JRC Scientific and Technical Reports

Simplified models/procedures for estimation of secant-to-yielding stiffness, equivalent damping, ultimate deformations and shear capacity of bridge piers on the basis of numerical analysis

LESSLOSS Project / Sub-Project 8: Deliverable 69 – Displacement-Based Design Methodologies

Carlo PAULOTTO, Gustavo AYALA, Fabio TAUCER, Artur PINTO

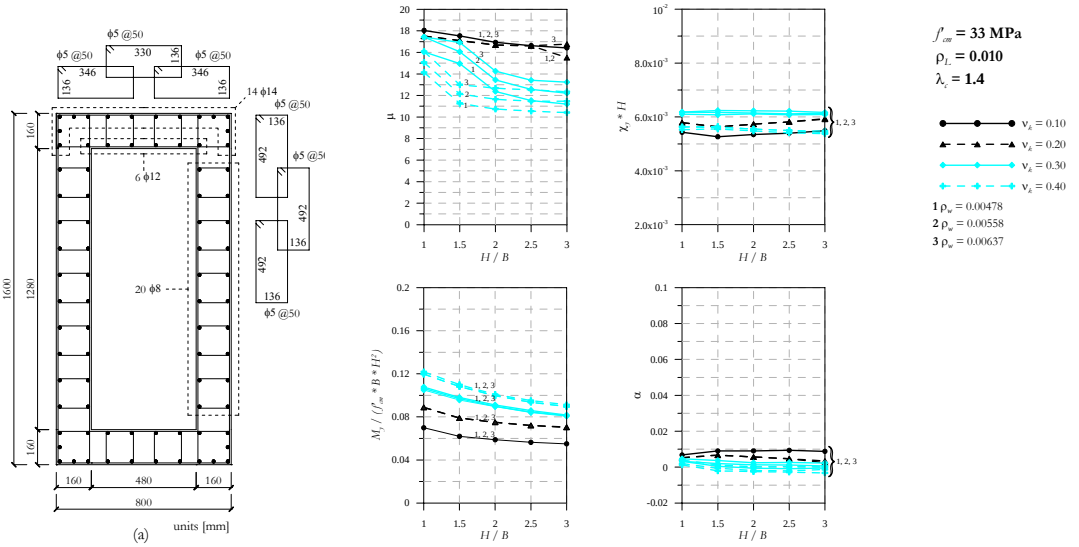

EUR 22885 EN - 2007

JRC EUROPEAN COMMISSION

ipsc Institute for the Protection and Security of the Citizen

less loss

The Institute for the Protection and Security of the Citizen provides researchbased, systems-oriented support to EU policies so as to protect the citizen against economic and technological risk. The Institute maintains and develops its expertise and networks in information, communication, space and engineering technologies in support of its mission. The strong crossfertilisation between its nuclear and non-nuclear activities strengthens the expertise it can bring to the benefit of customers in both domains.

European Commission
Joint Research Centre
Institute for the Protection and Security of the Citizen

Contact information
Address: Fabio TAUCER
E-mail: fabio.taucer@jrc.it
Tel.: +39 0332 78.5886
Fax: +39 0332 78.9049

http://ipsc.jrc.ec.europa.eu
http://www.jrc.ec.europa.eu

PUBSY 8009

EUR 22885 EN
ISSN 1018-5593

Luxembourg: Office for Official Publications of the European Communities

Printed in Italy

Simplified models/procedures for estimation of secant-to-yielding stiffness, equivalent damping, ultimate deformations and shear capacity of bridge piers on the basis of numerical analysis

EXECUTIVE SUMMARY

Current seismic evaluation and design tendencies for reinforced concrete bridges, in which performances under design conditions need to be estimated, require, even in the most simplified methods, an accurate description of the stiffness and energy dissipation characteristics of the piers forming the substructure. This description involves not only the use of sound analytical techniques, but also their calibration against existing results from experimental tests on large scale specimens.

Considering that the most widely used approach for the Displacement Based Design of bridges is based on the use of secant stiffness and equivalent viscous damping of the piers, both evaluated at maximum pier displacement, in this report the stiffness and energy dissipation characteristics, necessary to estimate these parameters, are obtained for reinforced concrete hollow rectangular bridge piers. This work involves the use, first of a continuous non-linear behaviour section model and then a pier model based on the plastic hinge approach and on the results obtained by the section model of the previous step.

The analysis starts from the identification of the parameters that play a major role in determining the behaviour of pier sections and their ranges of variation. The following parameters were chosen: the section aspect ratio, the mechanical properties of the reinforcement steel and concrete, the longitudinal reinforcement ratio, the normalized axial force and the confinement level. The range of variation of each of these parameters was determined on the basis of current practice and the prescriptions contained in the Eurocodes. As a result of this preliminary analysis, 2700 possible section designs were considered.

To determine the moment-curvature envelope of all the sections considered, nonlinear finite element analyses (using a 2D fibre model) under monotonically increasing curvatures were carried out. These capacity curves, representing the envelope curves of each section, are approximated with bilinear curves to be used either for evaluation or design purposes. In this way, the capacity curve of the generic section may be represented through four parameters: yield curvature and moment, and ultimate curvature and moment, which were used to summarize the results in a series of charts. The cyclic behaviour of each section is reproduced through nonlinear analysis under increasing cyclic loading, for which experimental results were also available. The results of these analyses were expressed in terms of a dimensionless parameter that is related to the energy dissipated per unit length by the section in a cycle. It was found that this parameter does not depend on the section aspect ratio, while it depends strongly on the normalized axial force, although this dependence becomes less strong as the longitudinal reinforcement ratio increases.

The properties derived at the section level are used to compute the force-displacement envelope and the energy dissipation characteristics of a pier of length L for a given level of ductility of the section; the calculations are performed assuming an expression derived from literature for the computation of the plastic length.

The equivalent properties of bridge piers, namely, equivalent stiffness and equivalent damping at maximum displacement, are calculated for rectangular hollow sections, and represent a significant design tool of direct application to the Displacement Based Design (DBD) of bridges, based on the concept of a substitute linear structure as originally defined by Gulkan and Sozen in 1967.

From the analysis of the experimental data it was observed that the shear contribution to the pier displacements can be significant. A state of art was produced concerning the different approaches that may be adopted to model the shear effects in reinforced concrete columns. The following models were analysed: the truss model, the classical Ritter-Morsch model, the concrete contribution model, the variable truss model, the strut and ties model, Compression Field Theory (CFT) and the Modified CFT (MCFT).

TABLE OF CONTENTS

LIST OF TABLES

LIST OF FIGURES

LIST OF SYMBOLS AND ABBREVIATIONS

PART A

b = Dimension of the concrete core perpendicular to the direction of the confinement under consideration, measured to outside of the perimeter hoop

b_0 = Width of the confined core in a column (to centreline of hoops)

d_{bL} = Diameter of longitudinal rebars

f_c = Compressive strength of concrete

f_{cd} = Design value of concrete compressive strength

f_{ck} = Characteristic compressive cylinder strength of concrete at 28 days

f_{cm} = Mean value of concrete cylinder compressive strength

f_{ctk} = Characteristic axial tensile strength of concrete

f_{ctm} = Mean value of axial tensile strength of concrete

f_t = Tensile strength of reinforcement

f_{tk} = Characteristic tensile strength of reinforcement

f_y = Yield strength of reinforcement

f_{yd} = Design value of yield strengtht of steel

f_{yk} = Characteristic yield strength of reinforcement

f_{ym} = Mean value of the yield strength of reinforcement

f_{ys} = Yield strength of the longitudinal reinforcement

f_{yt} = Yield strength of the tie

f_{yw} = Yield strength of transverse reinforcement

h_0 = Depth of the confined core in a column (to centreline of hoops)

n = Total number of longitudinal bars laterally engaged by hoops or cross ties on perimeter of column section

s = Spacing of transverse reinforcement, distance between tie legs

s_L = Maximum (longitudinal) spacing

s_T = Distance between hoop legs or supplementary cross ties

A_c = Cross sectional area of concrete

A_{cc} = Confined (core) concrete area of the section

A_s = Cross sectional area of reinforcement

A_{st} = Area of one leg of transverse reinforcement

A_{sw} = Total area of hoops or ties in the considered direction of confinement

A_t = Area of one tie leg

B = Width of the section

E = Energy stored by the section

E_c = Tangent modulus of elasticity of normal weight concrete at a stress $\sigma_c = 0$ and at 28 days

E_d = Energy stored by the pier

H = Depth of the section

K = Lateral stiffness of the pier

L = Distance from the plastic hinge to the point of zero moment

L_h = Plastic hinge length

M = Bending moment

N_{Ed} = Axial force corresponding to the design seismic combination

P = Axial load

V = Shear force

W = Energy dissipated by the section in one cycle

W_d = Energy dissipated by the pier in one cycle

α = Confinement effectiveness factor; post-yield stiffness ratio

χ = Curvature

δ = Parameter depending on the ratio f_t/f_y

ε_c = Compressive strain in the concrete

ε_{c1} = Compressive strain in the concrete at peak stress f_c

ε_{cu} = Ultimate compressive strain in the concrete

ε_u = Strain of reinforcement steel at maximum load

μ = Curvature ductility

μ_d = Displacement ductility

ν_k = Normalized axial force

ρ_L = Reinforcement ratio of the longitudinal reinforcement

ρ_w = Shear reinforcement ratio

σ_c = Compressive stress in concrete

ω_{wd} = Mechanical volumetric ratio of confining reinforcement

ξ = Equivalent damping ratio

Δ = Displacement

PART B

a = Shear span (distance from maximum moment section to point of inflection); maximum aggregate size

b = Width of the member; width of concrete layer

b_v = Effective web width taken as minimum web width within effective shear depth d_v

d_v = Effective shear depth taken as flexural lever arm which, for non-prestressed element

d_b = Bar diameter

f_{c1} = Principal tensile stress in concrete

f_{c2} = Principal compressive stress in concrete

f_{cx} = Stress in concrete in x-direction

f_{cy} = Stress in concrete in y-direction

f_{sx} = Average stress in x-reinforcement

f_{sxc} = Stress in x-reinforcement at crack location

f_{sy} = Average stress in y-reinforcement

f_{syc} = Stress in y-reinforcement at crack location

f_v = Tensile stress existing in the stirrups

f_{vy} = Yielding stress of transverse reinforcement

f_x = x-direction axial stress; stress applied to element in x-direction

f_y = y-direction axial stress; stress applied to element in y-direction

f_{yx} = Yield stress of x-reinforcement

f_{yy} = Yield stress of y-reinforcement

f'_c = Maximum compressive stress observed in a cylinder test

h = Depth of concrete layer

k_c = Factor for shear strength of concrete shear resisting mechanism

s = Stirrup spacing

s_{mx} = Indicator of the crack control characteristics of the x-reinforcement

s_{my} = Indicator of the crack control characteristics of the y-reinforcement

s_θ = Diagonal crack spacing

v_{ci} = Shear stress on crack surface

v_{cx} = Shear stress on x-face of concrete

v_{cxy} = Shear stress on concrete relative to x,y axes

v_{cy} = Shear stress on y-face of concrete

v_{sx} = Shear stress on x-reinforcement

v_{sy} = Shear stress on y-reinforcement

v_{xy} = Shear stress; shear stress on element relative to x, y-axis

w = Crack width

x = Distance from the column axis perpendicular to the applied shear force

y = Distance from top of beam section

$\overline{y}$ = Distance from top to centroid of section

A_g = Gross area of the member section

A_h = Area of one hoop leg

A_v = Total area of transverse reinforcement in the shear direction within a distance s

C = Compressive force acting on layer face

C_s = Compressive force acting in longitudinal bar

D = Diameter of a circular column

D' = Diameter of a spiral hoop

E_c = Young's modulus of concrete

$\overline{E}_c$ = Secant modulus of concrete

E_s = Young's modulus of reinforcement

$\overline{E}_s$ = Secant modulus of reinforcement

F = Force

M = Moment acting on member section

N = Axial force acting on member section

P = Axial load

S = Spacing between member cross sections

V = Shear resistance; shear force acting on a member section

V_c = Concrete contribution to the shear resistance

V_s = Transverse reinforcement contribution to the shear resistance

α = Angle between tangent to spiral and direction of shear force; angle formed between the column axis and the strut from the point of load application to the centre of the flexural compression zone at the column plastic hinge critical section; reinforcement orientation

γ_{xy} = Shear strain relative to x,y-axis

$\gamma^{p}_{\alpha xy}$ = Plastic shear strain in concrete relative to x, y-axes

ε = Instantaneous strain in concrete

ε_b = Bottom fibre strain in beam sections

ε^{e}_{c} = Elastic strain of concrete

ε^{p}_{c} = Residual (plastic offset) strain of concrete

ε_t = Top fibre strain in beam sections

ε_x = Strain in *x*-direction

ε_y = Strain in *y*-direction

ε_1 = First principal strain in concrete

1. INTRODUCTION

A number of important bridges and viaducts which incorporate reinforced concrete thin-walled hollow piers have been constructed during the past decades in seismic prone regions. The main advantage of this type of piers is that their mass is significantly smaller than that of piers with solid column sections of equivalent performance, thus reducing the amount of material used and decreasing the size of the inertial forces induced by earthquake loads. In spite of the more complex reinforcement layout and formwork construction, hollow columns are considered, in general, to be cost effective for large scale projects and for pier heights exceeding 20 m.

In spite of the use of hollow column sections for the construction of large bridge piers, their behaviour has not been extensively studied; in particular, a limited number of experimental tests have been performed to describe the load-deformation and energy dissipation characteristics of such members. The aim of this report is to describe these characteristics for different levels of deformation to be used within the context of Performance Based Design (PBD).

The report is subdivided in two parts: the first part (Part A) describes the moment-curvature relations and the energy dissipation characteristics of rectangular pier hollow sections of various design configurations, and the second part (Part B) describes the shear effects on reinforced concrete bridge piers.

In Part A, the stiffness and energy dissipation characteristics of the pier are derived based on energy principles from the section properties at the base of the pier. The stiffness properties of the section are described by a bilinear moment-curvature model defined by the bending moments and curvatures at yield and at the ultimate capacity of the section, derived from nonlinear analysis using a 2D fibre model initially calibrated from experimental results. The energy dissipation characteristics of the section are derived directly from the numerical model at increasing levels of ductility. Parametric analysis is performed for a large number of design configurations of the pier section, including the aspect ratio of the section, the normalised axial load, the percentage of longitudinal reinforcement, the level of confinement, and the strength of concrete and steel, and the results are summarised in series of charts that can be used by the designer to defined the moment-curvature diagram (including stiffness to yield and maximum curvature capacity) for a particular section. Similarly, a number of charts are presented, describing the energy dissipation for several section configurations for different levels of ductility.

In Part B, the state-of-the-art on the different approaches to model the effects of shear on reinforced concrete column sections is presented, starting from the truss model, that considers only the contribution of the steel stirrups, up to the modified compression field theory, that takes into account the three dimensional contribution along the section of both shear and bending. The theoretical explanation is supported by experimental tests performed on reinforced concrete hollow sections considering shear, as well as on walls that may be approximated to the webs of the pier. However, there is a need to extend the more detailed models to cyclic loading and to perform target tests on large scale piers to model the combined effects of shear and flexure.

PART A: STIFNESS AND ENERGY DISSIPATION EQUIVALENT PROPERTIES

2. SELECTION OF THE EXPERIMETAL DATA

2.1 GENERALITIES

The numerical models used in this research were calibrated against the results of experimental tests conducted on large-scale models of hollow reinforced concrete piers at the European Laboratory for Structural Assessment (ELSA) in Ispra (Italy) [Pinto *et al.*, 1996]. These experimental models used in the tests were chosen with the aim to reduce as much as possible the consequences of the scale effect in the calibration process.

Only a few number of documents are found in the technical literature focused on the scale effect on experimental tests of reinforced concrete bridge piers: [Stone and Cheok, 1989], [Hoshikuma *et al.*, 2002] and [Yeh *et al.*, 2002]. Stone and Cheok [1989] conducted a series of cyclic loading tests on full-scale circular columns, with a diameter of 1524 mm, and their relative well-scaled replica model, to determine the size effect on inelastic behaviour of reinforced concrete columns subjected to seismic forces. They found that the scale effect does not appear when reinforcement details including bar diameter and vertical hoop spacing are precisely scaled.

Hoshikuma *et al.* [2002] tested a full-scale column with a 2400 mm square section and a 1/4 scale replica model. The columns were subjected to a quasi-static, cyclically reversed horizontal load until the columns were completely failed. No vertical loads were applied to the prototype nor to the model. As Stone and Cheok [1989], they concluded that if the reinforcement details are precisely scaled, the size effect on the inelastic ductile behaviour of reinforced concrete bridge columns is not significant.

Yeh *et al.* [2002] carried out experimental tests on square hollow reinforced concrete bridge columns. Two prototypes and four models of such columns were tested under constant axial loads and quasi-static, cyclically reversed horizontal loads. The prototype cross sections were 1500 x 1500 mm and the scale factor of the models was equal to 1/3. Yeh *et al.* [2002] found that the prototypes have greater ductility factors than those given by the models and pointed out two possible sources for this discrepancy: a difference in the yielding characteristics between the rebars used as longitudinal reinforcement in the prototypes and those used in the models, and the effect of low-cycle fatigue, which has a stronger influence on the small size rebars used in the models. However, it should be noted that the scaling criteria applied by Stone and Cheok [1989] and in Hoshikuma *et al.* [2002] were not completely satisfied by Yeh *et al.* [2002]. It is opinion of the author that this could be the reason for the strong scale effect observed by Yeh *et al.* [2002], since differences in the yielding characteristics of the reinforcement and low-cycle fatigue affects were also present in Stone and Cheok [1989] and in the Hoshikuma *et al.* [2002] tests.

On the basis of these results, it can be concluded that the models tested by Pinto *et al.* [1996] can reasonably represent the actual behaviour of hollow reinforced concrete bridge piers, since they satisfy the scaling criteria applied by Stone and Cheok [1989] and Hoshikuma *et al.* [2002]. In fact, Pinto *et al.* [1996] used rebars with diameters ranging between 10 mm and 14 mm as longitudinal reinforcement in the flanges of the models (according to Mander [1984], the flange walls determine the behaviour of hollow rectangular concrete piers). Considering that the model scale factor was 1:2.5, these rebars correspond to prototype rebars having diameters in the range of 25-35 mm, which are commonly used in current practice for this type of structures. Analogous considerations can be made for the size of transverse reinforcement (5 mm for the models and 12.5 mm for the prototypes) and spacing of transverse reinforcement along the pier (50 mm for the models and 125 mm in the prototypes). If a criticism can be made on these models, is that the longitudinal reinforcement is not uniformly distributed on the section, as generally happens in current practice.

2.2 DESCRIPTION OF THE EXPERIMENTAL SET-UP AND RESULTS

The experimental tests preformed by Pinto *et al.* [1996] consisted in testing single piers subjected to cyclic loading, as well as testing of a complete bridge structure by means of the pseudo-dynamic (PSD) sub-structured test method, which integrates physical testing of the pier models for which the load-displacement behaviour is to be determined, with numerical models of those parts of the bridge for which the force-displacement response is known or remains elastic (i.e., the deck). Several bridge configurations composed of three piers were studied, according to their degree of irregularity in terms of the heights and capacities of the piers. The results obtained from the medium pier of the bridge B232 configuration were used for the calibration of the numerical model.

The geometric characteristics and the reinforcing steel lay-out of the pier model are presented in Figure 1. In order to determine the mechanical characteristics of concrete and steel, a set of specimens from the construction of the model were tested. The mechanical characteristics of concrete and steel reinforcement (Tempcore B500B) are reported in Table 1 and Table 2.

The footing of the pier was rigidly attached to the strong floor of the laboratory by means of post-tensioned steel bars passing through the floor. The footing was prestressed in order to limit cracking when developing the maximum strength at the base of the pier.

A stiff steel cap was connected with bolts and epoxy resin to the top of the pier (see Figure 1b). The cap was used to apply the horizontal loads coming from the PSD test method, and to impose the vertical loads needed to simulate the weight of the bridge superstructure.

2.2.1 Applied Horizontal Displacements

Two actuators were connected by spherical joints to the steel cap of the pier, on one side, and to a steel plate attached to the reaction wall on the opposite side, and were used to impose horizontal displacements. The pier was tested as part of a bridge configuration for two consecutive earthquakes using the PSD technique. The first earthquake, hereafter denoted as "design earthquake", was a stationary artificial earthquake with a PGA of 0.35g compatible with the prEN 1998-2 [CEN, 1993] spectrum for soil type B. The second earthquake was obtained by multiplying the ordinates of the first one by a factor 2. In Figure 2 and Figure 3 are reported the displacement and force time-histories measured at the top of the considered pier during these two tests. Finally, the pier was isolated from the bridge model and tested cyclically until failure. Figure 4 illustrates the displacement and force time-histories applied at the top of the pier during the cyclic test.

2.2.2 Applied Vertical Load

A vertical force of 1700 kN, corresponding to a 10% normalized axial force, was applied at the top of the pier and was kept practically constant during the whole duration of the test. The vertical load was applied by means of four actuators resting on top of the steel cap and hinged connected to post-tensioning steel rods running through the hollow core of the pier section; the steel rods were embedded at the base of the pier footing and instrumented with strain gages to monitor the axial load. The direction of the axial force follows the direction of post-tensioning (see Figure 5a) and can be decomposed into a horizontal (P·sin α) and a vertical component (P·cos α), so that the moment M at the column interface with the footing can be evaluated as:

$$M = V \cdot L + P' \cdot \Delta = V \cdot L + P \cdot \cos\alpha \cdot \Delta \qquad (2.1)$$

while the total lateral force applied to the column is:

$$V' = V - P \cdot \sin\alpha \qquad (2.2)$$

When a horizontal displacement history is applied to the pier, the gravity loads of the deck keep on acting along the vertical direction while the structure undergoes deformations (see Figure 5b). For this reason, Dutta *et al.* [1999] concluded that the post-tensioning method does not correctly model the P-Δ effect. Nevertheless, as noted by Asadollah and Xiao [2002], it can be asserted that the conventional method of post-tensioning is valid without any deficiency as long as the true forces P' and V' are used in the data analysis. It is worth noting that α is typically small: during the cyclic test it attained a maximum value of about 0.03 rad, as a result P' can be assumed to be equal to P.

2.2.3 Moment-Curvature Time-Histories

The evaluation of the moment-curvature behaviour along the column was carried out on the basis of the data given by a set of displacements transducers (LVDT) placed along the two external opposite faces of the pier model. (See Figure 1b). The average curvature in a slice can be expressed as:

$$\chi = \frac{\Delta_{v,i} - \Delta_{v,j}}{D \cdot l} \qquad (2.3)$$

where χ is the average curvature over the considered slice, Δ_{vi} and Δ_{vj} are the relative vertical displacements measured by two transducers at the same height on the two sides of the pier, D is the distance in plan between the two transducers and l is the height of the slice. The corresponding moment is calculated at the middle height of the slice, using the recorded values for the horizontal force and axial load and the relative horizontal deflection at the corresponding step.

Figure 6 and Figure 7 show the moment-curvature responses of slice #1 (at the base of the pier) of the medium pier of bridge B232 subjected to the design earthquake and to the design earthquake multiplied by a factor of two, respectively. Figure 8 shows the analogous response of the pier tested under increasing cyclic displacements until failure.

3. NUMERICAL MODEL

3.1 GENERALITIES

With the purpose of simulating the behaviour of pier sections with characteristics different from those in the laboratory, a fibre model was implemented in Castem 2000 [Maillard, 1993] and checked against the experimental results described in Section 0.

Four different material models: reinforcement steel in the longitudinal direction, unconfined concrete, flange confined concrete and web confined concrete, were used to build the section model.

3.2 STEEL AND CONCRETE MODELS

The monotonic behaviour of the steel fibre is represented by a three-stage stress-strain curve: linear elastic followed by a yielding plateau and a hardening zone modelled with a fourth degree polynomial. The model for cyclic loading follows the monotonic curve until the strain falls below a pre-established level after unloading from a postyielding position. From this point on, the stress-strain curve follows the Menegotto-Pinto [1973] model.

The rebar buckling is modelled after Monti and Nuti [1992]. This model, which neglects the influence of concrete and transverse reinforcement, was calibrated against experimental tests conducted on Italian reinforcing rebars FeB 44k characterized by a more pronounced hardening when compared with that shown by the modern Tempcore B500B rebars. This difference implies that Tempcore B500B bars are more prone to inelastic buckling than the FeB 44k rebars. For this reason, a recalibration of the model, which at present has not been performed, would have been desirable.

The values reported in Table 1 were assigned to the parameters of the steel model. The ultimate tensile strain was reduced by 30%, recognizing that under cyclic loading involving sequential tensile and compressive strains, the ultimate tensile strain is in general smaller than that obtained from monotonic testing [Priesley *et al.* 1996b]. The onset of strain hardening was assumed at a strain equal to 2%.

The Hognestad [1951] model was adopted for the concrete under monotonic compressive loading. A parabolic function defines the ascending part of the curve from zero to the maximum compression stress point. A straight line represents the concrete softening behaviour after maximum strength until failure. The slope of this line depends on the degree of confinement of concrete (see Figure 9). In order to improve the model for confined concrete, a third branch is considered after the softening compression branch and before reaching failure: a zero slope straight line defining a compression plateau. This additional condition accounts for the residual strength of the concrete core for important axial post-peak deformations. Following the recommendations of Park *et al.* [1982], a residual strength equal to 20% of the peak strength was assumed in the model.

The compression monotonic curve models the envelope of the behaviour of concrete under compression cyclic loading. Unloading from the envelope follows a law similar to the one proposed by Mercer and Martin [1987]: a straight line with a slope that depends on the maximum

strain reached during the loading history (see Figure 10). The degradation of the material stiffness is taken into account by decreasing the slope of the unloading branch as the maximum strain increases. The reloading compression curve is also a straight line from the zero stress point to the last loading point reached on the envelope; no strength degradation is considered.

A bilinear model was used to represent the behaviour of concrete under monotonic tensile loading: a first linear branch with a slope equal to the initial compression Young's modulus, from zero to the maximum tensile stress point, and a second linear branch from the maximum tensile stress point to a zero stress point (see Figure 10); the post-cracking softening behaviour models the "tension-stiffening" effect. Details on the model for cyclic tensile loading can be found in Guedes *et al.* [1994].

No attempt was made to simulate the crack closing, since no reliable model has been implemented in Castem 2000 [Maillard, 1993] yet. As a result, the numerical model is expected to show more pinching than the actual behaviour of the pier-section.

3.2.1 Confined Concrete

The behaviour of the confined concrete in the flanges of the pier section plays a major role in determining the seismic performance of the pier. For this reason, special effort has been devoted to model its behaviour. Many different stress-strain relationships have been developed for confined concrete: Sheik *et al.* [1982], Fafitis and Shah [1985], Mander *et al.* [1988], Saatcioglu and Razvi [1992], Sakino et al. [1993]. Among the aforementioned models, that proposed by Mander *et al.* [1988] is the only one that can be applied to all section shapes at all levels of confinement, furthermore it has also been accepted in prEN1998-2 [CEN, 2003], Annex E.

Unfortunately, the model proposed by Mander *et al.* [1998] is not implemented in Castem 2000 [Maillard, 1993]. As a result, an effort was made to evaluate the differences between the two models.

In Castem 2000 [Maillard, 1993] the confinement effect is modelled through the confinement parameter β, which affects the strength, the strain at the maximum strength and the slope of the post peak branch, as shown in the Equations (3.1), (3.2) and (3.3)

$$f_{c,c} = \beta \cdot f_c \tag{3.1}$$

$$\varepsilon_{c1,c} = \beta^2 \cdot \varepsilon_{c1} \tag{3.2}$$

$$Z = \frac{\beta - 0.85}{\beta \cdot \left(0.1 \cdot \alpha \cdot \omega_w + 0.0035 + \varepsilon_{c,c}\right)} \tag{3.3}$$

where $f_{c,c}$ and $\varepsilon_{c1,c}$ represent the maximum strength and the strain at the maximum strength for confined concrete, while f_c and ε_{c1} represent the analogous parameters for unconfined concrete; Z is the slope of the post peak branch (see Figure 9). The parameter β is defined as:

$$\beta = \min\left(1 + 2.5 \cdot \alpha \cdot \omega_w, 1.125 + 1.25 \cdot \alpha \cdot \omega_w\right) \tag{3.4}$$

where

$$\omega_w = \frac{A_{st} \cdot f_{yw} \cdot \sum\left(l_w / s\right)}{b_0 \cdot h_0 \cdot f_c} \tag{3.5}$$

represents the mechanical volumetric ratio of the stirrups and

$$\alpha = \left(1 - \frac{8}{3 \cdot n}\right) \cdot \left(1 - \frac{s}{2 \cdot b_0}\right) \cdot \left(1 - \frac{s}{2 \cdot h_0}\right) \tag{3.6}$$

expresses the effect of the number of longitudinal restrained rebars n and the density of the stirrups on the degree of confinement of the concrete core. In Equations (3.5) and (3.6) A_{st}, f_{yw} and l_w represent the area of the cross-section of the leg, the yielding stress and the total length of the stirrups, respectively; s is the distance between stirrups along the member axis, and b_0 and h_0 are the dimensions of the confined concrete core measured from the centre-line of the stirrups.

In Mander *et al.* [1998], the behaviour of the confined concrete is represented through a continuous equation:

$$\frac{\sigma_c}{f_{c,c}} = \frac{x \cdot r}{r - 1 + x^r} \tag{3.7}$$

where

$$x = \frac{\varepsilon_c}{\varepsilon_{c1,c}} \tag{3.8}$$

$$r = \frac{E_c}{E_c - E_{\sec}} \tag{3.9}$$

$$E_{\sec} = \frac{f_{c,c}}{\varepsilon_{c1,c}} \tag{3.10}$$

The confinement is taken into account by the confinement parameter λ_c:

$$\lambda_c = 2.254 \cdot \sqrt{1 + 7.94 \cdot \frac{\sigma_e}{f_c}} - \frac{2 \cdot \sigma_e}{f_c} - 1.254 \tag{3.11}$$

which directly affects the maximum concrete strength and the corresponding strain:

$$f_{c,c} = f_c \cdot \lambda_c \tag{3.12}$$

$$\varepsilon_{c1,c} = 0.002 \cdot \left[1 + 5 \cdot \left(\frac{f_{c,c}}{f_c} - 1\right)\right] \tag{3.13}$$

The confinement parameter λ_c is a function of the effective confinement pressure:

$$\sigma_e = \alpha \cdot \rho_w \cdot f_{yw} \tag{3.14}$$

where:

$$\alpha = \alpha_n \cdot \alpha_s \tag{3.15}$$

$$\alpha_n = 1 - \sum_n \frac{b_i^2}{6 \cdot b_0 \cdot h_0} \tag{3.16}$$

$$\alpha_s = \left(1 - \frac{s}{2 \cdot b_0}\right) \cdot \left(1 - \frac{s}{2 \cdot h_0}\right) \tag{3.17}$$

$$\rho_w = \frac{A_{sw}}{s \cdot b} \tag{3.18}$$

where b_i is the distance between consecutive engaged bars, A_{sw} is the total area of hoops or ties in the direction of confinement and b is the dimension of the concrete core perpendicular to the direction of the confinement under consideration, measured to the outside of the perimeter hoop.

For rectangular sections, the confinement effects should be evaluated in two orthogonal directions, say directions 2 and 3. When the values of ρ_w in these two directions are not equal, the effective confining stress may be estimated as:

$$\sigma_e = \sqrt{\sigma_{e2} \cdot \sigma_{e3}} \tag{3.19}$$

The Mander et al. [1998] and the Castem 2000 [Maillard, 1993] models were compared for the confined concrete of the flanges of the medium pier of bridge B232. The parameters of the two models corresponding to this case are reported in Table 3 and Table 4. Figure 11 shows the results given by the two models. It can be seen that the two models give different values for the maximum concrete strength, with large differences in the softening branch. The results given by the Castem 2000 [Maillard, 1993] model has been in part improved by equating the maximum concrete strength given by the two models. The value of the parameter β is set equal to the value of the λ_c parameter in Mander's model and the corresponding value of the product $\alpha \cdot \omega_w$ is determined through Equation (3.19). The results are shown in Figure 11.

3.3 VALIDATION OF THE NUMERICAL MODEL

In order to judge the ability of the numerical model to represent the actual behaviour of pier sections, the numerical results were compared with those obtained by the tests described in Section 0.

The comparison was first focused on the initial stiffness of the sections. With this aim, the results relative to the initial part of the design earthquake were considered. The results of the comparison are shown in Figure 12, Figure 13, Figure 14 and Figure 15, for slice #1, #2, #3 and #4, respectively. It can be observed that the cracked stiffness of the section is well predicted for all the four pier slices considered in the analysis. The uncracked stiffness is well predicted for slices #3 and #4, while for slice #2, it was not possible to derive any considerations as the experimental data was affected by noise. For slice #1 the initial stiffness is equal to the cracked stiffness, showing that this portion of the pier was already cracked at the beginning of the test. This was probably due to the presence of a cold joint between the plinth and the pier. In fact, the pier was made in a precast concrete workshop and then transported to the ELSA site where the plinth was cast in a separate phase.

Finally, the ability of the numerical model to predict the section behaviour after the yielding point was checked. With this aim, the numerical results were compared with the experimental ones which had been obtained applying the design earthquake to the bridge model. The results are shown from Figure 16 to Figure 19. From these results, it is evident that the numerical model is able to follow the skeleton curve of the section. Furthermore, it can be observed that the behaviour predicted by the numerical model is characterized by a very pronounced pinching that is not exhibited by the experimental results. This discrepancy, as previously mentioned, is due to the lack of a good crack opening-closure law in the numerical model.

On the basis of the comparison between the numerical and the experimental results relative to the design earthquake, it is concluded that the considered numerical model can be reasonably used to obtain the skeleton curve of the behaviour of a generic rectangular hollow section. It is

less clear if the numerical model is able to represent the hysteretic energy dissipated by sections due to a more pronounced pinching of the numerical model. With the aim of clarifying this point, a cyclic path of curvatures with increasing amplitude was applied to the numerical model and the results were compared with those obtained experimentally from the cyclic test described in Section 2.2. From Figure 20 it can be observed that the numerical model gives a rather good estimation of the energy dissipated by the section, at least in the case of cyclic tests. It should be noticed that overall, the different curvature paths used for the experimental and numerical tests seem not to affect the results.

4. PARAMETRIC ANALYSIS OF THE SECTIONS

4.1 GENERALITIES

The aim of this parametric analysis is to evaluate the moment-curvature behaviour of bridge pier sections within the framework of Displacement Based Design (DBD) according to the prescriptions prEN 1998 [CEN, 2003].

The analysis started from the identification of the parameters that play a major role in determining the behaviour of the section. The parameters that were considered are: the concrete class and the steel reinforcement yield strength, the wall thickness, the section aspect ratio, the longitudinal reinforcement ratio, the axial load level, and the confinement level.

The definition of the range of variation for each of these parameters is discussed in Sections 4.2 to 4.7, while the values that were considered in the analysis are reported in Table 22. For each of the 2700 combinations of these values, two nonlinear static analyses, one monotonic, and one cyclic, were performed in order to obtain the skeleton curve and the damping properties of the corresponding pier section. Finally, each skeleton curve was approximated through a bilinear curve.

4.2 STEEL AND CONCRETE CHARACTERISTICS

According to prEN 1998-1 5.3.2 (1)P [CEN, 2003], class B or C steel reinforcement, as defined in Table C.1 in Normative Annex C of prEN 1992-1-1 [CEN, 2003], should be used in primary seismic elements. Tempcore B500B reinforcing steel, which belongs to class B as defined by Normative Annex C, was considered in the analysis, with the following assumptions: steel tensile strength f_t equal to $1.19 \cdot f_y$ [Priestley *et al.*, 1996b]; elongation at maximum force ε_u and strain at the beginning of hardening equal to 0.11 and 0.02, respectively.

According to prEN 1998-1 7.2.1 (1) [CEN, 2003], the prescribed concrete class in plastic regions should not be lower than C20/25, and not higher than C40/50. In the parametric analysis, concrete classes C25, C30 and C35 were considered.

According to prEN 1998-1 4.3.3.4 (4) [CEN, 2003], the element properties should be based on the mean values of the material properties. For new structures, the mean values of the material properties may be estimated from the corresponding characteristic values on the basis of information provided in Annex E of prEN 1998-2 [CEN, 2003] and Table 3.1 of prEN 1992-1-1 [CEN, 2003] (see Table 5 and Table 6) for the values assumed in the parametric analysis). This provision recognizes the difference between designing for gravity loads and for earthquake

actions. In the case of gravity load design, it is important to have an adequate reserve of strength in order to avoid structural failure: the member properties are derived from a lower percentile of material properties (characteristic values). On the contrary, in the case of seismic design, structures are allowed to respond inelastically *e.g.,* the action level overcomes the structural strength, therefore there is no point in providing for a reserve of strength.

4.3 WALL THICKNESS

From a survey of a number of bridge designs it was observed that the thickness of the walls that constitute the hollow sections varies between 0.30 m and 0.50 m. In the parametric analysis a constant value of 0.40 m was chosen for the wall thickness.

4.4 SECTION ASPECT RATIO

Poston *et al.* [1985] conducted experimental tests on four bridge pier models. The objective of this work was to investigate the axial-load-moment-curvature behaviour of hollow columns and to examine the validity of the plane-section assumption. On the basis of their results and from those obtained by Proctor [1976, 1977] and Jobse [1982], Poston *et al.* [1985] concluded that the assumption is completely valid when the cross-sectional unsupported wall length to thickness ratio does not exceed 6. For ratios greater than 6, a strength reduction due to non-planar action and local instability is recommended. Taylor and Breen [1994], on the basis of the aforementioned experimental results and from those obtained after testing twelve piers models, concluded that wall slenderness ratios greater than 35 should not be allowed in practice, and that the normal design procedure used to design solid piers should only be applied to hollow piers when the slenderness ratio is lower than 15. For wall slenderness ratios greater than 15, Taylor and Breen [1994] proposed a simplified design method that formed the basis for the provisions contained in the AASHTO Specification [1998]. The validity of the results obtained by Taylor and Breen [1994] was confirmed by Santa Maria [2001], who tested five models of concrete bridge piers. It is worth noting that all the previous tests where conducted monotonically and quasi-statically. Furthermore, only the effect of axial loads and bending moments were considered in the analyses, with no reference to the effects of shear.

According to prEN 1998-2 6.2.4 (2) [CEN, 2003], in plastic regions the wall slenderness ratio should not exceed 8. Since in the parametric analysis the wall thickness was equal to 0.40 m, the maximum clear width of the wall is equal to 3.20 m. Furthermore, in the parametric analysis it was considered a monocellular hollow pier with the outer dimension of the flange constant and equal to 2.00 m resulting in a section aspect ratio of 2.0 when the maximum wall slenderness ratio allowed by prEN 1998-2 [CEN, 2003] is considered. In the parametric analysis aspect ratio values ranging between 1.0 and 3.0 have been considered, exceeding the maximum allowed slenderness ratio for aspect ratios larger than 2.

4.5 LONGITUDINAL REINFORCEMENT RATIO

The longitudinal reinforcement ratio is defined as:

$$\rho_L = \frac{A_s}{A_c} \tag{3.20}$$

where A_s and A_c are the total areas of longitudinal reinforcement and concrete cross-section.

Lower and upper limits to longitudinal reinforcement ratio are usually specified by design codes. There is, however, an important variation in codified limits and in common design practice among different countries [Priestley *et al.*, 1996b]. In the United States, it is permitted to vary the

longitudinal reinforcement ratio for columns between 0.01 and 0.08. In New Zealand, the permitted range is from 0.008 to 0.08. In Japan much lower reinforced ratios are permitted, and values as low as 0.005 are common. According to prEN 1998-1 5.4.3.2.2 (1) [CEN, 2003], the total longitudinal reinforcement ratio should not be less than 0.01 and not more than 0.04. In design practice, reinforcement ratios are usually between 0.01 and 0.03. In the present study, reinforcement ratios between 0.005 and 0.04 were considered, distributed in two layers as commonly observed in practice. Furthermore, it was assumed that the reinforcement rebars, having all the same size, are uniformly distributed across the section.

4.6 AXIAL LOAD LEVEL

The normalized axial force is defined as:

$$\nu_k = \frac{N_{Ed}}{A_c \cdot f_{ck}} \tag{3.21}$$

where N_{ed} is the axial force corresponding to the seismic design condition, A_c is the area of the concrete section and f_{ck} is the characteristic value of concrete strength.

According to prEN 1998-2 2.2.2.1 5(P) [CEN, 2003], plastic hinges shall not be formed in reinforced concrete sections where the normalized axial force exceeds 0.6. Furthermore, if the normalized axial force is greater than 0.30, even in a single ductile member, the value of the bridge behaviour factor should be reduced (prEN 1998-2 4.1.6 5(P) [CEN, 2003]). As a result, in design practice, normalized axial force values usually range between 0.10 and 0.30.

4.7 CONFINEMENT LEVEL

The confinement level of concrete in a section is related to the amount of transverse reinforcement and its arrangement, which in turn is related to the amount and arrangement of the longitudinal reinforcement. The confinement level can be evaluated through Mander's parameter λ_c, as suggested by Annex E of prEN 1998-2 [CEN, 2003], using Equations from (3.7) to (3.19).

In order to evaluate the range of variation of λ_c, a 1.00 m section of a wall with a thickness of 0.40 m was considered (see Figure 21). By assuming a value i for the distance between the centres of two consecutive rebars, the rebar size can be evaluated in terms of the longitudinal reinforcement ratio (see Table 7). It is reasonable to assume that the diameter of the longitudinal reinforcement of bridge piers may vary between ϕ16 mm and ϕ32 mm, so that any bar diameter resulting from the combination of the selected distance i and longitudinal reinforcement ratio ρ is discarded if it falls out of this range (see Table 7).

For each spacing value i, the distance b_i between two consecutive engaged rebars is evaluated. According to prEN 1998-2 6.2.4 (4) [CEN, 2003], if $\nu_k \leq 0.2$ the requirements concerning buckling of longitudinal compression reinforcement given in Section 6.2.2 need to be met; otherwise the confinement provisions given in Section 6.2.1 need to be met as well.

According to prEN 1998-2 6.2.2 [CEN, 2003], longitudinal rebars should be restrained against outward buckling through: i) a perimeter tie engaged by intermediate cross-ties at alternate locations of longitudinal bars at a horizontal spacing not exceeding 200mm (see Table 8); ii) transverse reinforcement at a vertical spacing not exceeding the value of the product between the diameter of the longitudinal rebars and factor δ (see Table 10), defined as:

$$5 \leq \delta = 2.5 \cdot \left(f_{tk} / f_{yk} \right) + 2.25 \leq 6 \tag{3.22}$$

where f_{tk} and f_{yk} are the characteristic values of the tensile and yield strength of the transverse reinforcement, respectively. Following Priestley *et al.* [1996b], a value equal to 1.19 has been assumed for the ratio f_{tk}/f_{yk}, resulting in a value of δ equal to 5.

According to prEN 1998-2 6.2.1 [CEN, 2003], the transverse distance between hoop legs or supplementary cross-ties should not exceed 1/3 of the smallest dimension of the concrete core to the hoop centreline, nor 200 mm (see Table 9) and the spacing of hoops or ties in the vertical direction should be smaller than 6 times the longitudinal bar diameter and 1/5 of the smallest dimension of the concrete core measured to the hoop centreline.

For each of the considered reinforcement arrangements, the values of the parameters α_n, α_s and α, defined according to Equations (3.16), (3.17) and (3.15), are evaluated. The results are shown in Table 12 and Table 17.

According to prEN 1998-2 6.2.2 (4)P [CEN, 2003], if $\nu_k \leq 0.2$, the minimum amount of transverse ties is given by:

$$\min\left(\frac{A_t}{s_T}\right) = \frac{\sum A_s \cdot f_{ys}}{1.6 \cdot f_{yt}} \quad (\text{mm}^2/\text{m}) \tag{3.23}$$

where A_t is the area of one tie leg (in mm^2), s_T is the vertical distance between tie legs (in m), ΣA_s is the sum of the areas of the longitudinal bars restrained by the tie (in mm^2), f_{yt} is the yield strength of the tie and f_{ys} is the yield strength of the longitudinal reinforcement. From Equation (3.23), A_t and the relative transverse reinforcement ratio can be determined for each considered couple of A_s and s_T values (see Table 18 and Table 19).

For $\nu_k > 0.2$, both prEN 1998-2 6.2.1 (provisions against buckling) and 6.2.2 (confinement provisions) [CEN, 2003] should be met. The quantity of confining reinforcement is defined through the mechanical reinforcement ratio:

$$\omega_{wd} = \rho_w \cdot f_{yd} / f_{cd} \tag{3.24}$$

where ρ_w is the transverse reinforcement ratio defined as:

$$\rho_w = \frac{A_{sw}}{s_L \cdot b} \tag{3.25}$$

where A_{sw} is the total area of hoops or ties in one direction of confinement; s_L is the spacing of hoops or ties in the vertical direction, b is the dimension of the concrete core perpendicular to the direction of confinement under consideration, measured outside of the perimeter hoop.

The minimum amount of confining reinforcement is determined, for rectangular hoops and cross ties, as follows:

$$\omega_{wd,r} \geq \max\left(\omega_{w,req}, \frac{2}{3}\omega_{w,\min}\right) \tag{3.26}$$

where:

$$\omega_{w,req} = \frac{A_c}{A_{cc}} \cdot \lambda \cdot \nu_k + 0.13 \cdot \frac{f_{yd}}{f_{cd}} \cdot \left(\rho_L - 0.01\right) \tag{3.27}$$

where A_c is the concrete gross section area; A_{cc} is the confined concrete area of the section to the hoop centreline, $\omega_{w,min}$ and λ are factors specified in Table 20 and ρ_L is the reinforcement ratio of the longitudinal reinforcement. From Figure 22 it is possible to observe that the plot of Equation (3.27) in the ν_k-ρ_L-$\omega_{wd,r}$ space is represented by a plane with a slope that depends on the values of the parameter λ given in Table 20. Figure 22 also shows the maximum transverse reinforcement ratio 0.016 ($\omega_{wd,r}$ = 0.346) needed to achieve a ductile seismic behaviour when ν_k = 0.60 and ρ_L = 0.04.

It can be concluded then that the transverse reinforcement ratios range between a minimum of 0.003, obtained for $\nu_k \leq 0.20$ and a low amount of longitudinal reinforcement (see Table 19), and a maximum ratio of 0.016. Assuming that the transverse reinforcement ratio is the same in both directions, orthogonal and parallel to the wall of Figure 21, the range of values of the confinement pressure σ_e and of the confinement parameter λ_c can be evaluated through Equations (3.14) and (3.11), respectively. The results are reported in Table 21.

In the parametric analysis, λ_c ranges between 0.0 and 2.0. For the concrete classes given in Table 5 and the λ_c values considered in the parametric analysis, the corresponding values of σ_e are evaluated (see Figure 23) as a function of the transverse reinforcement ratio ρ_w. The limits of this range correspond to the minimum and maximum values attained by the confinement effectiveness parameter α (from about 0.6 to about 0.8) (see Table 14 and Table 17).

4.8 FAILURE CRITERIA OF THE SECTIONS

Failure of the reinforced concrete section is achieved when one of the following conditions occurs: i) the reinforcing steel attains its ultimate tensile strain; ii) the confined concrete reaches its ultimate compressive strain.

In design and analysis of members subjected to earthquake loads, a reduced effective ultimate tensile strain should be adopted, since there is evidence that under cyclic loading involving sequential tensile and compressive strains, the ultimate tensile strain is less than that obtained under monotonic testing [Priestley *et al.*, 1996b]. The requirement that the reinforcement tensile strain ε_s should not be greater than $0.70 \cdot \varepsilon_{su}$, where ε_{su} is the reinforcement steel elongation at maximum stress, is generally conservative, except for members with high axial compression forces.

The confined concrete attains its ultimate compressive strain, according to prEN1998-2 E.2.1 [CEN, 2003], when:

$$\varepsilon_{cu,c} = 0.004 + \frac{1.4 \cdot \rho_s \cdot f_{ym} \cdot \varepsilon_{um}}{f_{cm,c}} \qquad (3.28)$$

where $\rho_s = 2 \cdot \rho_w$ for orthogonal hoops, f_{ym} and ε_{um} are the mean values of the yield stress and elongation at maximum stress of the reinforcement steel, respectively, and $f_{cm,c}$ is the mean value of the compressive strength of the confined concrete. It should be noted [Priestley *et al.*, 1996b] that Equation (3.28) has been formulated from considerations of confined sections under axial compression. When used to estimate the ultimate compression strains of sections subjected to bending, or combined bending and axial compression, Equation (3.28) tends to be conservative by at least 50%.

4.9 IDEALIZED MOMENT-CURVATURE RELATIONSHIP

The nonlinear skeleton curves obtained from the parametric analysis were approximated through bilinear curves. With this aim, the first yield point and the point corresponding to failure are evaluated for each nonlinear skeleton curve.

The first yield point corresponds to the point on the moment-curvature relationship at which either the first steel fibre reaches the yield strain in tension or the extreme compression fibre attains a strain of 0.002, whichever occurs first. The latter condition only applies when the column axial load is high, typically for values of $\nu_k \geq 0.35$. [Priestley *et al.*, 1996a].

The failure point is obtained when one of the conditions given in Section 4.8 is reached. The line that joins the origin and the first yield point gives the initial slope of the bilinear curve; the line that extends through the failure point and balances the areas between the actual and the idealized moment-curvature relationships beyond the first yield point gives the slope of the second branch (see Figure 24).

It is worth noting that sections with different detailing, and hence with different reinforcement ratios ρ_w (see Figure 23), may lead to the same value of the confinement parameter λ_c. Since the ultimate compressive strain $\varepsilon_{cu,c}$ depends on the amount of ρ_w (see Equation (3.28)), for the same value of λ_c, different values of $\varepsilon_{cu,c}$ are obtained. However, in the parametric analysis, the skeleton nonlinear curves are derived, among other parameters, as a function of λ_c, with ρ_w only determining the level at which the maximum curvature is attained. As a result, during the bilinearization procedure previously described, for the same skeleton curve (i.e., same λ_c), different bilinear diagrams are obtained for different levels of the ultimate curvature (i.e., different values of ρ_w).Some examples of bilinear curves obtained by the parametric analysis are shown in Figure 25 and Figure 26.

5. RESULTS ON EQUIVALENT SECTION PROPERTIES: MOMENT-CURVATURE AND ENERGY DISSIPATION

With the purpose of serving as a tool for the analysis and design of rectangular hollow bridge pier sections, the results of the parametric analysis are represented in terms of dimensionless parameters.

Concerning the bilinear skeleton curves, the following parameters have been chosen (see Figure 24):

(dimensionless curvature) $\chi \cdot H$ (4.1)

(curvature ductility) $\mu = \chi_u / \chi_y$ (4.2)

(dimensionless yield moment) $\dfrac{M_y}{f'_{cm} \cdot B \cdot H^2}$ (4.3)

(post yielding stiffness ratio) $\alpha = \dfrac{\left(M_u - M_y\right)}{\left(\chi_u - \chi_y\right)} \Big/ \dfrac{M_y}{\chi_y}$ (4.4)

where B and H are the section width and depth, respectively, and f'_{cm} is the mean value of the concrete compressive strength. The results of the parametric analysis, for class C25 concrete and normalized axial load ranging between 0.10 and 0.40, are shown from Figure 27 to Figure 55.

The hysteretic energy dissipated by the section in a cycle is represented in a dimensionless form by the following parameters:

$$\eta = \frac{W}{2 \cdot \pi \cdot M_{\max} \cdot \chi_{\max}} \tag{4.5}$$

where W is the energy dissipated in one cycle, $M_{\max}$ and $\chi_{\max}$ are the maximum moment and curvature cyclic amplitude, respectively. The obtained results are shown in Figure 56. It can be observed that η does not depend on the section aspect ratio, while it depends strongly on the normalized axial force, although this dependence becomes less important when the longitudinal reinforcement ratio increases.

6. FROM SECTION TO MEMBER PROPERTIES

The charts that represent the results of the parametric analysis of reinforced concrete hollow sections were derived with the purpose of serving as a tool for the performance based assessment/analysis of bridges, which need the evaluation of two main parameters: equivalent stiffness and equivalent damping, both evaluated for a cantilevered pier in terms of top displacement and shear force; this section explains how to derive these properties from the properties of the section at the base of the pier.

The equivalent stiffness of the pier is defined as the secant stiffness K and is computed in terms of the secant-to-yield stiffness K_y and the ductility of the pier μ_d corresponding to the evaluation of K. Considering that the force-displacement envelope of the pier is bilinear with a post-yield stiffness ratio a_d, the secant stiffness of the pier is expressed as:

$$\begin{cases} K = K_y & \text{when } \mu_d \le 1 \\ K = \dfrac{1+\alpha_d\left(\mu_d - 1\right)}{\mu_d} K_y & \text{when } \mu_d > 1 \end{cases} \tag{5.1}$$

The secant-to-yield stiffness K_y of the pier is computed in terms of the yield moment M_y and the yield curvature χ_y of the section, such that for a pier of length L with an inverted triangular bending moment distribution the following expression is obtained:

$$K_y = \frac{3 \cdot M_y}{\chi_y \cdot L^3} \tag{5.2}$$

The ductility μ_d may be expressed as a function of the plastic and yield displacements Δ_p and Δ_y, respectively, at the top of the pier:

$$\mu_d = 1 + \frac{\Delta_p}{\Delta_y} \tag{5.3}$$

Where the yield and plastic displacements are equal to:

$$\Delta_y = \frac{\chi_y L^2}{3} \tag{5.4}$$

$$\Delta_p = \left[\frac{M_u}{M_y} - 1\right]\Delta_y + L_p\left(\chi_u - \chi_y\right)\left(L - 0.5L_p\right) \tag{5.5}$$

By substituting Equations (5.4) and. (5.5) into Equation (5.3), and by relating M_u to M_y through the post yield stiffness ratio α and curvature ductility μ of the section, μ_d is expressed as follows, for a pier height L and plastic hinge length L_p:

$$\mu_d = 1 + (\mu - 1)\left[\alpha + \frac{3L_p}{L}\left(1 - 0.5\frac{L_p}{L}\right)\right] \tag{5.6}$$

The plastic hinge length is computed from [Priestley et al., 1996b]:

$$L_p = 0.08 \cdot L + 0.022 \cdot d_{bL} \cdot f_y \qquad \text{(MPa)} \tag{5.7}$$

where d_{bl} and f_y are the diameter and yield stress of the longitudinal steel reinforcement, respectively.

The post yield stiffness ratio α_d of the pier is computed in terms of the plastic hinge length L_p and the post yield stiffness ratio α of the section, such that for a pier length L the following expression is obtained:

$$\alpha_d = \frac{1}{1 + \frac{3L_p}{\alpha L}\left(1 - 0.5\frac{L_p}{L}\right)} \tag{5.8}$$

Equation (5.8) shows that α_d is larger than α, as the post yield stiffness of the pier takes into account the stiffness contribution of the elastic portion of the pier. The value of α_d is practically independent of the length of the pier, as L_p is nearly proportional to L, especially for large values of L (see Equation (5.7)).

Experimental tests performed on bridge piers with varying span ratios [Pinto *et al.*, 1995 and 1996] using Tempcore steel have shown that for pier ductilities larger than one, the ratio of secant stiffness K with respect to the secant to yield stiffness K_y of the pier can be approximated by using Equation (5.1) with α_d equal to zero, such that the following simplified expression may be used:

$$\begin{cases} K = K_y & \text{when } \mu_d \le 1 \\ K = \dfrac{1}{\mu_d} & \text{when } \mu_d > 1 \end{cases} \tag{5.9}$$

The results of the tests performed by [*Pinto et al.,* 1995 and 1996] are presented in graphical form in Figure 57, showing good agreement with Equation (5.9).

The equivalent damping ratio of the pier ξ is calculated from the total dissipated energy W_d and the total energy E_d stored by the pier at a ductility μ_d:

$$\xi = \frac{W_d}{2\pi E_d} \tag{5.10}$$

where

$$E_d = \frac{\chi_y L}{3} \mu_d M_y \left[1 + \alpha\left(\mu - 1\right)\right] \tag{5.11}$$

Considering that the portion of the pier that remains elastic does not dissipate energy, W_d can be approximated by:

$$W_d = W \cdot L_p \tag{5.12}$$

where W is the energy dissipated by the section and is expressed as a function of the dimensionless hysteretic energy η and the energy E stored by the section:

$$W = 2\pi \eta E \tag{5.13}$$

where

$$E = \chi_y \mu M_y \left[1 + \alpha\left(\mu - 1\right)\right] \tag{5.14}$$

By substituting Equation (5.11) through (5.14) into (5.10), it is possible to express ξ as follows:

$$\xi = 3\eta \frac{\mu}{\mu_d} \frac{L_p}{L} \tag{5.15}$$

Summarising, the expressions proposed in the present section allow constructing the force displacement envelope (K_y, Δ_y, α_d and μ_d) and the equivalent viscous damping ratio ξ of a pier of length L, as a function of the properties M_y, χ_y, α and η of the section for a given ductility μ at the base of the pier.

PART B – SHEAR EFFECTS ON BRIDGE PIERS

7. SHEAR TESTS ON HOLLOW COLUMNS

The correct evaluation of the seismic performance of reinforced concrete hollow piers is a fundamental step for the reliable assessment of the seismic performance of large bridges in seismic prone areas. It is well known that compared to steel, the inelastic response of reinforced concrete members to cyclic loading is in general more difficult to evaluate. This is due to many factors: cracking, crushing and shrinking of concrete; yielding, strain hardening, buckling and rupture of the steel reinforcement; bond-slip of the longitudinal reinforcement and the degree of confinement of concrete offered by the transverse steel reinforcement. The influence of these factors on the behaviour of reinforced sections has been modelled with more or less success for the case of axial and flexural forces, however, the behaviour in shear, especially for the case of short hollow column sections, is yet not well understood.

In this part of the document, the results of experimental tests conducted by several research groups on hollow piers are first reported. Then, the different approaches to the problem of modelling shear effects in the design and assessment of bridge columns are presented. These approaches range from the original truss model proposed by Ritter (1899) and Mörsch (1909) to the very recent Modified Compression Field Theory (CFT) proposed by Vecchio & Collins (1986). Finally, some short considerations are made about the shear effects in the case of hollow reinforced concrete piers.

Mander [1984] carried out experimental tests on small models of hollow reinforced concrete bridge piers with the purpose of assessing their seismic performance and checking the applicability of the New Zealand Concrete Design Code [1982] for the detailing of plastic hinge regions. The main conclusions of Mander were that the seismic performance of hollow reinforced concrete piers is dominated by the behaviour of the flanges, therefore, good performances in terms of strength and energy dissipation characteristics are attained by designing the flanges as solid column members.

Pinto *et al.* [1995] reported on the experimental results obtained from the testing of a squat hollow bridge pier scaled model (1:2.5) designed according to ENV 1998-2 [CEN, 1993] and subjected to a step-wise increasing displacement history. In spite of the low shear span ratio (1.75), the pier attained a displacement ductility of six while maintaining its load carrying capacity. It was observed that the shear deformations contributed to one third of the total displacements at the top of the pier, while the energy dissipated in shear represented 10% of the total energy dissipation. During the experimental tests the warping of one section of the pier was measured, showing that up to a ductility of three the deformed section assumes the well-known S-shape profile, while for higher levels of ductility this profile is modified by the severe amount of shear cracking that takes place along the pier.

Another series of tests carried out by Pinto *et al.* [1996] on similar piers as those tested in [1995], but with higher span ratios of 3.5 and 5.25, showed that even though the failure mechanism was determined by flexure, shear deformations play a role in contributing to the total deformations of the pier, but to a more limited extent than for the squat pier. Likewise, the maximum ductility attained for these piers was on the order of six, similar to the maximum ductility observed for the pier with the lower span ratio of 1.75.

Inoue and Egawa [1996] investigated and compared the flexural and shear behaviour of a set of solid and hollow reinforced concrete beams subjected to cyclic deflections. It was observed that for the hollow beams, diagonal cracks are generated at an early stage of loading, leading to a considerable increase in the strain of the stirrups, thus increasing the contribution of shear to the total displacement of the beam. It was observed that shear deformations contributed up to 50% of the ultimate deflection of the hollow beam. For the solid beams, diagonal cracks appeared at the onset of yielding of the longitudinal reinforcement, while the contribution of shear deformations to the total deflection of the beam was rather limited, even when reaching the ultimate deflection. Furthermore, Inoue and Egawa [1996] found that the strains of stirrups and the principal strain in concrete could be well evaluated using the CFT.

Takahashi and Iemura [2000] investigated the seismic performance of hollow reinforced concrete piers using both static cyclic tests and pseudo dynamic tests on small scale models. The results of the static cyclic tests showed that the flexural cracks in the flange change drastically into diagonal cracks when these progress into the web. These diagonal cracks intersecting each other generate vertical cracks at the centre of the web, inducing large strains in stirrups. On the base of these observations, Takahashi and Iemura [2000] concluded that the influence of shear cannot be neglected and a rational shear design method, which is able to account for the effects of the deterioration of concrete resistance due to cyclic loading, should be established. Comparing the results of cyclic loading and pseudo dynamic tests, different crack patterns were observed: in the latter it was found that the flexural cracks did not turn into shear cracks, even when progressing into the web. Takahashi & Iemura suggested that this difference can be explained considering the non-symmetric damage distribution induced in the pier by the considered earthquake; concluding that the loading history may strongly influence the performance of the pier.

Yeh *et al.* [2002] performed pseudo-dynamic and cyclic tests on two prototypes and four models of hollow bridge piers subjected to constant levels of axial load. The tested piers were found to have acceptable seismic performance, reaching flexural failure with ductility factors for the model and prototype of 5.26 and 11.1, respectively. An important result from the test was that the prototypes showed higher ductilities than the models, and that the ductility capacity of the sections is reduced as the level of axial load increases.

8. RITTER – MÖRSCH TRUSS MODEL

Current design procedures for reinforced concrete members in shear stem from the original truss model proposed by Ritter [1899] and Mörsch [1909]. In this model it is assumed that a cracked reinforced concrete beam acts like a truss with parallel longitudinal chords and a web composed of steel ties and diagonal concrete struts inclined 45° with respect to the longitudinal axis (Figure 58); the tensile stresses in the diagonally cracked concrete are neglected. According to this model, when transverse loads act on a reinforced concrete member, the diagonal compressive concrete stresses push apart the loaded faces, while the tensile stresses in the stirrups pull them together.

Shear failure of reinforced concrete members can be classified as either diagonal tension failure or diagonal compression failure. The former occurs after the formation of cracks inclined with respect to the member axis. As loading continues, crack opening may disrupt the load carrying mechanism, thus leading to failure. The latter may occur either before or after the formation of inclined cracks and results in crushing of the concrete along a diagonal compression strut. Diagonal compression failure may occur when either the column axial force or the transverse reinforcement ratio, or both, are relatively high, or alternatively, if the aspect ratio[1] is relatively low. However, for the case of elements with an aspect ratio greater than 2 with axial load near or below the balanced point, diagonal tension failure seems to be the controlling mechanism. In this case the shear resistance is given by:

$$V = \frac{A_v \cdot d_v \cdot f_{ry}}{s} \tag{7.1}$$

where A_v is the area of shear reinforcement within a distance equal to the stirrup spacing s, d_v is the effective shear depth taken as the flexural lever arm of the member and f_{ry} is the yield stress of the shear reinforcement.

For rectangular columns, the appropriate definition of A_v may be illustrated through the example reported in Figure 59, taken from Priestley *et al.* [1996]. In this example a column reinforced with 12 longitudinal bars and two possible arrangements of transverse reinforcement is considered. Both arrangements include a peripheral hoop: in one alternative the eight internal longitudinal bars are confined by an octagonal hoop, whereas in other alternative the bars are confined by two independent rectangular hoops, shown as dashed lines in Figure 59.

Considering a flexure-shear crack inclined at $\theta = 45°$ to the column axis, as shown in Figure 59, the resisting force crossing the crack depends on whether the crack crosses the hoop layer in the outer regions, indicated by lines 1-1, or in the centre region, indicated by line 2-2. The peripheral hoop contributes fully at all sections, but in the outer sections the yield force in the octagonal hoop is at 45° with respect to the direction of the applied shear force and must be resolved back to the line of action on V_s. Considering the case where the section is reinforced by the peripheral and octagonal hoops, the resisting force F parallel to the applied shear force is:

Octagonal case, section 1-1:

$$F = \left(2 + \frac{2}{\sqrt{2}}\right) \cdot A_h \cdot f_{ry} = 3.41 \cdot A_h \cdot f_{ry} \tag{7.2}$$

Octagonal case, section 2-2:

$$F = (2 + 2) \cdot A_h \cdot f_y = 4.00 \cdot A_h \cdot f_{ry} \tag{7.3}$$

where A_h is the area of one leg of the hoops.

Similarly, for the case with peripheral hoop and overlapping internal hoops, four hoop legs are crossed by the crack at section 1-1 and six legs are crossed at section 2-2. Hence:

Rectangular case, section 1-1:

$$F = 4 \cdot A_h \cdot f_{ry} \tag{7.4}$$

---

[1] The aspect ratio of an element is defined as the ratio between the shear span and the width of the element cross section.

Rectangular case, section 2-2:

$$F = 6 \cdot A_h \cdot f_{ry} \tag{7.5}$$

Since an inclined crack will cross approximately twice as many hoop sets in the outer (1-1) than in the inner (2-2) section, the average effective area of transverse reinforcement for the two cases is:

Octagonal case:

$$A_v = \left(\frac{2 \cdot 3.41 + 1 \cdot 4}{3} \right) \cdot A_h = 3.61 \cdot A_h \tag{7.6}$$

Rectangular case:

$$A_v = \left(\frac{2 \cdot 4 + 1 \cdot 6}{3} \right) \cdot A_h = 4.67 \cdot A_h \tag{7.7}$$

It can readily be shown that the efficiency of the two alternatives (shear strength divided by volume of steel) is the same. The octagonal case will generally be preferable because of the reduced steel congestion in the core.

In applying Equation (7.1) to circular sections reinforced with spirals or circular hoops, codes have generally recommended taking $A_v = 2 \cdot A_h$ and $d = 0.8 \cdot D$. However, it is clear from the discussion above, that resolving hoop forces parallel to the applied shear force is inappropriate. In Figure 59, the component F of the hoop force exposed by a diagonal flexure-shear crack and parallel to the applied shear force is:

$$F = A_h \cdot f_{ry} \cdot \cos\alpha \tag{7.8}$$

where α is the angle between the tangent to the spiral and the direction of the shear force, and varies from 0° to 90° as the distance x perpendicular to the column axis varies from 0 to 0.5 of diameter D' of the spiral or hoop. It can readily be shown that the total shear resistance, assuming a 45° crack inclination, is:

$$V = \frac{\pi}{2} \cdot \frac{A_h \cdot f_{ry} \cdot D'}{s} \tag{7.9}$$

Although this assumes that the crack traverses the full diameter of the section, the error resulting from a compression zone extending into the core is negligible, since the contribution of the hoop force to resist shear in the regions where x is maximum is negligible.

Experimental tests have revealed that the results given by the model proposed by Ritter and Mörsch are generally quite conservative. In fact, it neglects important sources of shear resistance as aggregate interlock, dowel action of the longitudinal steel and shear carried across the uncracked concrete. It is also evident that this model does not account for the effects of axial force on shear resistance.

9. TRUSS MODELS

Considering that the results obtained with the Ritter – Mörsch truss model underestimate the actual shear strength of reinforced concrete members, most construction standard and norms (*e.g.* ACI 318–2002, CSA - Canadian Standard Association 1994) have accepted to add an empirical correction term to the original truss equations. This term, known as the "concrete contribution", and generally denoted as V_c, is meant to represent those sources of shear resistance that the basic truss model is not able to capture. With this assumption, the nominal shear resistance can be expressed as:

$$V = V_s + V_c \tag{8.1}$$

where V_s represents the transverse reinforcement contribution to shear resistance. This contribution is equal to Equation (7.1) in which f_{ty} has been replaced by the tensile stress f_v of the stirrups. The concrete contribution is taken as the shear force corresponding to the initiation of diagonal cracking, which has been assessed empirically from experimental data and may be expressed from the following expressions as found in the ACI and CSA construction codes:

$$\text{ACI 318 - 2002} \quad V_c = 0.166 \cdot \left(1 + \frac{P}{13.8 \cdot A_g}\right) \cdot \sqrt{f_c'} \cdot b \cdot d_v \quad \text{(MPa)} \tag{8.2}$$

$$\text{CSA 1994} \quad V_c = 0.20 \cdot \sqrt{f_c'} \cdot b \cdot d_v \quad \text{(MPa)} \tag{8.3}$$

where f'_c is the compressive strength of concrete, b is the width of the member, d_v is the effective depth of the member, A_g is the gross area of the member section, and P is the axial load (positive if compressive).

When comparing Equation (8.2) and Equation (8.3), it is possible to observe that only the first equation takes into account the effect of axial force on shear resistance: axial compressive loads increase the shear load at which flexural and inclined cracking occurs. The dependency of V_c on the axial load may be thought as a way to account for the effects of axial loads on the shear mechanisms neglected in the Ritter - Mörsch truss model, *i.e.*, axial compression forces generate a larger compression zone characterized by a greater shear strength; on the contrary, axial tensile forces reduce the depth of the compression zone and may lead to premature yielding of the longitudinal reinforcement, which in turn rapidly destroys the aggregate interlock mechanism. It is worth noting that some codes (*e.g.* ACI 318-89) consider the beneficial effect of axial loads on shear resistance only for the case of axial forces coming from external sources, such as gravity loads, while for axial forces generated from self-equilibrated systems, no beneficial effects are considered.

Acknowledging the conservative results given by the Ritter – Mörsch truss model, the European Code prEN 1992-1 [CEN, 2003] does not use the corrective term V_c, instead adopts a method known as the "variable – angle truss method" [2], which is based on a truss model in which the

[2] A combination of the variable-angle truss and a concrete contribution has also been proposed. This procedure has been referred to as the modified truss model approach [CEB, 1978; Ramirez and Breen, 1991]

concrete struts can form with the member axis an angle θ that can vary up to a value of 45°. The method recognises that due to shear mechanisms different from those considered by the Ritter–Mörsch truss model, the compressive stresses in the member web may have an inclination lower than 45°. According to this model the shear resistance of a member may be reached either for yielding of the stirrups:

$$V = \frac{A_v}{s} \cdot d_v \cdot f_{vy} \cdot \cot\theta \tag{8.4}$$

or for crushing of the concrete web struts:

$$V = b \cdot d_v \cdot \nu \cdot f_c' / \left(\cot\theta + \tan\theta\right) \tag{8.5}$$

where ν is the strength reduction factor for concrete cracked in shear and is computed as a function of the compressive stress f'_c derived from cylinder tests:

$$\nu = 0.6 \cdot \left(1 - \frac{f_c'}{250}\right) \quad (f'_c \text{ in MPa}) \tag{8.6}$$

Equation (8.6) accounts for the lower compression resistance of the concrete forming the struts with respect to the compression resistance derived from standard cylinder tests. This reduction in resistance is due to the high tensile strains that exist in the struts normal to the direction of the struts and to the effects of the stirrups crossing the struts.

For a given amount of transverse reinforcement the maximum shear resistance is attained when the yielding of the shear reinforcement and the crushing of the web concrete struts are reached simultaneously. This assumption leads to the following condition for angle θ:

$$\cot\theta = \sqrt{\frac{1-\omega_v}{\omega_v}} \tag{8.7}$$

With the mechanical percentage of web reinforcement ω_v equal to:

$$\omega_v = \frac{A_v \cdot f_{vy}}{s \cdot b \cdot \nu \cdot f_c'} \tag{8.8}$$

Considering the values of θ given by Equation (8.7), the shear strength may be expressed as a function of the amount of shear reinforcement, and may be plotted in a dimensionless format as shown in Fig. 2.1, indicating that larger shear capacities are obtained with respect to the Ritter – Mörsch truss model, which assumes a strut inclination of θ equal to 45°.

The norm prEN 1992-1 [CEN, 2003] suggests to use as shear resistance of a member the lowest value resulting from Equations (8.4) and (8.5) for a given amount of shear reinforcement and for a given value of θ. For members subjected to axial compressive forces, the same code suggests to multiply the value given by Equation (8.5) by a factor α_c ranging between 0 and 1.25 (see Fig. 2.2), which depends on the mean compressive stress σ_p acting on the section of the member. prEN 1992-1 [CEN, 2003] does not consider any distinction between the loads inducing the compressive stresses, which may be either external (i.e., gravity loads) or due to prestressing or postensioning. It should be noted that prEN 1992-1 [CEN, 2003] does not give any indication on the effects on shear resistance associated to loads inducing tensile stresses on the section.

Both of the approaches presented in the previous paragraphs (*e.g.*, concrete contribution method as given by Equation (8.1) and the variable angle truss model) are insensitive to the magnitude and consequences of the member deformations. Mechanisms such as tension stiffening,

aggregate interlock and dowel action, all fail as the deformation of the section increases or after several cycles of load reversal. It is evident that this model deficiency becomes crucial when the seismic response of a reinforced concrete member has to be evaluated.

In view of the difficulty of modelling the concrete behaviour, a number of codes reduce or even neglect the concrete contribution term. For example, in the case of bridges subjected to seismic actions, prEN1998-2 [CEN, 2003] suggests to assume a value of θ equal to 45° when designing plastic hinge regions for shear, *i.e.*, the Ritter - Mörsch truss model should be adopted with no concrete contribution. In other codes, the concrete contribution reduction depends on the value of the compressive stress: if it is less than a small fraction of f'_c, the concrete contribution is set equal to zero, otherwise it is taken as a fraction of its value corresponding to the static case, as given for example by Equations (8.2) and (8.3). Unfortunately, experiments have shown that the resulting estimate of the nominal shear strength is over-conservative at low values of displacement ductility demand and under-conservative at higher values of displacement ductility.

The dependence of shear strength on deformation demand has been acknowledged as early as 1975 in a comprehensive study of reinforced concrete columns subjected to large transverse displacements reversal [Wight and Sozen, 1975][3]. In 1983, the Applied Technology Council [ATC, 1983] published guidelines for seismic retrofit of bridges in which a conceptual model was proposed to model the relationship between shear demand and supply at different ductility levels (see Figure 62). This model has inspired some of the contemporary approaches that have been proposed in order to modify the concrete contribution term in the design code guidelines. In general, the contribution of concrete V_c is assumed to be independent on the level of deformation at low displacement ductility values.

Most of the proposed models suggest a constant initial value for V_c up to a displacement ductility of 1 [Wong *et al.*, 1993; Lehman *et al.*, 1996] or 2 [Ang *et al.*, 1989; Priestley *et al.*, 1994]. At larger displacement ductilities (usually in excess of 4), V_c is assigned a fixed residual value, with the exception of the expression reported in Lehman *et al.* [1996], where V_c is set to zero for displacement ductility values greater than 4. The shear contribution of concrete is assumed to decay linearly for displacement ductilities that fall between these two limits.

In some experimental studies [Ang *et al.*, 1989, Aschheim and Moehle, 1992; Wong *et al.*, 1993], it has been observed that the concrete contribution is enhanced by an increase in the amount of shear reinforcement. This behaviour is represented by the models proposed by Ang *et al.* [1989] and Aschheim and Moehle [1992]: in the former, the residual shear stress is proportional to the amount of transverse reinforcement, while in the latter, the concrete shear contribution increases with the amount of transverse reinforcement. In the experimental studies by Ang *et al.* [1989] and Wong *et al.* [1993] it was also observed that when the flexural ductility increases to values above two (>2), the inclination of the diagonal compression struts of the truss mechanism with respect to the longitudinal axis decreases (< 45°), thus increasing the shear carried by the transverse reinforcement and hence that of the overall truss.

Hereafter, two models, developed by Priestley *et al.* [1994] and Sezen and Moehle [2004], are presented in more detail.

---

[3] It should be noticed that some researchers (*e.g.* Konwinsky *et al.* 1995) have found that column shear strength was independent on displacement ductility demand.

9.1 PRIESTLEY *ET AL.* [1994]

According to this model, the shear strength of columns subjected to cyclic lateral loads results from the summation of three contributions: concrete, V_c; a truss mechanism, V_s; and an arch mechanism, V_p:

$$V_n = V_c + V_s + V_p \tag{8.9}$$

The concrete component is given by:

$$V_c = k \cdot \sqrt{f'_c} \cdot \left(0.8 \cdot A_g\right) \qquad \text{(psi)} \tag{8.10}$$

in which the parameter k, within plastic end regions, depends on the member displacement ductility demand as defined in Figure 63, where the concrete contribution is reduced to one-third of its initial value for large ductility demands. For columns subjected to ductile demands in the two orthogonal directions, the reduction factor k assumes even lower values than for the uniaxial ductility demand. For regions of columns outside the plastic end regions, the concrete component is computed with the value of k corresponding to a ductility demand of one.

The contribution of transverse reinforcement to shear strength is based on a truss mechanism using an angle θ equal to 30° between the diagonal compression struts and the column longitudinal axis. For rectangular columns this contribution is given by:

$$V_s = \frac{A_v \cdot f_{ty} \cdot D'}{s} \cdot \sqrt{3} \tag{8.11}$$

and for circular columns by:

$$V_s = \frac{\pi}{2} \cdot \frac{A_h \cdot f_{ty} \cdot D'}{s} \cdot \sqrt{3} \tag{8.12}$$

where A_h is the area of one hoop leg; f_{ty} is the yield strength of transverse reinforcement; s is the spacing of the layers of stirrups or hoops along the member axis; A_v is the total area of transverse reinforcement in a layer in the direction of the shear force; D' is the core dimension, from centre to centre of the peripheral hoop.

The shear strength enhancement resulting from axial compression is considered as an independent component of shear strength, resulting from a diagonal compression strut, as shown in Figure 64, given by:

$$V_p = P \cdot \tan\alpha \tag{8.13}$$

For a cantilever column, α is the angle formed between the column axis and the strut from the point of load application to the centre of the flexural compression zone at the column plastic hinge critical section. For a column in reverse or double bending, α is the angle between the column axis and the line joining the centres of flexural compression at the top and bottom of the column. The justification for the foregoing approach is that since the axial load must be transmitted through the flexural compression zone, an angle is formed between the column axis and the compression strut, thus creating a horizontal component of force that opposes the external action of the shear force.

9.2 SEZEN AND MOEHLE [2004]

More recently, Sezen and Moehle [2004] have proposed a shear strength model for lightly reinforced concrete columns (*e.g.*, characterized by a diagonal tension failure). In this model, the concrete contribution is estimated using the following considerations: it is assumed that the onset of diagonal tension cracking in an element under a uniform stress state can be related to the nominal principal tension stress acting on the element. Assuming a plain stress condition within the *x*-*y* plane, the principal tension stress σ_1 is defined as:

$$\sigma_1 = \frac{\sigma_x + \sigma_y}{2} + \sqrt{\left(\frac{\sigma_x - \sigma_y}{2}\right)^2 + \tau^2} \qquad (8.14)$$

where σ_x, σ_y are the normal tension stresses in the x and y directions, respectively, and τ represents the shear stresses acting on the faces normal to the x and y directions. In reinforced concrete columns the normal stress σ_y in the direction of the shear force is equal to zero, based on the assumption that the confinement effect of poorly detailed transverse reinforcement is very small. σ_x. The normal stress σ_x, parallel to the direction of the column longitudinal axis, is defined as P/A_g. Assuming that tensile cracking occurs when σ_1 reaches the nominal tensile strength f_{ct} = $0.5\cdot(f'_c)^{0.5}$ (in MPa), Equation (8.14) can be solved to find the shear stress at the onset of diagonal tension cracking:

$$\tau = 0.5 \cdot \sqrt{f'_c} \cdot \sqrt{1 - \frac{P}{0.5 \cdot \sqrt{f'_c} \cdot A_g}} \quad \text{(MPa)} \qquad (8.15)$$

According to Equation (8.15) the shear stress corresponding to the onset of diagonal tension cracking will increase as the axial load level increases.

The stress state in a reinforced concrete column subjected to axial and lateral loading is further complicated by the non-homogeneous nature of reinforced concrete, and by the presence of bond and flexural cracks. As a result Equation (8.15) does not provide a direct measure of the onset of inclined cracking, as it overestimates the inclined cracking load. This is especially true for columns with larger ratios between shear span (distance from the maximum moment section to the point of inflection) and the effective section depth.

Using an effective concrete area of $0.8\cdot A_g$ and the shear stress τ at the onset of cracking from Equation (8.15) the concrete contribution to shear strength may be expressed as:

$$V_c = \frac{\tau}{a/d} \cdot 0.8 \cdot A_g \quad \text{(MPa)} \qquad (8.16)$$

where $2 \leq a / d \leq 4$.

Considering that experimental results have shown that shear strength decreases with the increase of the displacement ductility demand, Sezen and Mohele [2004] suggested to introduce a ductility-related k factor similar to the one introduced by Priestley *et al.* [1994]. It should be noted that Priestley *et al.* [1994] applied the factor k only to the concrete contribution, based on the fact that crack opening leads only to degradation of the load-carrying capacity of concrete, with no associated degradation of the reinforcement. However, the damage of concrete leads to a loss of anchorage of the transverse reinforcement as well as to a reduction in the bond capacity of the longitudinal and transverse reinforcement, thus reducing the strength of the truss mechanisms. Based on these considerations, Sezen and Mohele [2004] decided to apply the k factor to both the concrete and truss contributions. Considering that the truss contribution V_s to shear strength

is given by Equation (7.1), the proposed model to compute shear strength is expressed by the following equation:

$$V = V_s + V_c = k \cdot \frac{A_v \cdot f_{vy} \cdot d}{s} + k \cdot \frac{\tau}{a/d} \cdot 0.8 \cdot A_g \quad \text{(MPa)} \tag{8.17}$$

The k factor is defined equal to 1.0 for displacement ductilities less than 2 and equal to 0.7 for displacement ductilities exceeding 6, varying linearly for intermediate displacement ductilities.

9.3 STRUT-AND-TIE MODEL

The strut and tie model is strictly an equilibrium model and is based on the lower theorem of the plasticity theory. The "strut and tie" term is generally reserved for disturbed or D-regions and the term "truss" is used for beam or B-regions. In B-regions, plane sections remain plane and a uniform compression fields developed. In D-regions, arch action, as opposed to beam action, is exhibited. D-regions extend about one member depth at both ends from the concentrated loads, reactions, or abrupt changes in the section or direction of the member. The regions between the D-regions are treated as B-regions. As the slenderness of the reinforced concrete member increases, the behaviour shifts from a D-region to a B-region dominant behaviour.

Concerning shear, the difference in behaviour of the two regions can be expressed as follows [MacGregor, 1992]:

$$V = \frac{\mathrm{d}M}{\mathrm{d}x} = \frac{\mathrm{d}\left(T \cdot d_v\right)}{\mathrm{d}x} = \frac{\mathrm{d}T}{\mathrm{d}x} \cdot d_v + T \cdot \frac{\mathrm{d}d_v}{\mathrm{d}x} \tag{8.18}$$

where M and T represent the bending moment and the shear force demand and x is the distance of the generic cross section from one member end.

In B-regions, the lever arm remains constant and the tension force adjusts to equilibrate the internal moment:

$$V = \frac{\mathrm{d}T}{\mathrm{d}x} \cdot d_v \tag{8.19}$$

The quantity $\mathrm{d}T/\mathrm{d}x$ is the shear flow (shear stress multiplied by the beam width) across any horizontal plane between the longitudinal reinforcement and the compression zone and is typical of beam behaviour.

In D-regions, the tension force remains constant and the lever arm adjusts to equilibrate the internal moment:

$$V = T \cdot \frac{\mathrm{d}d_v}{\mathrm{d}x} \tag{8.20}$$

The strut and tie, and the truss models, provide a consistent design approach for B- and D-regions. If the level of accuracy and simplicity used in the design of D-regions were considered satisfactory for B-regions, the "endless discussion on shear can be put to bed" [Schläich *et al.*, 1987]. Although the behaviour of short (or deep) members and slender members is different, the models are consistent, being important to account for arching action where it exists. As the shear span ratio of a member decreases, the role of the web reinforcement changes from that of carrying primarily direct tension to that of serving primarily as shear friction reinforcement, thus preventing sliding failure along the inclined crack.

Strut-and-tie models are discrete representations of statically equivalent distributed stress fields. Upon cracking of concrete, some stress redistribution occurs, which is limited by the plastic deformation capacity of the concrete. It is therefore important, in highly stressed regions, to orient the strut-and-tie model along the internal forces predicted by the theory of elasticity. In less stressed regions, significant deviations from the theory of elasticity can be accommodated without exceeding the ductility of the structure. Schläich *et al.* (1987) suggest two guidelines in selecting a workable strut-and-tie model:

- The compatibility of deformations may be approximately considered by orienting the struts and ties within 15° of the force systems obtained from a linear elastic analysis of uncracked members and connections.
- The most valid model tends to be one which minimizes the amount of reinforcement, since this corresponds to the minimum strain energy solution.

Marti (1985) recommends three rules when using strut-and-tie models:

- Draw truss models to scale.
- Visualize the force flow using consistent equilibrium considerations.
- Ensure that truss member forces can be developed and transferred at the required locations.

10. COMPRESSION FIELD THEORY (CFT)

Discussing the problem concerning the evaluation of the inclination angle θ of the compressive struts in the truss model, Mörsch [1922] stated, "it is absolutely impossible to mathematically determine the slope of the secondary inclined cracks according to which one can design the stirrups". Seven years after Mörsch's statement, another German engineer, Wagner [1929], solved an analogous problem while dealing with the post-buckling shear resistance of thin-webbed metal girders. Wagner assumed that after buckling, the thin metal skin continues to carry shear by transverse frames and longitudinal stringers. He assumed that the angle of inclination of the diagonal tensile stresses in the buckled thin metal skin would coincide with the angle of inclination of the principal tensile strain as determined from the deformations of the skin, of the transverse frame and of the longitudinal stringers. This approach became known as the tension field theory.

Shear design procedures for reinforced concrete that, in the same way as the tension field theory, determine the angle θ by considering the deformations of the transverse reinforcement, the longitudinal reinforcement, and the diagonally stressed concrete, have become known as compression field approaches. With these methods, equilibrium conditions, compatibility conditions and stress-strain relationships for both the reinforcement and the diagonally cracked concrete are used to predict the load-deformation response of a section subjected to shear.

To illustrate the Compression Field Theory (CFT) a membrane element representing a uniform thickness and relatively small portion of a reinforced concrete structure containing an orthogonal grid of reinforcement is used (see Figure 65). The considered x and y axes are chosen to coincide with the directions of longitudinal and transverse reinforcement, respectively. Loads acting on planes at the edges of the element are assumed to consist of uniform axial stresses f_x and f_y, and shear stress $v_{xy,}$ (see Figure 65a). Deformation of the element is assumed to occur such that the

edges remain straight and parallel (Figure 65b). The deformation state is defined by the two normal strains ε_x, ε_y, and by the shear strain γ_{xy}.

The problem at hand is to determine how the three in-plane stresses f_x, f_y and v_{xy} are related to the three in-plane strains ε_x, ε_y and γ_{xy}. To solve this problem, the following additional assumptions need to be made:

- For each strain state exists only one corresponding stress state. Situations in which the influence of loading history is significant are ignored.
- The considered strains are average values: they are measured over base lengths that are greater than the crack spacing. In a similar manner the stresses are also average values; *i.e.*, they are averaged over a length greater than the crack spacing.
- The concrete and the reinforcing bars are perfectly bonded together at the boundaries of the element.
- The longitudinal and transverse reinforcing bars are uniformly distributed over the element.

10.1 COMPATIBILITY CONDITIONS

Having assumed that the reinforcement is perfectly bonded to the surrounding concrete, compatibility requires that any deformation experienced by the concrete must be matched by an identical deformation of the reinforcement (see Figure 66a), *i.e.*, non-prestressed reinforcement has the same initial strain as the surrounding concrete. Hence:

$$\varepsilon_{sx} = \varepsilon_{cx} = \varepsilon_x \tag{9.1}$$

and

$$\varepsilon_{sy} = \varepsilon_{cy} = \varepsilon_y \tag{9.2}$$

If the three strain components ε_x, ε_y and γ_{xy} are known, the strain in any other direction can be easily determined by using the Mohr's circle (see Figure 66b). Useful relationships, which can be derived from its geometry, include:

$$\gamma_{xy} = \frac{2 \cdot (\varepsilon_x - \varepsilon_2)}{\tan\theta} \tag{9.3}$$

$$\varepsilon_x + \varepsilon_y = \varepsilon_1 + \varepsilon_2 \tag{9.4}$$

$$\tan^2\theta = \frac{\varepsilon_x - \varepsilon_2}{\varepsilon_y - \varepsilon_2} = \frac{\varepsilon_1 - \varepsilon_y}{\varepsilon_1 - \varepsilon_x} = \frac{\varepsilon_1 - \varepsilon_y}{\varepsilon_y - \varepsilon_2} = \frac{\varepsilon_x - \varepsilon_2}{\varepsilon_1 - \varepsilon_x} \tag{9.5}$$

where θ is the angle of inclination of the principal strains to the x-axis; ε_1 and ε_2 are respectively the principal tensile strain and the principal compressive strain.

10.2 EQUILIBRIUM CONDITIONS

The forces applied to the reinforced concrete element are resisted by the stresses in the concrete and in the reinforcement. For the free-body diagram shown in Figure 67a, the requirement that the forces add up to zero in the x-direction can be written as:

$$\int_A f_x \, dA = \int_{A_c} f_{cx} \, dA_c + \int_{A_s} f_{sx} \, dA_s \tag{9.6}$$

where A is the area of the element section normal to the x-axis; A_c and A_s are respectively the concrete area and the steel area of the section.

Ignoring the small reduction in concrete cross-sectional area due to the presence of reinforcement, Equation (9.6) becomes:

$$f_x = f_{cx} + \rho_{sx} \cdot f_{sx} \tag{9.7}$$

where ρ_{sx} denotes the reinforcement ratio in the x-direction.

In a similar way, the following equilibrium conditions can be derived:

$$f_y = f_{cy} + \rho_{sy} \cdot f_{sy} \tag{9.8}$$

$$v_{xy} = v_{cx} + \rho_{sx} \cdot v_{sx} \tag{9.9}$$

and

$$v_{xy} = v_{cy} + \rho_{sy} \cdot v_{sy} \tag{9.10}$$

Assuming that:

$$v_{cx} = v_{cy} = v_{cxy} \tag{9.11}$$

The stress conditions in the concrete are completely defined if f_{cx}, f_{cy} and v_{cxy} are known. A Mohr's circle for concrete stresses is drawn so that the following relationships can be deduced (see Figure 67b):

$$f_{cx} = f_{c1} - v_{cxy} / \tan\theta_c \tag{9.12}$$

$$f_{cy} = f_{c1} - v_{cxy} / \tan\theta_c \tag{9.13}$$

and

$$f_{c2} = f_{c1} - v_{cxy} \cdot \left(\tan\theta_c + 1/\tan\theta_c\right) \tag{9.14}$$

where f_{c1} and f_{c2} are respectively the principal tensile stress and principal compressive stress in concrete, and θ_c is the angle of inclination of the principal stresses along the concrete with respect to the x-axis.

10.3 STRESS-STRAIN RELATIONSHIP

Since the CFT was published, a large amount of experimental research aimed at determining the stress-strain characteristics of diagonally cracked concrete has been conducted. This work has typically involved testing of reinforced concrete elements subjected to uniform membrane stresses in special-purpose machines.

The results of these experimental studies have shown that it is reasonable to assume that the principal strain and principal stress axes coincide for concrete. In the case of reinforced concrete elements loaded in combined tension and shear, and containing reinforcement only in the direction of tension, the direction of the principal stresses in concrete can differ up to 20° from the direction of the principal strains [Bhide and Collins, 1989]. The predicted angle, based on the assumption that the direction of the principal stress coincides with the direction of the principal strain, lays about half-way between the observed strain and the stress directions. In case of reinforced concrete elements with both longitudinal and transverse reinforcement, the direction

of principal stresses in the concrete typically deviates less than 10° from the direction of the principal strains [Vecchio and Collins, 1986].

The same experimental results indicate that the concrete compressive stress f_{c2} is a function not only of compressive strain ε_2, but also of the co-existing principal tensile strain ε_1. Thus, cracked concrete subjected to high tensile strains in the direction normal to the compression strut is softer and weaker than concrete in a standard cylinder test. Vecchio and Collins [1986] suggested the following relationship:

$$f_{c2} = f_{c2\max} \cdot \left[2 \cdot \frac{\varepsilon_2}{\varepsilon'_c} - \left(\frac{\varepsilon_2}{\varepsilon'_c} \right)^2 \right] \tag{9.15}$$

where

$$\frac{f_{c2\max}}{f'_c} = \frac{1}{0.8 - 0.34 \cdot \varepsilon_1 / \varepsilon'_c} \leq 1.0 \tag{9.16}$$

Considering that ε'_c is usually set equal to -0.002, Equation (9.16) becomes (see Figure 68):

$$\frac{f_{c2\max}}{f'_c} = \frac{1}{0.8 + 170 \cdot \varepsilon_1} \leq 1.0 \tag{9.17}$$

Note that $f_{c2\max}/f'_c$ decreases with the increase of ε_1.

The CFT assumes that after cracking, no tensile stresses in the concrete can occur. However, tests on reinforced concrete elements have demonstrated that even after extensive cracking, tensile stresses still exist in the cracked concrete, and that these stresses significantly increase the ability of the cracked concrete to resist shear stresses. Vecchio and Collins [1986] proposed the modified compression field theory (MCFT), which is a further development of the CFT that accounts for the influence of the tensile stresses in the cracked concrete.

Based on Vecchio & Collins' [1986] tests on reinforced concrete panels, Collins & Mitchell [1991] proposed a relationship between the average principal tensile stress and the average tensile strain in concrete. The suggested relationship prior to cracking (*i.e.* $\varepsilon_1 < \varepsilon_{cr}$) is (see Figure 69):

$$f_{c1} = E_c \cdot \varepsilon_1 \tag{9.18}$$

where E_c is the modulus of elasticity of concrete, which is taken as $2f'_c/\varepsilon'_c$. The suggested relationship after cracking (*i.e.* $\varepsilon_1 > \varepsilon_{cr}$) is (see Figure 69):

$$f_{c1} = \frac{0.33 \cdot \sqrt{f'_c}}{1 + \sqrt{500 \cdot \varepsilon_1}} \quad \text{(MPa)} \tag{9.19}$$

Concerning reinforcement, the MCFT assumes that the axial stress depends only on axial strain, and that the average shear stress on the plane normal to the reinforcement is equal to zero. The axial stress is related to the axial strain through the bilinear uniaxial stress-strain relationship as follows:

$$f_{sx} = E_s \cdot \varepsilon_x \leq f_{yx} \tag{9.20}$$

$$f_{sy} = E_s \cdot \varepsilon_y \leq f_{yy} \tag{9.21}$$

$$v_{sx} = v_{sy} = 0 \tag{9.22}$$

where E_s is the modulus of elasticity of the reinforcement, and f_{xy} and f_{yy} are the yield stresses of the x and y-reinforcement, respectively.

The stress-strain formulations presented in the previous equations are related with average values and do not give any information regarding local variations. However, local variations are important, because failure may be governed by local stresses that occur at a crack, rather than by the size of the average stresses.

Figure 70 compares the calculated average stresses (a) with the actual local stresses that occur at a crack (b); the crack direction is assumed normal to the principal tensile strain direction. While on a plane parallel to the crack direction the calculated average shear stress is zero (*i.e.*, in terms of average stresses the plane parallel to the crack direction is a principal plane), there may be local non-zero shear stresses v_{ci} at the crack.

As the applied external forces f_x, f_y and v_{xy} are fixed, the two sets of stresses shown in Figure 70 have to be statically equivalent. Assuming that in both cases the considered inclined plane has a unit area, the equivalence in x-direction requires that:

$$\rho_{sx} \cdot \left(f_{sxcr} - f_{sx} \right) = f_{c1} + \frac{v_{ci}}{\tan\theta} \tag{9.23}$$

and in the y-direction:

$$\rho_{sy} \cdot \left(f_{sycr} - f_{sy} \right) = f_{c1} - \frac{v_{ci}}{\tan\theta} \tag{9.24}$$

Equations (9.23) and (9.24) can only be satisfied for the non shear stress condition on the crack if:

$$\rho_{sx} \cdot \left(f_{sxcr} - f_{sx} \right) = \rho_{sy} \cdot \left(f_{sycr} - f_{sy} \right) = f_{c1} \tag{9.25}$$

considering that the stress in the reinforcement at a crack cannot exceed the yield strength:

$$f_{sxcr} \leq f_{yx} \tag{9.26}$$

and

$$f_{sycr} \leq f_{yy} \tag{9.27}$$

Hence, if the calculated average stress in either of the x or y reinforcement is high, it may not be possible to satisfy Equation (9.25). In this case, the condition of equilibrium requires the existence of shear stresses on the crack.

For normal concrete, cracking occurs along the interface between the cement paste and the aggregate particles[4], so that the resulting rough cracked surface can transfer shear by aggregate interlocking. The maximum possible value of v_{ci} is taken by Bhide and Collins [1989] to be related to the crack width w and the maximum aggregate size a by the following relationship:

---

[4] This is not the case for high-strength concrete, *i.e.*, concrete characterized by a compressive strength greater than 50 MPa. The shear failure surface in high-strength concrete members is smoother than in normal-strength concrete members, with cracks propagating through coarse aggregate particles rather than around them.

$$v_{ci\max} = \frac{0.18 \cdot \sqrt{f'_c}}{0.3 + (24 \cdot w)/(a + 16)} \quad \text{(MPa, mm)} \tag{9.28}$$

The average crack width w may be taken as the product of the principal tensile strain and the diagonal crack spacing s_θ:

$$w = \varepsilon_1 \cdot s_\theta \tag{9.29}$$

where

$$s_\theta = \frac{1}{\frac{\sin\theta}{s_{mx}} + \frac{\cos\theta}{s_{my}}} \tag{9.30}$$

s_{mx} and s_{my} are indicators of the crack control characteristics of the x-reinforcement and y-reinforcement, respectively. These indicators can be roughly estimated by the relationships: s_{mx} = 1.5 x (maximum distance from x-bars) and s_{my} = 1.5 x (maximum distance from y-bars) or by using more refined formulas such as the equation given by the CEB-FIP Model Code [1990]:

$$\begin{aligned} s_{mx} &= 2 \cdot \left(c_x + \frac{s_x}{10} \right) + 0.25 \cdot k_1 \cdot \frac{d_{bx}}{\rho_x} \\ s_{my} &= 2 \cdot \left(c_y + \frac{s_y}{10} \right) + 0.25 \cdot k_1 \cdot \frac{d_{by}}{\rho_y} \end{aligned} \tag{9.31}$$

where c is the distance to reinforcement, s is the bar spacing, d_b is the bar diameter, ρ is the reinforcement ratio and k_1 is equal to 0.4 for deformed bars or 0.8 for plain bars. The subscripts x and y denote the x- and y-directions, respectively.

Assuming that the y-reinforcement is weaker than the x-reinforcement, at high loads the average strain ε_y exceeds the yield strain of the reinforcement. In this case, both f_{sy} and f_{syer} are equal to the yield stress in the y-reinforcement and Equation (9.24) becomes:

$$f_{c1} = v_{ci} \cdot \tan\theta \tag{9.32}$$

Substituting Equation (9.28) into Equation (9.32), the following relationship is obtained:

$$f_{c1} \le \frac{0.18 \cdot \sqrt{f'_c} \cdot \tan\theta}{0.3 + (24 \cdot w)/a + 16} \quad \text{(MPa, mm)} \tag{9.33}$$

11. ANALYSIS OF RC MEMBERS SUBJECTED TO SHEAR, MOMENT AND AXIAL LOAD USING THE MCFT

The MCFT was developed to analyze reinforced concrete elements under general in-plane stress conditions. Vecchio and Collins [1988] extended the theory to the analysis of reinforced concrete beams loaded in combined shear, moment and axial load. In their procedure the considered beam is considered to be composed of a series of m concrete layers and n steel elements (see Figure 71). Each individual concrete layer is defined by its width b_i, depth h_i, amount of transverse

reinforcement ρ_{yi} and position relative to the top of the beam y_{ci}. The steel elements are defined by their cross-sectional area A_{sj} and position y_{sj} relative to the top of the beam. At the level of layers and elements, conditions of compatibility and equilibrium are controlled by the MCFT, while uniform stress conditions are assumed to exist in each layer. At the section level, the only compatibility requirement used is the Bernoulli's hypothesis (*i.e.*, plane sections remain plane). Thus, the longitudinal strains in each of the concrete layers and reinforcing bar elements are determined as a function of the top and bottom fibre strains ε_t and ε_b of the section:

$$\varepsilon_{xi} = \varepsilon_t + \frac{(\varepsilon_b + \varepsilon_t)}{\sum_i^n h_i} \cdot y_i \tag{9.34}$$

At the section level, equilibrium requires that the following conditions are satisfied: i) to balance the shear, moment, and axial load acting on the section; ii) to balance the horizontal shear.

The procedure estimates the longitudinal strain distribution along the member and the shear stress distribution across the section; each individual layer is analyzed separately. The stresses f_{sxj} in the steel elements are determined from the longitudinal strains, while the longitudinal stresses f_{cxi} in the concrete layers are calculated according to the MCFT, as the longitudinal strains and the shear stresses normal to the layers are known. The resultant of these stresses must satisfy the following conditions:

$$\sum_{i=1}^{n} f_{cxi} \cdot b_i \cdot h_i + \sum_{j=1}^{m} f_{sxj} \cdot A_{sj} = N \tag{9.35}$$

$$\sum_{i=1}^{n} f_{cxi} \cdot b_i \cdot h_i \cdot (y_{ci} - \overline{y}) + \sum_{j=1}^{m} f_{sxj} \cdot A_{sj} \cdot (y_{sj} - \overline{y}) = M \tag{9.36}$$

$$\sum_{i=1}^{n} v_{ci} \cdot b_i \cdot h_i = V \tag{9.37}$$

where N, M and V are the axial load, moment and shear acting about the centroid of the section; $\overline{y}$ is the distance from the top to the centroid of the section. If these conditions are not satisfied, the assumed longitudinal strain gradient is readjusted and the analysis is repeated until equilibrium at the section level is satisfied.

The correct shear stress distribution is obtained by analyzing a second section of the beam located at a small distance from the first. According to this method, often referred as "dual section analysis", both sections are analyzed for the same shear stress distribution to satisfy the equilibrium of the section.

Let C_{i1} denote the compressive force acting on the face of concrete layer i at Section 1; C_{i2} denotes the force acting on the face at Section 2. Section 1 and 2 are separated by a distance S usually taken equal to $H/6$. The compressive force C_i is computed as:

$$C_i = f_{cxi} \cdot b_i \cdot h_i + C_{si} \tag{9.38}$$

where C_{si} is the force in the steel element, set equal to zero if the considered concrete layer does not contain any reinforcing bars. If concrete layer k, shown in Figure 72, is considered, the horizontal shear forces acting on layers F_{k-1} and F_k are determined as follows:

$$F_{k-1} = \sum_{i=1}^{k-1} (C_{i1} - C_{i2}) \tag{9.39}$$

$$F_k = F_{k-1} + C_{k1} - C_{k2} \tag{9.40}$$

The normal shear force V_k can then be determined from rotational equilibrium of the free-body shown in Figure 72 as:

$$V_k = \frac{\left(F_k + F_{k-1}\right)}{2} \cdot \frac{h_k}{S} \tag{9.41}$$

Hence, the average shear stress acting on the vertical face of concrete layer k is calculated as:

$$v_k = \frac{V_k}{b_k \cdot h_k} \tag{9.42}$$

The shear stresses calculated following the present procedure should match, for each layer, the shear stresses initially assumed. If they do not, then the assumed shear flow distribution is corrected and the analysis repeated until convergence.

12. DESIGN PROCEDURE BASED ON THE MCFT

Collins and Mitchell [1991] suggested a shear design method based on the MCFT. This method has been adopted by a number of codes, such as the Ontario Highway Bridge Design Code [1991], the Norwegian Code [1992], the Canadian Standards Association Concrete Design Code [1994] and the AASHTO LRFD [1994] specifications.

According to this method, the shear stresses are assumed to be uniform over the effective shear area, $b \cdot d_v$. Assuming that the x- and y-directions are parallel to the member axis and the transverse reinforcement, respectively, the largest longitudinal strain ε_x occurring within the web is used to calculate the principal tensile stress ε_1. For the design of non-prestressed elements (see Figure 73), ε_x can be approximated as the strain in the flexural tension reinforcement, equal to:

$$\varepsilon_x = \frac{\left(M/d_v\right) + 0.5 \cdot N + 0.5 \cdot V \cdot \cot\theta}{E_s \cdot A_s} \quad \geq -0.2 \cdot 10^{-3} \tag{10.1}$$

where A_s is the area of longitudinal reinforcement on the flexural tension side of the member. According to strain compatibility conditions, the principal tensile strain ε_1 can be related to ε_x, the direction of the principal compressive stresses θ, and the magnitude of the principal compressive strain ε_2:

$$\varepsilon_1 = \varepsilon_x + \left(\varepsilon_x - \varepsilon_c\right) \cdot \cot^2\theta \tag{10.2}$$

Solving Equation (9.15) with respect to ε_2:

$$\varepsilon_2 = \varepsilon'_c \cdot \left(1 - \sqrt{1 - f_{c2}/f_{c2\max}}\right) \tag{10.3}$$

where ε'_c is generally taken equal to -0.002 and the principal compressive stress f_{c2} can be conservatively taken as:

$$f_{c2} = v_{xy} \cdot \left(\tan\theta + \cot\theta\right) \tag{10.4}$$

where:

$$v_{xy} = \frac{V}{b \cdot d_v} \tag{10.5}$$

From Equations (10.2), (10.3) and (10.4) ε_1 can be expressed as:

$$\begin{aligned} \varepsilon_1 &= \varepsilon_x + \left[\varepsilon_x + \varepsilon_x^*\right] \cdot \cot^2 \theta \\ \varepsilon_x^* &= 0.002 \cdot \left(1 - \sqrt{1 - \frac{v_{xy}}{f_c'} \cdot \left(\tan\theta + \cot\theta\right) \cdot \left(0.8 + 170 \cdot \varepsilon_1\right)} \right) \end{aligned} \tag{10.6}$$

Considering the MCFT as a truss model with a concrete contribution equal to the transverse component of the shear stresses v_{ci} transferred across the crack (see Figure 70), the shear strength may be expressed as:

$$\begin{aligned} V \;=\; V_s + V_c \;&=\; \frac{A_v \cdot f_{vy}}{s} \cdot d_v \cdot \cot\theta + v_{ci} \cdot b \cdot d_v \\ &=\; \frac{A_v \cdot f_{vy}}{s} \cdot d_v \cdot \cot\theta + f_{c1} \cdot \cot\theta \cdot b \cdot d_v \end{aligned} \tag{10.7}$$

Substituting Equation (9.19) into Equation (10.7):

$$V = \frac{A_v \cdot f_{vy}}{s} \cdot d_v \cdot \cot\theta + \beta \cdot \sqrt{f_c'} \cdot b \cdot d_v \tag{10.8}$$

where

$$\beta = \frac{0.33 \cdot \cot\theta}{1 + \sqrt{500 \cdot \varepsilon_1}} \le \frac{0.18}{0.3 + \dfrac{24 \cdot w}{a + 16}} \quad \text{(MPa,mm)} \tag{10.9}$$

In order to use Equation (10.8) for the evaluation of the required amount of transverse reinforcement, it is necessary to determine appropriate values of θ and β which must satisfy Equation (10.6). These values are generally given as function of the longitudinal strain ε_x and shear stress level v_{xy}/f'_c in the form of tables or diagrams. The values given as example in Table 23 ensure that the tensile strain in the stirrups is at least equal to 0.002 and that the compressive stress f_{c2} does not exceed the crushing strength f_{c2max} of concrete. In determining these values it was assumed that the amount and spacing of the stirrups would limit the crack spacing to about 300 mm.

13. CYCLIC LOAD MODELING THROUGH THE MCFT

It is worth discussing why some codes have maintained an approach based on the truss model even when more rational methods exist, such as the MCFT, which is now adopted, for example, in the Canadian, Norwegian and AASHTO LRFD codes. As observed in Duthinh and Carino [1996], the reason may be behind the fact that a whole generation of engineers has learned and used methods based on the truss approach. However, design engineers should take into account

that there is a fundamental difference between the two approaches. According to ACI-ASCE Committee 326 [1962], "diagonal tension is a combined stress problem in which horizontal stresses due to bending as well as shear stresses must be considered".

Collins [1993] explains that this combination of flexure and shear is what has made the shear problem so intractable. He contrasts the traditional type of shear tests (beam), which are simple to perform, but difficult to analyze, with the more recent tests (panel), which are more difficult to perform but simpler to analyze. In the tests of beams simply supported with two concentrated loads, the behaviour of the member changes from section to section along the shear span and also over the depth of the beam. In contrast, the state of stresses in a panel loaded in pure shear, or in a combination of shear and axial forces, is uniform.

Because shear is studied independently of bending, the shear carried by the compression zone is not taken into account by the MCFT. In addition, the shear carried by dowel action is neglected; only the shear carried by aggregate interlock is accounted for.

The contribution to shear strength due to dowel action is rather small, while the contribution related to the shear carried by the compression zone can account for 25-30% of the total concrete contribution in beams with typical reinforcement ratios. Nevertheless, when the MCFT is applied to traditional beam tests, it performs rather well as a predictor of strength. The reason of this good agreement is related to the choice of the location (mid-span) of ε_x, which reflects the redistribution of shear stresses transferred from the most highly strained portions of the cross section to the less highly strained portions. However, it would be conservative to use the highest value of ε_x, as an increase in ε_x decreases the shear capacity. So, implicitly, the higher shear capacity of the uncracked or least strained region is taken into consideration.

The Seismic Shear Wall International Standard Problem documented by the Nuclear Power Engineering Corp. of Japan [1996] has brought to the fore the inability of the proposed methods of analysis and modelling of concrete to give a reliable evaluation of the peak strength and the ductility of structural walls subjected to reversed cyclic loading. Among these methods the smeared crack approach[5], which assumes fixed cracks, tends to be the most favoured. Okamura and Maekawa [1991] and Sittipunt and Wood [1995], among others, have documented models assuming a fixed crack approach and have demonstrated a good agreement with experimental results. However, the fix cracked method requires separate formulations to model the normal stress and the shear stress hysteretic behaviour. This is somewhat at odds both with the test observations and with common elasticity approaches to constitutive modelling.

An alternative approach based on the smeared rotating crack assumption was proposed by Vecchio [1989, 1990]. The procedure was based on an iterative, secant stiffness formulation, where the concrete is treated as an orthotropic material with its principal axes corresponding to the directions of the principal average tensile strains and principal average compressive strains, modelled according to the constitutive relations of the MCFT. The secant stiffness formulation is marked by excellent convergence and numerical stability characteristics. Correlations to experimental data for structures subjected to monotonic loading conditions are generally very good. Vecchio [1999] has demonstrated that secant stiffness based procedures can be also used to effectively model reversed cyclic load effects in reinforced concrete structures. This result has been obtained employing strain offsets to model the plastic components of strain in the concrete and reinforcement, as hereafter illustrated in some details (Palermo and Vecchio [2003]).

---

[5] Smeared crack approach simulate cracking with a fictious constitutive model, thereby avoiding the need for changing geometry and mesh model.

Palermo and Vecchio [2004] verified their algorithm through analyses that include slender walls, which are controlled by flexural effects, and squat walls, where the response is dominated by shear-related mechanisms. The results have shown that ultimate strength, ductility, energy dissipation and failure mechanisms are well simulated. The procedure proposed by Palermo and Vecchio [2003] was also able to simulate second-order mechanisms such as the elongation of the flange wall and the horizontal expansion of the web wall. The first mechanism can be considered a measure of the extent of flexural cracking and ratcheting[6] in the flange walls, while the second mechanism represents the dilatation of the web wall due to cracking and yielding of the web reinforcement, and the extent of compression softening of the concrete in the web wall.

13.1 PLASTIC OFFSET FORMULATION

The concrete average strain in the average principal direction may be expressed as the sum of the elastic strain component ε_c^e and the plastic strain component (or plastic offset) ε_c^p:

$$\varepsilon_c = \varepsilon_c^e + \varepsilon_c^p \tag{13.1}$$

The elastic strain is then used to compute the secant modulus of concrete on the base of the concrete average stress f_c:

$$\overline{E}_c = f_c \big/ \varepsilon_c^e \tag{13.2}$$

In a similar way, the average strain in the reinforcement may be computed from the sum of the elastic and plastic components of strain:

$$\varepsilon_{si} = \varepsilon_{si}^e + \varepsilon_{si}^p \tag{13.3}$$

and the secant modulus for the reinforcement is calculated on the base of the steel average stress f_{si}:

$$\overline{E}_{si} = f_{si} \big/ \varepsilon_{si}^e \tag{13.4}$$

Plastic offsets may be incorporated in a finite element algorithm in the form of prestrains ([Vecchio and Collins, 1990], [Vecchio, 1992]). With this aim the concrete plastic offsets in the principal directions and the reinforcement plastic strain are first resolved into components relative to the reference axes, giving the vectors:

$$\left[\varepsilon_c^p\right] = \begin{bmatrix} \varepsilon_{cx}^p \\ \varepsilon_{cy}^p \\ \gamma_{cxy}^p \end{bmatrix} \tag{13.5}$$

and

$$\left[\varepsilon_{si}^p\right] = \begin{bmatrix} \varepsilon_{si}^p \cdot \left[1+\cos\left(2\alpha_i\right)\right]/2 \\ \varepsilon_{si}^p \cdot \left[1-\cos\left(2\alpha_i\right)\right]/2 \\ \varepsilon_{si}^p \cdot \sin\left(2\alpha_i\right) \end{bmatrix} \tag{13.6}$$

---

[6] Ratcheting is a term used to describe the vertical stretching of the flange due to irrecoverable strains that accumulate in the postyield cycles.

where α_i defines the reinforcement orientation. The unconstrained joint displacements are determined from prestrains and the element geometry. Then, given the unconstrained displacements, the plastic prestrain nodal force vectors of concrete [F_c^p] and reinforcement [F_s^p] can be separately evaluated as the product of the corresponding element secant stiffness matrices [K_c] and [K_s] and the unconstrained joint displacements. The forces thus obtained are added to the externally applied joint loads to determine the total nodal forces [F].

The total nodal displacements are obtained by multiplying the total nodal force vector by the inverse of the global stiffness matrix [K], equal to the sum of the stiffness contributions of concrete and steel reinforcement:

$$[K] = [K_c] + \sum_i [K_s]_i \tag{13.7}$$

From these displacements the strains and stresses are recalculated, and the new secant moduli of concrete and steel reinforcement are evaluated; the procedure is repeated until convergence on the secant stiffness is achieved.

The plastic strains that take place in the concrete are defined through the Mohr's circle. For this, the principal direction θ is determined on the basis of the elastic strain components, and the plastic strains in the directions corresponding to the principal axes are computed from the concrete plastic strains in the x and y axes:

$$\varepsilon_{c1}^p = \frac{\varepsilon_{cx}^p + \varepsilon_{cy}^p}{2} + \frac{\varepsilon_{cx}^p - \varepsilon_{cy}^p}{2}\cos(2\theta) + \frac{\gamma_{cxy}^p}{2}\sin(2\theta) \tag{13.8}$$

$$\varepsilon_{c2}^p = \frac{\varepsilon_{cx}^p + \varepsilon_{cy}^p}{2} - \frac{\varepsilon_{cx}^p - \varepsilon_{cy}^p}{2}\cos(2\theta) - \frac{\gamma_{cxy}^p}{2}\sin(2\theta) \tag{13.9}$$

For calculations performed at increasing or varying load steps, further plastic straining may occur. Let $\Delta\varepsilon_{c1}^e$ and $\Delta\varepsilon_{c2}^p$ represent the increments (negative or positive, regardless of whether the total strains are tensile or compressive) of the plastic strains in the principal directions, the parameters defining the envelope of plastic strains are updated as follows:

$$\varepsilon_{cx}^{p'} = \varepsilon_{cx}^p + \frac{\Delta\varepsilon_{c1}^p}{2}\left[1 + \cos(2\theta)\right] + \frac{\Delta\varepsilon_{c2}^p}{2}\left[1 - \cos(2\theta)\right] \tag{13.10}$$

$$\varepsilon_{cy}^{p'} = \varepsilon_{cy}^p + \frac{\Delta\varepsilon_{c1}^p}{2}\left[1 - \cos(2\theta)\right] + \frac{\Delta\varepsilon_{c2}^p}{2}\left[1 + \cos(2\theta)\right] \tag{13.11}$$

$$\gamma_{cxy}^{p'} = \gamma_{cxy}^p + \Delta\varepsilon_{c1}^p \cdot \sin(2\theta) - \Delta\varepsilon_{c2}^p \cdot \sin(2\theta) \tag{13.12}$$

Mohr's circle approach can also be used to approximately calculate the maximum concrete strain corresponding to an arbitrary direction: the maximum concrete strain attained during the load history is evaluated in order to calculate the concrete stress from the stress-strain constitutive model used to model the hysteretic behaviour of concrete. For example, the maximum compressive strains in the principal directions attained during the loading history are given by:

$$\varepsilon_{cm1} = \frac{\varepsilon_{cmx} + \varepsilon_{cmy}}{2} + \frac{\varepsilon_{cmx} - \varepsilon_{cmy}}{2}\cos(2\theta) + \frac{\gamma_{cmxy}}{2}\sin(2\theta) \tag{13.13}$$

$$\varepsilon_{cm2} = \frac{\varepsilon_{cmx} + \varepsilon_{cmy}}{2} - \frac{\varepsilon_{cmx} - \varepsilon_{cmy}}{2}\cos(2\theta) - \frac{\gamma_{cmxy}}{2}\sin(2\theta) \tag{13.14}$$

where ε_{cmx}, ε_{cmy} and γ_{cmxy} are quantities defining maximum compressive strains relative to the x,y – axes.

If the current total compressive strains are greater than those previously recorded, the maximum strain envelope must be updated. Thus, the strain increments $\Delta\varepsilon_{m1}$ and $\Delta\varepsilon_{m2}$ are defined as:

$$\Delta\varepsilon_{cm1} = \begin{cases} 0 & \text{if} \quad \varepsilon_1 > \varepsilon_{cm1} \\ \varepsilon_1 - \varepsilon_{cm1} & \text{if} \quad \varepsilon_1 < \varepsilon_{cm1} \end{cases} \tag{13.15}$$

$$\Delta\varepsilon_{cm2} = \begin{cases} 0 & \text{if} \quad \varepsilon_2 > \varepsilon_{cm2} \\ \varepsilon_2 - \varepsilon_{cm2} & \text{if} \quad \varepsilon_2 < \varepsilon_{cm2} \end{cases} \tag{13.16}$$

The parameters defining the compressive strain envelope are then updated as follows:

$$\varepsilon'_{cmx} = \varepsilon_{cmx} + \frac{\Delta\varepsilon_{cm1}}{2}\left[1+\cos(2\theta)\right] + \frac{\Delta\varepsilon_{cm2}}{2}\left[1-\cos(2\theta)\right] \tag{13.17}$$

$$\varepsilon'^{'}_{cy} = \varepsilon_{cmy} + \frac{\Delta\varepsilon_{cm1}}{2}\left[1-\cos(2\theta)\right] + \frac{\Delta\varepsilon_{cm2}}{2}\left[1+\cos(2\theta)\right] \tag{13.18}$$

$$\gamma'^{'}_{cxy} = \gamma_{cmxy} + \Delta\varepsilon_{cm1}\cdot\sin(2\theta) - \Delta\varepsilon_{cm2}\cdot\sin(2\theta) \tag{13.19}$$

An envelope for the maximum tensile strains in the concrete is developed in a similar manner. Note that the Mohr's circle used for computing the maximum strain does not represent a compatible strain condition, however, it represents a convenient way of keeping track of the maximum strain in any given direction.

13.2 CONCRETE STRESS-STRAIN MODEL

In the following description of the concrete model it is assumed that compression and tension responses occur along the average principal strain directions 2 and 1, respectively.

13.2.1 Compression response

The backbone curve typically follows the monotonic response, *i.e.*, Hognestad [1955] parabola or Popovics [1973] formulation, including the compression softening effects according to the MCFT. The shape and the slope of the unloading and reloading responses depend on the plastic offset strain. The plastic offset is used as a parameter in defining the unloading path and in determining the degree of damage in concrete due to cycling. Palermo and Vecchio [2003] have suggested for the plastic strain offset the following relation:

$$\varepsilon_c^{p'} = \varepsilon^p \cdot \left[0.166 \cdot \left(\frac{\varepsilon_{2c}}{\varepsilon_p} \right)^2 + 0.132 \cdot \left(\frac{\varepsilon_{2c}}{\varepsilon_p} \right) \right] \tag{13.20}$$

where ε_p is the strain at peak stress and ε_{2c} is the strain at the onset of unloading from the backbone curve. The plastic offset strain remains unchanged unless the previous maximum strain in the history of loading is exceeded. Tests conducted by Buyukozturk and Tseng [1984] have shown that the plastic offset is not affected by the confining stresses or strains.

In order to describe the unloading branch of concrete, Palermo & Vecchio (2003) have adopted a Ramberg – Osgood formulation (see Figure 74):

$$f_c(\Delta\varepsilon) = f_{2c} + E_{c2}(\Delta\varepsilon) + \left[\frac{(E_{c3} - E_{c2}) \cdot \Delta\varepsilon^N}{N \cdot (\varepsilon_c^p - \varepsilon_{2c})^{N-1}}\right] \tag{13.21}$$

where

$$\Delta\varepsilon = \varepsilon - \varepsilon_{2c} \tag{13.22}$$

and

$$N = \frac{(E_{c2} - E_{c3}) \cdot (\varepsilon_c^p - \varepsilon_{2c})}{f_{2c} + E_{c2} \cdot (\varepsilon_c^p - \varepsilon_{2c})} \tag{13.23}$$

with ε equal to the instantaneous strain in the concrete. The initial unloading stiffness E_{c2} is assigned a value equal to the initial tangent stiffness of concrete E_c, calculated as f'_c/ε'_c. The unloading stiffness E_{c3}, which defines the stiffness at the end of the unloading phase, is defined as $0.071E_c$, while f_{2c} is the stress calculated from the backbone curve at the peak unloading strain ε_{2c}.

Reloading is modelled by a linear response that takes into account the degradation in the reloading stiffness resulting from load cycling. The reloading stiffness is defined as a degrading function of the strain recovery during unloading (see Figure 75):

$$f_c = f_{r0} + E_{c1} \cdot (\varepsilon_c - \varepsilon_{r0}) \tag{13.24}$$

where f_c and ε_c are the stress and the strain on the reloading path; f_{r0} is the stress in concrete at a reloading reversal and corresponds to the strain ε_{r0}; and E_{c1} is the reloading stiffness, calculated as:

$$E_{c1} = \frac{(\beta_d \cdot f_{\max}) - f_{r0}}{\varepsilon_{2c} - \varepsilon_{ro}} \tag{13.25}$$

where

$$\beta_d = \frac{1}{1 + 0.10 \cdot (\varepsilon_{rec}/\varepsilon_p)^{0.5}} \quad \text{for} \quad |\varepsilon_c| < |\varepsilon_p| \tag{13.26}$$

and

$$\beta_d = \frac{1}{1 + 0.175 \cdot (\varepsilon_{rec}/\varepsilon_p)^{0.6}} \quad \text{for} \quad |\varepsilon_c| > |\varepsilon_p| \tag{13.27}$$

and

$$\varepsilon_{rec} = \varepsilon_{\max} - \varepsilon_{\min} \tag{13.28}$$

β_d is a damage indicator, f_{max} is the maximum stress in concrete for the current unloading loop, and ε_{rec} is the amount of strain recovered in the unloading process and is the difference between the maximum strain ε_{max} and the minimum strain ε_{min} for the current hysteresis loop. The minimum strain is limited by the compressive plastic offset strain. β_d is calculated for the first unloading/reloading cycle and remains constant until the previous maximum unloading strain is attained or exceeded. Therefore, no additional damage is induced in the concrete for hysteresis

loops occurring at strains less than the maximum unloading strain. A model for partial unloading/reloading has also been proposed by Palermo and Vecchio [2003].

13.2.2 Tension response

For the tension model, Palermo and Vecchio [2003] have proposed as backbone curve the two branch curve adopted by the MCFT. Similar to the concrete in compression, the plastic offset in tension is dependent on the unloading strain from the backbone curve:

$$\varepsilon_c^p = 146 \cdot \varepsilon_{1c}{}^2 + 0.523 \cdot \varepsilon_{1c} \tag{13.29}$$

where ε_c^p is the tensile plastic offset, and ε_{1c} is the unloading strain from the backbone curve. To describe the unloading branch in tension, Palermo and Vecchio [2003] have adopted a Ramberg – Osgood formulation (see Figure 76):

$$f_c(\Delta\varepsilon) = f_{1c} - E_{c5}(\Delta\varepsilon) + \left[\frac{(E_{c5} - E_{c6}) \cdot \Delta\varepsilon^N}{N \cdot (\varepsilon_{1c} - \varepsilon_c^p)^{N-1}}\right] \tag{13.30}$$

where

$$\Delta\varepsilon = \varepsilon_{1c} - \varepsilon \tag{13.31}$$

and

$$N = \frac{(E_{c5} - E_{c6}) \cdot (\varepsilon_{1c} - \varepsilon_c^p)}{E_{c5} \cdot (\varepsilon_{1c} - \varepsilon_c^p) - f_{1c}} \tag{13.32}$$

f_{1c} is the unloading stress from the backbone curve, and E_{c5} is the initial unloading stiffness, equal to the initial tangent stiffness E_c. The unloading stiffness E_{c6}, which defines the stiffness at the end of the unloading phase, is calculated as:

$$E_{c6} = 0.071 \cdot E_c \cdot (0.001/\varepsilon_{1c}) \qquad \varepsilon_{1c} \le 0.001 \tag{13.33}$$

$$E_{c6} = 0.053 \cdot E_c \cdot (0.001/\varepsilon_{1c}) \qquad \varepsilon_{1c} > 0.001 \tag{13.34}$$

In order to model the reloading of concrete in tension, Palermo and Vecchio [2003] have suggested adopting a linear behaviour, taking into account the degrading reloading stiffness (see Figure 77). The reloading stress is then calculated as:

$$f_c = \beta_t \cdot tf_{\max} - E_{c4} \cdot (\varepsilon_{1c} - \varepsilon_c) \tag{13.35}$$

where

$$E_{c4} = \frac{(\beta_t \cdot tf_{\max}) - tf_{r0}}{\varepsilon_{1c} - t_{r0}} \tag{13.36}$$

f_c is the tensile stress on the reloading curve and corresponds to a strain of ε_c. E_{c4} is the reloading stiffness, β_t is a tensile damage indicator, tf_{max} is the unloading stress for the current hysteresis loop, and tf_{r0} is the stress in concrete at a reloading reversal corresponding to a strain t_{r0}. The damage parameter β_t is calculated from the following relation:

$$\beta_t = \frac{1}{1+1.15\cdot\left(\varepsilon_{rec}\right)^{0.25}} \tag{13.37}$$

where

$$\varepsilon_{rec} = \varepsilon_{\max} - \varepsilon_{\min} \tag{13.38}$$

ε_{rec} is the strain recovered during an unloading phase, and is equal to the difference between the unloading strain ε_{max} and the minimum strain at the onset of reloading ε_{min}, which is limited by the plastic offset strain. A model for partial unloading/reloading has been also proposed for concrete in tension by Palermo and Vecchio [2003].

13.2.3 Cracking-closing model

The re-contact strain, defined as the strain at which the two cracked surfaces come into contact, is assumed to be equal to the plastic offset strain of concrete in tension. The stiffness of the concrete during closing of cracks is smaller than that after cracks are completely closed. The latter is assumed equal to the initial tangent stiffness. The crack-closing stiffness E_{close} is calculated from:

$$E_{close} = \frac{f_{close}}{\varepsilon_c^p} \tag{13.39}$$

where f_{close} is the stress imposed on the concrete as cracked surfaces come into contact, and is given by:

$$f_{close} = -E_c \cdot \left(0.0016\cdot\varepsilon_{1c} + 50\cdot 10^{-6}\right) \tag{13.40}$$

The stress on the closing-of-cracks path is then determined from the following expression:

$$f_c = E_{close}\cdot\left(\varepsilon_c - \varepsilon_c^p\right) \tag{13.41}$$

After the cracks have completely closed and loading continues into the compression strain region, the reloading rules for concrete in compression are applicable, with the stress in concrete, at the reloading reversal point, equal to f_{close}.

For reloading from the closing-of-cracks curve into the tensile strain region, the stress in the concrete is assumed to be linear, following the reloading path previously established for the tensile reloading of concrete.

13.3 REINFORCEMENT MODEL

The monotonic response of steel reinforcement is assumed to be trilinear. The initial response is linear elastic, followed by a yield plateau and ending with a strain-hardening portion. The hysteretic response of the reinforcement is modelled after Seckin [1981], and the Bauschinger effect is represented by a Ramberg – Osgood formulation.

14. CONCLUSIONS

The present report has described the structural behaviour of rectangular reinforced concrete hollow piers of bridge structures subjected to lateral deformations.

The first part of the work focused on the derivation of equivalent properties in terms of load-displacement envelopes and energy dissipation characteristics based on the properties of the section at the base of the pier. The properties at the section were derived, for a large number of design configurations, based on nonlinear numerical analysis calibrated against experimental results. The results of this work can be summarised as follows:

- The nonlinear numerical model based on the discretization of the section in fibres offers a good representation of the nonlinear cyclic behaviour of sections of rectangular reinforced concrete hollow piers;
- The nonlinear monotonic skeleton curve of the moment-curvature relationship of the section can be well represented by a bilinear curve, defined by the yield and ultimate bending moment and curvatures of the section; the ultimate curvatures are determined based on the ultimate strains reached by either the concrete or the steel fibres;
- Parametric analyses were performed for a large combination of designs of the section, including the aspect ratio of the section, the normalised axial load, the percentage of longitudinal reinforcement, the level of confinement, and the strength of concrete and steel. The results of the parametric analysis are summarised in charts giving the yield and ultimate bending moment and curvatures in a dimensionless form, thus allowing the construction of the bilinear moment-curvature of the section;
- Similarly, the energy dissipation characteristics of the different designs of the section are given in the form of charts for different levels of curvature ductility of the section;
- The force-displacement bilinear diagram of the pier can be obtained by integrating the bi-linear moment-curvature diagram of the section along the plastic hinge length and by adding the elastic deformation of the remaining portion of the pier. Similarly, the equivalent damping of the pier can be computed from energy principles based on the damping characteristics of the section and the plastic hinge length.

The results given by the charts proposed in the present work offers the possibility to the designer to construct the equivalent properties of the pier in terms of secant stiffness and equivalent damping for a given level of ductility for a large combination of design possibilities in a more reliable way than the current expressions available in literature for solid reinforced concrete column sections. These properties can then be used within the context of Performance Based Design.

In the second part of the work, the different approaches to model shear effects on reinforced concrete beam-column elements are documented. Since at present the methods available to date do not allow a proper definition of the shear load-deformation characteristics of the pier in the same way as done for the first part of the report using a fibre model, a work on the state-of-the-art was presented, identifying the following main issues:

- Hollow reinforced concrete piers exhibit a good seismic performance, including shear and flexural behaviour, if the flanges are properly confined.
- For hollow reinforced concrete squat piers, the shear contribution to the total deformation is important and cannot be disregarded. The shear deformation, in general negligible for long span ratios of solid sections, needs also to be considered for for tall reinforced concrete hollow sections.

- Acknowledging that hollow sections are composed by thin walls, the MCFT seems to be the more effective way to take into account the effects of shear.

- It is necessary to extend and improve the MCFT to model the cyclic behaviour of reinforced concrete members and calibrate these models through dedicated tests to model the shear effects on rectangular reinforced concrete hollow.

REFERENCES

PART A

Comité Européen de Normalisation (CEN) [1993] *ENV 1998-2 Structures in seismic regions (bridges)*, Draft Document TC250/SC8/N76, Brussels, Belgium.

Comité Européen de Normalisation (CEN) [2003] *prEN 1992-1-1 Eurocode 2: Design of concrete structures for earthquake resistence - Part 1-1: General rules and rules for building*, Final Draft, Brussels, Belgium.

Comité Européen de Normalisation (CEN) [2003] *prEN 1998-1 Eurocode 8: Design of structures for earthquake resistence - Part 1: General rules, seismic actions and rules for building*, Final Draft, Brussels, Belgium.

Comité Européen de Normalisation (CEN) [2003] *prEN 1998-2 Eurocode 8: Design of structures for earthquake resistence Part 2: Bridges*, Draft Document TC250/SC8/N370, Brussels, Belgium.

Dutta, A., Mander, J.B., Kokorina, T. (1999) "Retrofit for control and repairability of damage", *Earthquake Spectra*, Vol. 15, No. 4, pp. 657-79.

Esmaeily-Gh., A., Xiao, Y. [1999] "Seismic behaviour of bridge column subjected to various loading patterns", *PEER Report 2002/15*, Pacific Earthquake Engineering Research Centre, College of Engineering, University of California, Berkeley, U.S.

Fafitis, A., Shah, S.P. [1985] "Prediction of ultimate behavior of confined columns subjected to large deformations", *Journal of the American Concrete Institute*, Vol. 82, No. 4, pp. 423-433.

Guedes, J., Pegon, P., Pinto, A.V. [1994] "A fibre/Timoshenko beam element in Castem 2000", Special publication No. I.94.31, Joint Research Center, European Commission, Ispra, Italy.

Hognestad, E. [1951] "A study of combined bending and axial load in reinforced concrete members", *Bulletin Series No. 399*, University of Illinois Engineering Experiment Station, U.S.

Hoshikuma, J., Unjoh, S., Nagaya, K. [2001] "Size effect on ductile behaviour of reinforced concrete columns under cyclic loading", *Proceeding of the 17th U.S. – Japan Bridge Engineering Workshop*, Tsukuba, Japan.

Jobse, H.J. [1982] Applications of high strength concrete for highway bridges, *Report No. FHWA/RD-82/097*, Concrete Technology Corporation, Tacoma, U.S.

Maillard A. [1993] "Castem 2000, Guide d'utilisation", *Rapport CEA 93/007*, CEA, Saclay, France.

Mander, J.B. [1984] "Experimenatl behaviour of ductile hollow reinforced concrete columns", *Proceeding of the 8th World Conference on Earthquake Engineering*, San Francisco, U.S.

Mander, J.B., Priestley, M.J.N., Park, R. [1988] "Theoretical stress-strain model for confined concrete", *Journal of Structural Engineering*, ASCE, Vol. 114, No. 8, pp. 1804-1826.

Menegotto, M., Pinto, P.E. [1973] "Method of analysis for cyclically loaded reinforced concrete plane frames including changes in geometry and non-elastic behaviour of elements under combined normal force and bending", *Proceedings of the IABSE Symposium on resistance and ultimate deformability of structures acted on by well-defined repeated loads*, Lisbon, Portugal.

Mercer, C., Martin, J. [1987] "A beam element for cyclically loaded reinforced concrete structures", *Technical Report No. 98*, FRD/UCT Centre for Research in Computational and Applied Mechanics, University of Cape Town, South Africa.

Monti, G., Nuti, C. [1992] "Nonlinear cyclic behavior of reinforcing bars including buckling", *Journal of Structural Engineering*, ASCE, Vol. 118, No. 112, pp. 3268-3284.

Park, R., Priestley, M.J.N., Gill, W.D. [1982] "Ductility of square-confined concrete columns", *Journal of the Structural Division*, Vol. 108, No. ST4, pp. 929-950.

Pinto, A.V., Verzelletti, G., Negro, P., Guedes, J. [1995] *Cyclic testing of a squat bridge-pier - Report EUR 16247 EN*, Joint Research Center, European Commission, Ispra, Italy.

Pinto, A.V., Verzelletti, G., Pegon, P., Magonette, G., Negro, P., Guedes, J. [1996] *Pseudo-dynamic testing of large-scale R/C bridges - Report EUR 16378 EN*, Joint Research Center, European Commission, Ispra, Italy.

Poston, R.W., Gilliam, T.E., Yamamoto, Y., Breen, J.E. [1985] "Hollow concrete bridge pier behaviour", *ACI Journal*, Vol. 82, No. 6, pp. 779-787.

Priestley, M.J.N., Ranzo, G., Benzoni, G., Kowalsky, M.J. [1996a] "Yield displacement of circular bridge column", *Proceedings of the Fourth Caltrans Workshop*, Sacramento, U.S.

Priestley, M.J.N., Seible, F., Calvi, G.M. [1996b] *Seismic design and retrofit of bridges*, John Wiley & Sons, New York, U.S.

Proctor, A.N. [1976] "Hollow concrete columns", *Civil Engineering*, September, pp. 53-55.

Proctor, A.N. [1977] "Hollow rectangular reinforced concrete columns", *Civil Engineering*, September, pp. 45-49.

Saatcioglu, M., Razvi, S. [1992] "Strength and ductility of confined concrete", *Journal of Structural Engineering*, ASCE, Vol. 118, No. 6, pp. 590-1607.

Santa Maria, R. [2001] "Behavior of hollow, rectangular concrete piers subjected to biaxial bending", *PhD Dissertation*, The Univesrity of Texas at Austin, U.S.

Sheikh, S.A., Uzumeri, S.M. [1982] "Analytical model for concrete confinement in tied columns", *Journal of Structural Division*, ASCE, Vol. 108, No. ST12, pp. 2703-2722.

Stone, W.C., Cheok, G.S. [1989] *Inelastic behavior of full-scale bridge columns subjected to cyclic loading*, NIST Building Science Series 166, National Institute of Standards and Technology, U.S. Department of Commerce, Washington, U.S.

Sun, Y., Sakino, K. [1993] "Experimental study on ductility improvement method for reinforced concrete columns using high-strength materials", *Proceedings of the Japan Concrete Institute*, Vol. 15, No. 2, pp. 719-724.

Taylor, A.W., Breen, J.E. [1994] "Design recommendations for thin-walled box piers and pylons", *Concrete International*, Vol. 16, No. 12, pp. 36-41.

Watson, S., Zahn, F.A., Park, R. [1992] "Confining reinforcement for concrete columns", *Journal of Structural Engineering*, Vol. 120, No. 6, pp. 1798-1823.

Yeh, Y.-K., Mo, Y.L., Yang, C.Y. [2002] "Seismic performance of rectangular hollow bridge columns", *Journal of Structural Engineering*, ASCE, Vol. 128, No. 1, pp. 60-68.

PART B

American Association of State Highway and Transportation Officials [1994] *AASHTO LRFD bridge design specifications and commentary*, Washington, D.C, U.S.

Ang, B.G., Priesley, M.J.N., Paulay, T. [1989] "Seismic shear strength and deformability of RC bridge columns subjected to inelastic cyclic displacements", *Rep. No. UCB/EERC-92/04*, Earthquake Engineering Research Center, University of California at Berkeley, Berkeley, CA, U.S.

Ang, B.G., Priestley, M.J.N., Paulay, T. [1989] "Seismic shear strength of circular reinforced concrete columns", *ACI Structural Journal*, Vol. 86, No. 1, pp. 45-59.

Applied Technology Council [1983] Seismic retrofitting guidelines for highway bridges, ATC 6-2, Redwood City, CA, U.S.

ASCE-ACI Committee 445 on shear and torsion [1998] "Recent Approaches to shear design of structural concrete", *Journal of Structural Engineering*, ASCE, Vol. 124, No. 12, pp. 1375-1417.

Bhide, S.B., Collins, M.P. [1989] "Influence of axial tension on the shear capacity of reinforced concrete members", *ACI Structural Journal*, Vol. 86, No. 5, pp. 570-581.

Buyukozturk, O., Tseng, T.M. [1984] "Concrete in biaxial cyclic compression", *Journal of Structural Engineering*, ASCE, Vol. 110, No. 3, pp. 461-476.

Comité Européen de Normalisation (CEN) [1993] *ENV 1998-2 Structures in seismic regions (bridges)*, Draft Document TC250/SC8/N76, Brussels, Belgium.

Collins, M.P., Mitchell, D. [1991] *Prestressed concrete structures*, Prentice Hall, Englewood Cliffs, New Jersey, U.S.

Collins, M.P. [1993] "The use of rational design methods for shear", *ACI SP 157 Proc. Thomas Paulay Symp. Recent developments in lateral force transfer in building*, September 1993, pp. 351-374, University California San Diego, U.S.

Comité Euro-International du Beton (CEB) – Fédération International de la Precontrainte (FIP) [1993] *Model Code 1990 (MC90)*, Thomas Telford, London, U.K.

Comité Euro-International du Beton (CEB) [1978] *Shear and torsion, June: Explanatory and viewpoint papers on Model Code Chapter 11 and 12*, prepared by CEB Committee V, CEB Bull. 12, Paris, France.

CSA Committee A23.3 [1994] *Design of concrete structures: structures (design) – A national standard of Canada*, Canadian Standards Association, Rexdale, Canada.

Duthinh, D., Carino, N.J. [1996] "Shear design of high-strength concrete beams: a review of the state-of-the-art", *NISTIR 5870*, Building and Fire Research Laboratory, National Institute of Standards and Technology, Gaithersburg, MD 20899, U.S.

Hognestad, E., Hansen, N.W., McHenry, D. [1955] "Concrete stress distribution in ultimate strength design", *ACI Journal*, Vol. 52, No. 12, pp. 455-479.

Inoue, S., Egawa, N. [1996] "Flexural and shear behavior of reinforced concrete hollow beams under reversed cyclic loading", *Proceedings of 11th World Conference on Earthquake Engineering*, Paper No. 1359, Mexico.

Konwinsky, C.M., Ramirez, J.A., Sozen, M.A. [1995] "Shear strength of reinforced concrete columns subjected to seismic loading", *Proceedings of National Seismic Conference on bridges and highways: progress in research and practice*, pp. 10-13, San Diego, U.S.

Lehman, D.E., Lynn, A.C., Aschleim, M.A., Moehle, J.P. [1996] "Evaluation methods for reinforced concrete columns and connections", *Proceedings of 11th World Conference on Earthquake Engineering*, Paper No. 673, Mexico.

MacGregor, J.G. [1988] *Reinforced concrete*, Prentice Hall, Englewood Cliffs, New Jersey, U.S., ISBN 0-13-771742-3.

Mander, J.B. [1984] "Experimental behaviour of ductile hollow reinforced concrete columns", *Proceedings of 8th World Conference on Earthquake Engineering*, San Francisco, U.S.

Marti, P. (1985) "Truss models in detailing", *Concrete International*, Vol. 7, No. 12, pp. 66-73

Mörsch [1909] *Concrete-Steel Construction (Der Eisenbetonbau)*, English translation of the 3rd German edition, McGraw-Hill Book Co., New York, U.S.

Mörsch, E. [1922] *Der Eisenbetonbau-seine theorie und anwendung*, 5th Ed., Vol. 1, Part 2., Wittwer, Stuttgart, Germany.

MTO, OHBDC Committee [1991] *Ontario Highway Bridge Design Code*, 3rd Edition, Ontario Ministry of Transportation Officials, Downsview, Canada.

Norwegian Council for Building Standardization [1992] *Norwegian Standard NS 3473 E*, Norwey.

Nuclear Power Engineering Corporation of Japan (NUPEC) [1996] "Comparison report, seismic shear wall ISP, NUPEC's seismic ultimate dynamic response test", *Report No. NU-SSWISP-D014*, Organization for Economic Co-Operation and Development, Paris, France.

Okamura, H., Maekawa, K. [1991] *Nonlinear analysis and constitutive models of reinforced concrete*, Giho-do Press, University of Tokyo, Japan.

Palermo, D., Vecchio, F.J. [2003] "Compression field modelling of reinforced concrete subjected to reversed loading: formulation", *ACI Structural Journal*, Vol. 100, No. 5, pp. 616-625.

Pinto, A.V., Verzelletti, G., Negro, P., Guedes, J. [1995] *Cyclic testing of a squat bridge-pier - Report EUR 16247 EN*, Joint Research Center, European Commission, Ispra, Italy.

Pinto, A.V., Verzelletti, G., Pegon, P., Magonette, G., Negro, P., Guedes, J. [1996] *Pseudo-dynamic testing of large-scale R/C bridges - Report EUR 16378 EN*, Joint Research Center, European Commission, Ispra, Italy.

Popovics, S. [1973] "A numerical approach to the complete stress-strain curve of concrete", *Cement and Concrete Research*, Vol. 3, No. 5, pp. 583-599.

Priestley, M.J.N., Seible, F., Benzoni, G. [1994] "Seismic response of columns with low longitudinal steel ratios", *Structural System Research Project*, Report SSRP-94/08, University of California, San Diego, U.S.

Priestley, M.J.N., Verma, R., Xiao, Y. [1994] "Seismic shear strength of reinforced concrete columns", *Journal of Structural Engineering*, ASCE, Vol. 120, No. 8, pp. 2310-2239

Priestley, M.J.N., Seible, F., Calvi, G.M. [1996] *Seismic Design and retrofit of bridges*, John Wiley & Sons, New York, U.S., ISBN 0-471-57998-X.

Ramirez, J.A., Breen, J.E. [1991] "Evaluation of a modified truss-model approach for beam in shear", *Struct. J. Am. Concrete Inst.*, Vol. 88, No. 5, pp. 562-571.

Ritter, W. [1899] "Die Bauweise Hennebique", *Schweizerische Bauzeitung*, Zürich, Switzerland.

Schläich, J., Schafer, K., Jennewein, M. [1987] "Toward a consistent design of structural concrete", *Precast/Prestressed Concrete Institute Journal*, Vol. 32, No. 3, pp. 74-150.

Seckin, M. [1981] "Hysteretic behaviour of cast-in-place exterior beam-column sub-assemblies", *PhD thesis*, University of Toronto, Toronto, Canada.

Sezen, H., Moehle, J.P. [2004] "Shear Strength Model for Lightly Reinforced Concrete Columns", *Journal of Structural Engineering*, ASCE, Vol. 130, No. 11, pp. 1692-1703.

Sittipunt, W., Wood, S.L. [1995] "Influence of web reinforcement on the cyclic response of structural walls", *ACI Structural Journal*, Vol. 92, No. 6, pp. 745-756.

Standards Association of New Zealand [1982] *The design of concrete structure*, Wellington, New Zealand.

Takahashy, Y., Iemura, H., [2000] "Inelastic seismic performance of RC tall piers with hollow sections", *Proceedings of 12th World Conference on Earthquake Engineering*, Paper No. 1353, New Zealand.

Vecchio, F.J. [1989] "Nonlinear finite element analysis of reinforced concrete membranes", *ACI Structural Journal*, Vol. 86, No. 1, pp. 26-35.

Vecchio, F.J. [1989] "Towards cyclic load modelling of reinforced concrete", *ACI Structural Journal*, Vol. 96, No. 2, pp. 132-202.

Vecchio, F.J. [1990] "Reinforced concrete membrane element formulations", *Journal of Structural Engineering*, ASCE, Vol. 116, No. 3, pp. 730-750.

Vecchio, F.J. [1992] "Finite element modelling of concrete expansion and confinement", *Journal of Structural Engineering*, ASCE, Vol. 118, No. 9, pp. 2390-2406.

Vecchio, F.J., Collins, M.P. [1986] "The modified compression-field theory for reinforced concrete elements subjected to shear", *ACI Journal*, Vol. 83, No. 2, pp. 219-231.

Wong, Y.L., Paulay, T., Priestley, M.J.N. [1993] "Response of circular reinforced concrete columns to multi-directional seismic attack", *ACI Structural Journal*, Vol. 90, No. 2, pp. 180-191.

Yeh, Y.K., Mo, Y.L., & Yang, C.Y. (2002) "Seismic performance of rectangular hollow bridge columns", ASCE Journal of Structural Engineering, Vol. 128, No. 1, pp. 60-68.

TABLES

PART A

Table 1 Mechanical properties of reinforcement steel (average values)

Nominal Bar Diameter [mm]	Number of Tests	Average Bar Diameter [mm]	f_y [MPa]	f_u [MPa]	ε_u [%]
Φ5	7	4.7	699.5	730.9	1.6
Φ8	4	8.2	503.4	563.0	12.3
Φ12	4	11.9	558.2	646.8	12.8
Φ14	4	13.8	477.2	577.7	13.0

Table 2 Mechanical properties of concrete (average values)

Cubic Compressive strength [MPa] (16 tests)	Tensile Strength [MPa] Brazilian Test (5 tests)	Initial Tangent Modulus [GPa]
35.4	3.1	29.4

Table 3 Values of the parameters of the model implemented in Castem2000 [Maillard, 1993] for confined concrete referred to the flanges of the section of the medium pier of bridge B232

A_h [mm²]	l_w [mm]	b_0 [mm]	h_0 [mm]	ω_w	α
19.64	2860	779	139	0.1969	0.642
β	$f_{c,c}$ [N/mm2]	$\varepsilon_{c1,c}$	Z		
1.2831	39.4	0.00441	28.8		

Table 4 Values of the parameters of the Mander's model for the confined concrete. They refer to the concrete in the flanges of the section of the medium pier of the bridge B232

A_{sw2} [mm²]	A_{sw3} [mm²]	b_{02} [mm]	b_{03} [mm]	ρ_2 [%]	ρ_3 [%]
157.1	39.3	779	139	0.336	0.471
α_n	α_s	α	σ_{e2} [N/mm²]	σ_{e3} [N/mm²]	σ_e [N/mm²]
0.768	0.754	0.579	1.361	1.908	1.612
$f'_{c,c}/f'_c$	$\varepsilon_{c1,c}$	E_{sec} [N/mm²]	E_c [N/mm²]	r	
1.324	0.00524	7757	30800	1.337	

Table 5 Stress and deformation characteristics of concrete according to prEN 1992-1-1 [CEN, 2003]: f_{ck} and f_{cm} are the characteristic and mean values of the compressive strength, respectively; f_{ctm} is the mean value of the tensile strength and E_{cm} is the mean value of the modulus of elasticity

	C25	C30	C35
f_{ck} [MPa]	25	30	35
f_{cm} [MPa][1]	33	38	43
f_{ctm} [MPa]	2.6	2.9	3.2
E_{cm} [GPa]	31	32	34

[1] $f_{cm} = 8 + f_{ck}$

Table 6 Stress and deformation characteristics of steel reinforcement according to prEN 1998-2 E.2.2 [CEN, 2003]: f_{yk} and f_{ym} are the characteristic and mean values of the yield stress, respectively. ε_{uk} and ε_{um} are the characteristic and mean values of elongation at maximum strength, respectively

Tempcore B500B	
f_{yk} [MPa]	500
f_{ym} [MPa]	$1.15 \cdot f_{yk}$
ε_{um}	ε_{uk}

Table 7 With reference to Figure 21, steel reinforcement diameter (mm) as a function of bar spacing i and rlongitudinal reinforcement ratio ρ_L; only bar diameters between 16mm and 32mm have been accepted.

	ρ_L				
i [mm]	0.005	0.010	0.020	0.030	0.040
100	11	16	23	28	32
150	14	20	28	34	39
200	16	23	32	39	45

Table 8 Allowed distances (mm), in the horizontal plane, between two consecutive engaged rebars for the case $v_k \leq 0.2$

	ρ_L				
i [mm]	**0.005**	**0.010**	**0.020**	**0.030**	**0.040**
100	-	100 200	100 200	100 200	100 200
150	-	150	150	-	-
200	200	200	200	-	-

Table 9 Allowed distance (mm), in the horizontal plane, between two consecutive engaged rebars for the case $v_k > 0.2$

	ρ_L				
i [mm]	**0.005**	**0.010**	**0.020**	**0.030**	**0.040**
100	-	100	100	100	100
150	-	-	-	-	-
200	-	-	-	-	-

Table 10 Allowed spacing (mm), along the vertical direction, for transverse reinforcement for the case $v_k \leq 0.2$

	ρ_L				
i [mm]	**0.005**	**0.010**	**0.020**	**0.030**	**0.040**
100	-	80	113	138	160
150	-	98	138	-	-
200	80	113	160	-	-

Table 11 Allowed spacing (mm), along the vertical direction, for transverse reinforcement for the case $v_k > 0.2$

	ρ_L				
i [mm]	**0.005**	**0.010**	**0.020**	**0.030**	**0.040**
100	-	68	683	68	68
150	-	68	68	-	-
200	68	68	68	-	-

Table 12 Values of the factor α_n defined according to Equation (3.16) for the case $v_k \leq 0.2$

	ρ_L				
i [mm]	**0.005**	**0.010**	**0.020**	**0.030**	**0.040**
100	-	0.902 0.804	0.902 0.804	0.902 0.804	0.902 0.804
150	-	0.853	0.864	-	-
200	0.804	0.804	0.804	-	-

Table 13 Values of factor α_s defined according to Equation (3.17) for the case $v_k \leq 0.2$

	ρ_L				
***i* [mm]**	**0.005**	**0.010**	**0.020**	**0.030**	**0.040**
100	-	0.847 0.847	0.787 0.787	0.742 0.742	0.704 0.704
150	-	0.814	0.742	-	-
200	0.847	0.787	0.704	-	-

Table 14 Values of the confinement effectivness factor α evaluated according to Equation (3.15) for the case $v_k \leq 0.2$

	ρ_L				
***i* [mm]**	**0.005**	**0.010**	**0.020**	**0.030**	**0.040**
100	-	0.764 0.681	0.710 0.633	0.669 0.596	0.635 0.566
150	-	0.695	0.641	-	-
200	0.681	0.633	0.566	-	-

Table 15 Values of factor α_n defined according to Equation (3.16) for the case $v_k > 0.2$

	ρ_L				
***i* [mm]**	**0.005**	**0.010**	**0.020**	**0.030**	**0.040**
100	-	0.902	0.902	0.902	0.902
150	-	-	-	-	-
200	-	-	-	-	-

Table 16 Values of factor α_s defined according to Equation (3.17) for the case $v_k > 0.2$

	ρ_L				
***i* [mm]**	**0.005**	**0.010**	**0.020**	**0.030**	**0.040**
100	-	0.869	0.869	0.869	0.869
150	-	0.869	0.869	-	-
200	0.869	0.869	0.869	-	-

Table 17 Values of the confinement effectiveness factor α evaluated according to Equation (3.15) for the case $v_k > 0.2$

	ρ_L				
***i* [mm]**	**0.005**	**0.010**	**0.020**	**0.030**	**0.040**
100	-	0.784	0.784	0.784	0.784
150	-	-	-	-	-
200	-	-	-	-	-

Table 18 Transverse reinforcement rebar sizes (mm) for the case $\nu_k \leq 0.2$

	ρ_L									
i [mm]	**0.005**	**0.010**		**0.020**		**0.030**		**0.040**	
100	-	6	8	8	11	10	14	11	16
150	-	8		12		-		-	
200	8	11		16		-		-	

Table 19 Transverse reinforcement ratios for the case $\nu_k \leq 0.2$

	ρ_L									
i [mm]	**0.005**	**0.010**		**0.020**		**0.030**		**0.040**	
100	-	0.003	0.003	0.004	0.004	0.005	0.005	0.006	0.006
150	-	0.004		0.005		-		-	
200	0.003	0.004		0.006		-		-	

Table 20 Coefficients of Equations (3.26) and (3.27), as given in Table 6.1 of prEN 1998-2 [CEN, 2003].

Seismic behaviour	λ	$\omega_{w,\min}$
Ductile	0.37	0.18
Limited ductile	0.28	0.12

Table 21 Confinement pressure and confinement parameter for different shear reinforcement ratios and classes of concrete

	ρ_w		σ_e [MPa]		λc	
	min	max	min	max	min	max
C25	0.003	0.018	1.23	6.27	1.24	1.94
C30	0.003	0.016	1.23	7.18	1.21	1.93
C35	0.003	0.014	1.23	8.08	1.19	1.93

Table 22 Values of the parameters considered in the parametric analysis

Parameter values	
Wall thickness [m]	0.40
Concrete	C25 C30 C35
H/B	1.0 1.5 2.0 2.5 3.0
steel	Tempcore B500B
ρ_L	0.005 0.010 0.020 0.030 0.040
ν_k	0.10 0.20 0.30 0.40
λ_c	1.0 1.2 1.3 1.4 1.6 1.8 2.0

PART B

Table 23 Values of θ and β for members containing at least the required minimum amount of stirrups

$\frac{v_{xy}}{f'_c}$	$\varepsilon_x \cdot 10^3$										
	-0.20	-0.10	-0.05	0	0.125	0.25	0.50	0.75	1.00	1.50	2.00
0.075	22.3° 6.32	20.4° 4.75	21.0° 4.10	21.8° 3.75	24.3° 3.24	26.6° 2.94	30.5° 2.59	33.7° 2.38	36.4° 2.23	40.8° 1.95	43.9° 1.67
0.100	18.1° 3.79	20.4° 3.38	21.4° 3.24	22.5° 3.14	24.9° 2.91	27.1° 2.75	30.8° 2.50	34.0° 2.32	36.7° 2.18	40.8° 1.93	43.1° 1.69
0.125	19.9° 3.18	21.9° 2.99	22.8° 2.94	23.7° 2.87	25.9° 2.74	27.9° 2.62	31.4° 2.42	34.4° 2.26	37.0° 2.13	41.0° 1.90	43.2° 1.67
0.150	21.6° 2.88	23.3° 2.79	24.2° 2.78	25.0° 2.72	26.9° 2.60	28.8° 2.52	32.1° 2.36	34.9° 2.21	37.3° 2.08	40.5° 1.82	42.8° 1.61
0.175	23.2° 2.73	24.7° 2.66	25.5° 2.65	26.2° 2.60	28.0° 2.52	29.7° 2.44	32.7° 2.28	35.2° 2.14	36.8° 1.96	39.7° 1.71	42.2° 1.54
0.200	24.7° 2.63	26.1° 2.59	26.7° 2.52	27.4° 2.51	29.0° 2.43	30.6° 2.37	32.8° 2.14	34.5° 1.94	36.1° 1.79	39.2° 1.61	41.7° 1.47
0.225	26.1 2.53	27.3 2.45	27.9 2.42	28.5 2.40	30.0 2.34	30.8 2.14	32.3 1.86	34.0 1.73	35.7 1.64	38.8 1.51	41.4 1.39
0.250	27.5 2.39	28.6 2.39	29.1 2.33	29.7 2.33	30.6 2.12	31.3 1.93	32.8 1.70	34.3 1.58	35.8 1.50	38.6 1.38	41.2 1.29

FIGURES

PART A

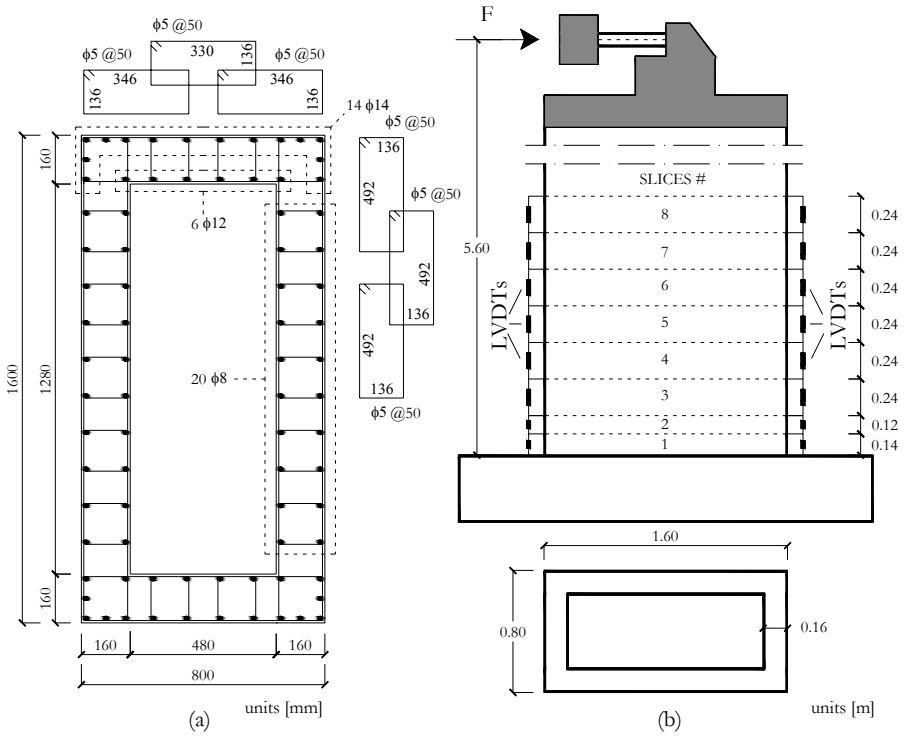

Figure 1 (a) Reinforcement layout of the pier section; (b) Geometric characteristics of the pier and instrumentation placement

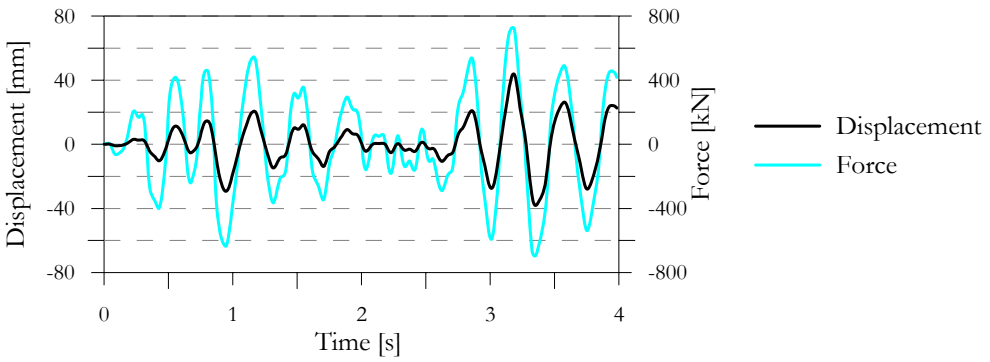

Figure 2 Displacement and force time-history applied at the top of the pier in the horizontal direction during the first PSD test (bridge subjected to the design earthquake)

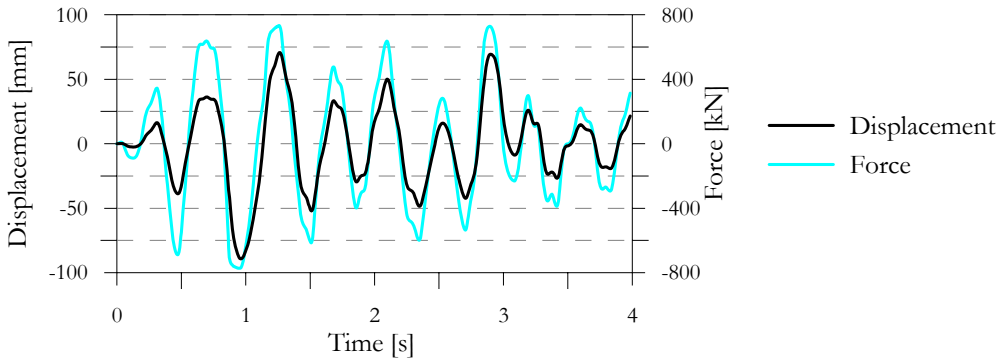

Figure 3 Displacement and force time-history applied at the top of the pier in the horizontal direction during the second PSD test (bridge subjected to two time the design earthquake)

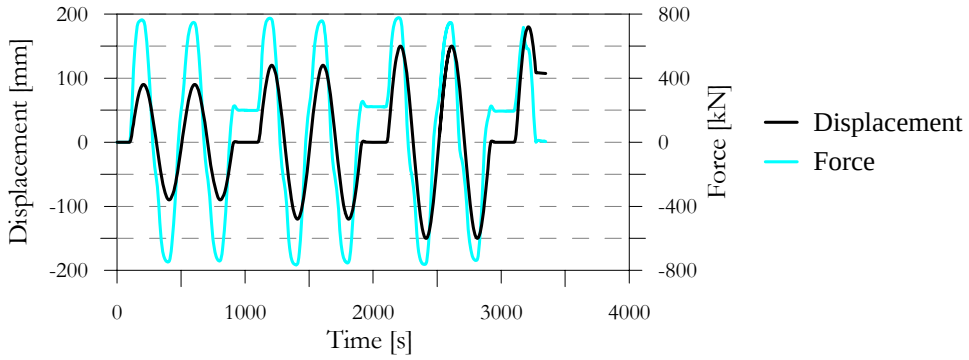

Figure 4 Displacement and force time-history applied at the top of the pier in the horizontal direction during the cyclic test

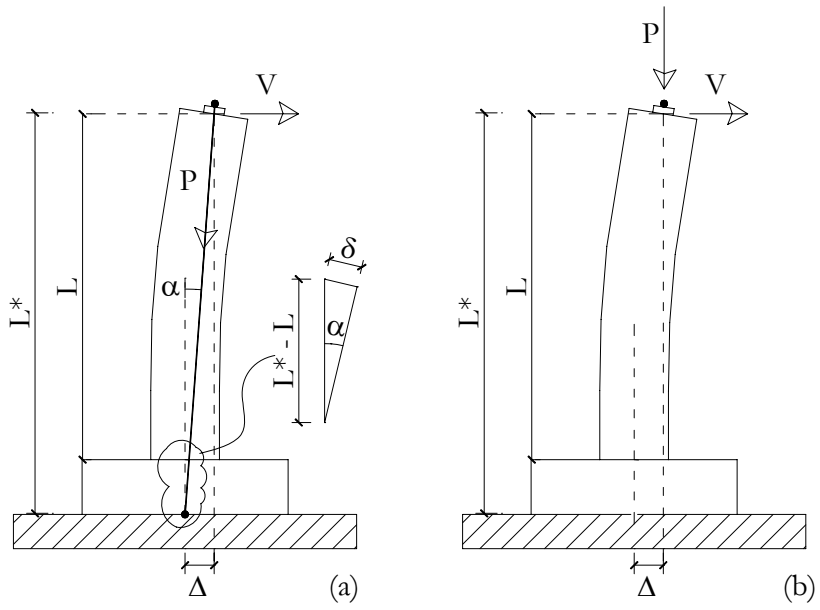

Figure 5 Application of the vertical load to the pier: (a) post-tensioning method; (b) correct approach needed for testing

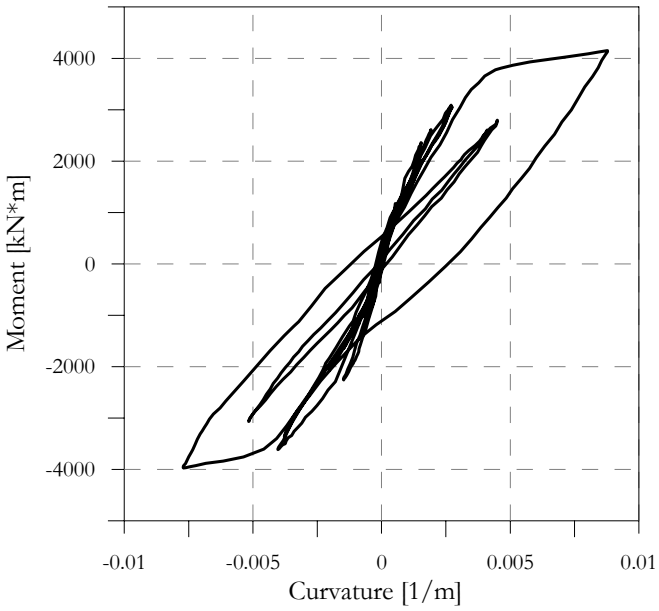

Figure 6 Moment-curvature plot of the response of the pier to the design earthquake at slice #1

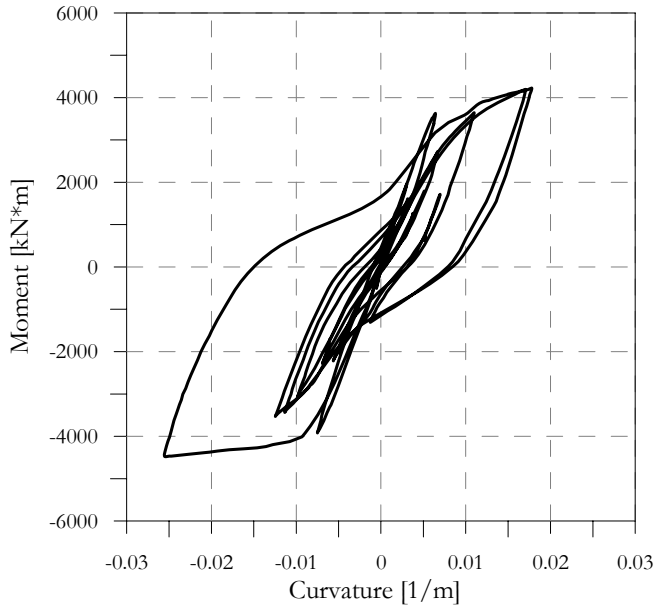

Figure 7 Moment-curvature plot of the response of the pier to two time the design earthquake at slice #1

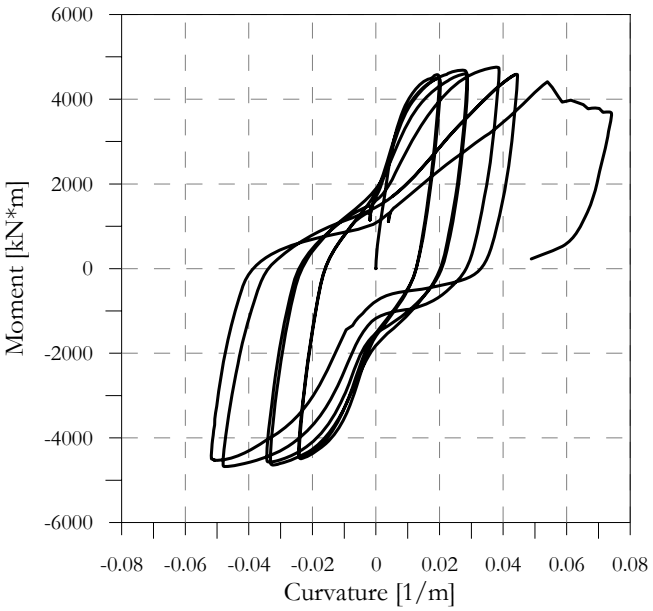

Figure 8 Moment-curvature plot of the response of the pier to the cyclic excitation at slice #1

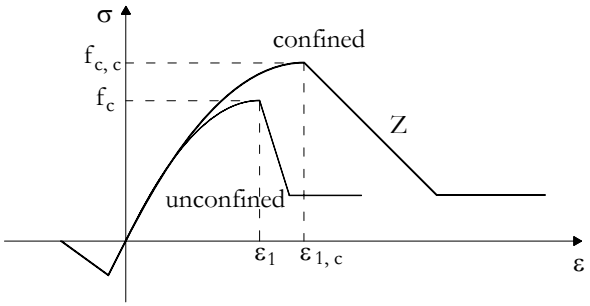

Figure 9 Concrete model for monotonic loading

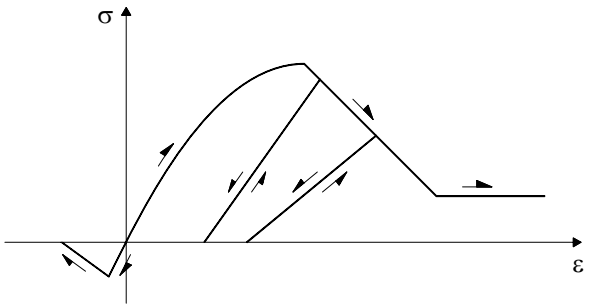

Figure 10 Concrete model for cyclic loading

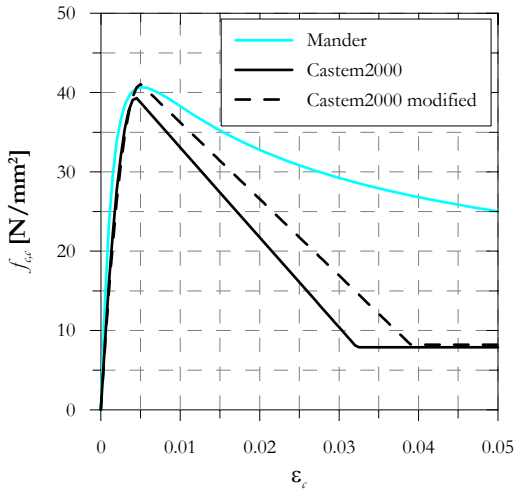

Figure 11 Comparison between Mander's model and Castem 2000 [Maillard, 1993] model for the confined concrete in the flanges of the section of the medium pier of bridge B232

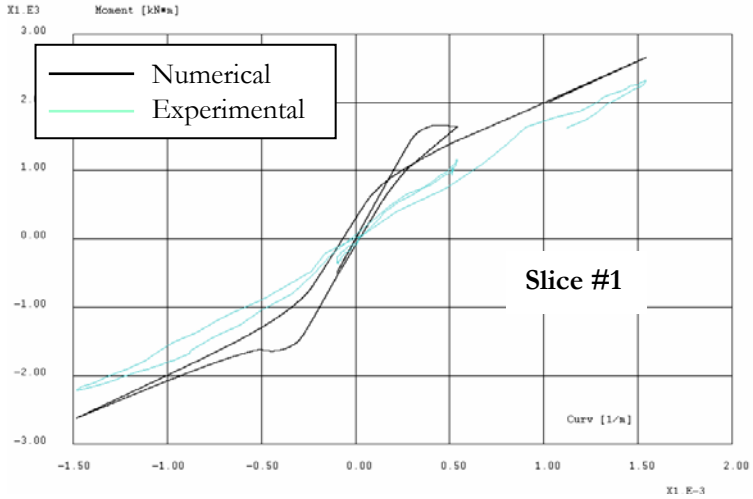

Figure 12 Comparison between the numerical and experimental results relative to slice #1 of the pier when subjected to the first few seconds of the design earthquake

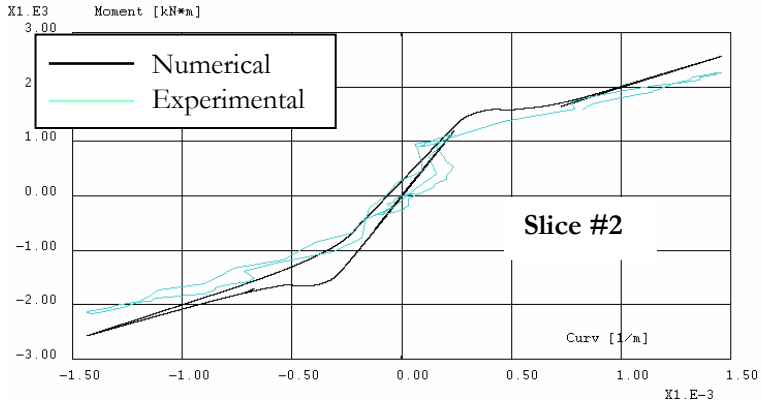

Figure 13 Comparison between the numerical and experimental results relative to slice #2 of the pier when subjected to the first few seconds of the design earthquake

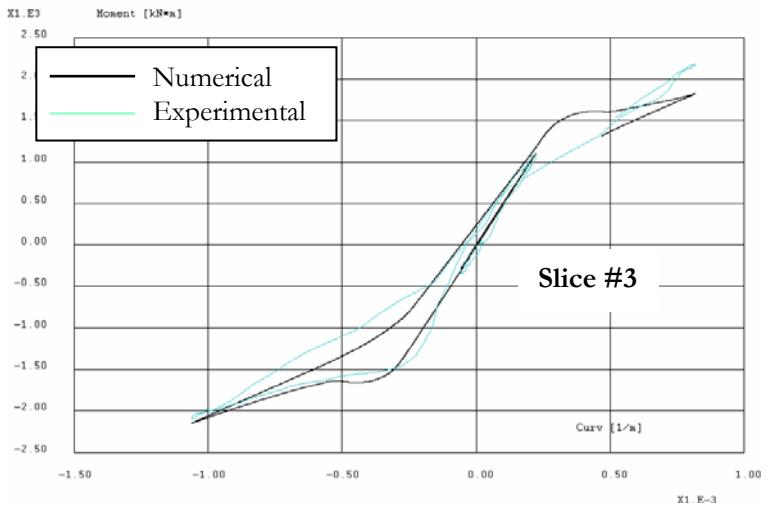

Figure 14 Comparison between the numerical and experimental results relative to slice #3 of the pier when subjected to the first few seconds of the design earthquake

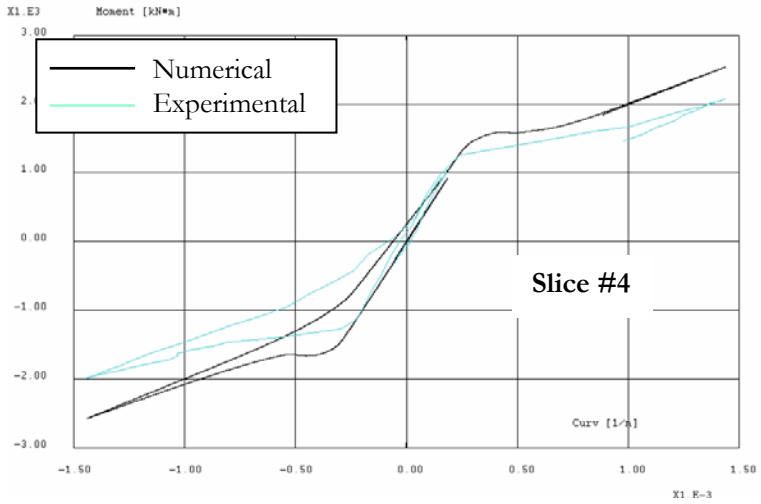

Figure 15 Comparison between the numerical and experimental results relative to slice #4 of the pier when subjected to the first few seconds of the design earthquake

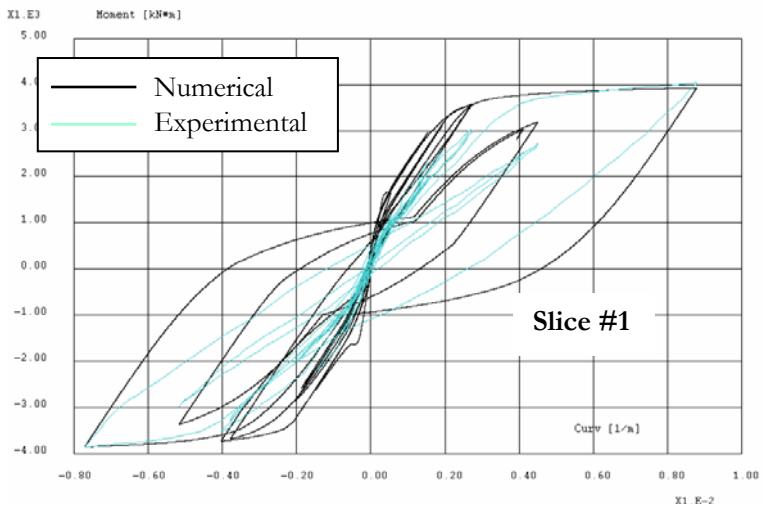

Figure 16 Comparison between the numerical and experimental results relative to slice #1 of the pier when subjected to the entire duration of the design earthquake

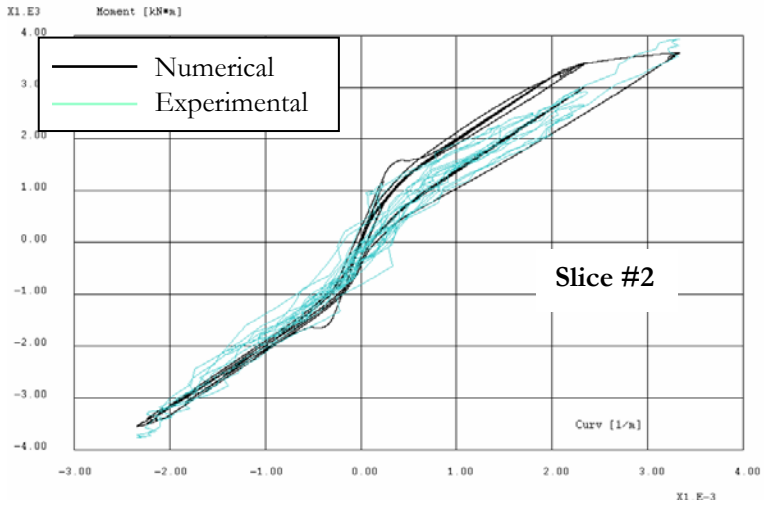

Figure 17 Comparison between the numerical and experimental results relative to slice #2 of the pier when subjected to the entire duration of the design earthquake

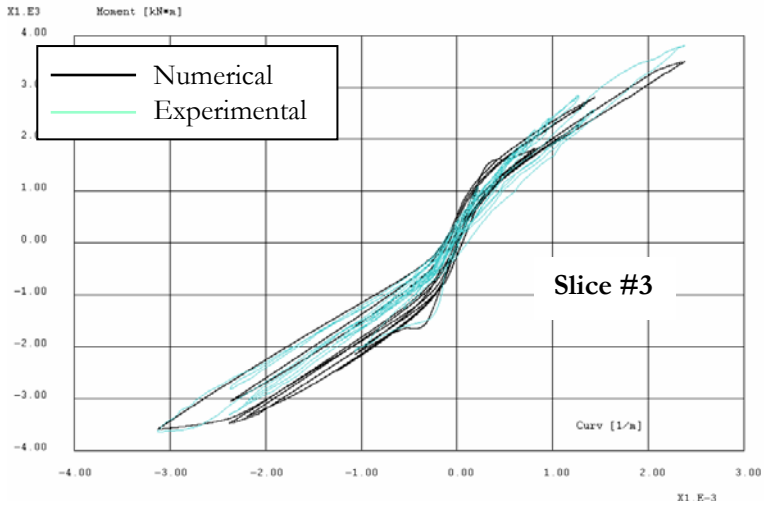

Figure 18 Comparison between the numerical and experimental results relative to slice #3 of the pier when subjected to the entire duration of the design earthquake

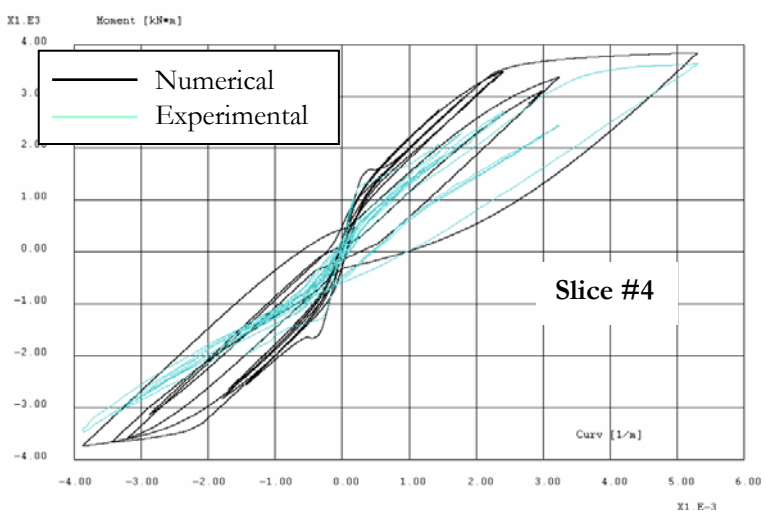

Figure 19 Comparison between the numerical and experimental results relative to slice #4 of the pier when subjected to the entire duration of the design earthquake

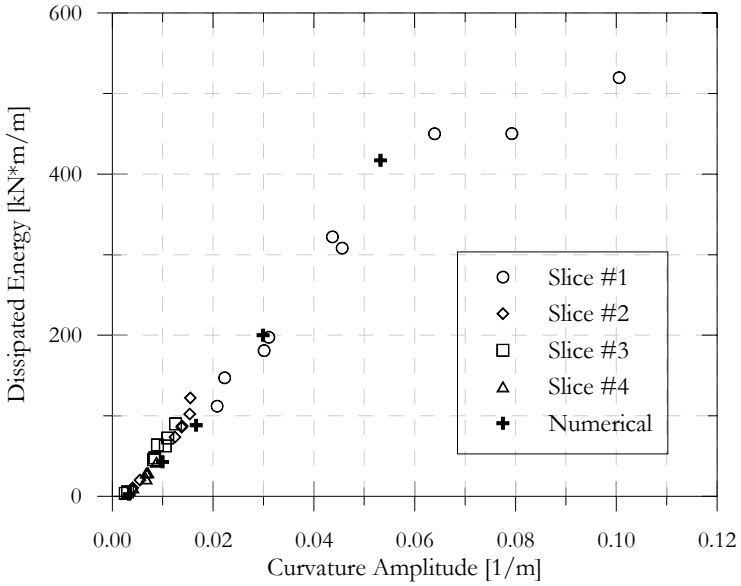

Figure 20 Comparison between the energy dissipated per cycle by the numerical model and by the sections belonging to different pier slices for cyclic tests of increasing amplitude

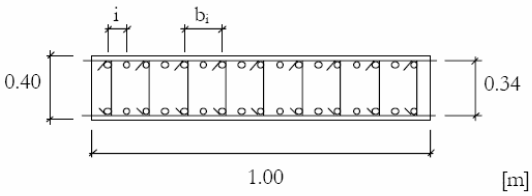

Figure 21 Typical section of the bridge pier wall considered in the parametric analysis

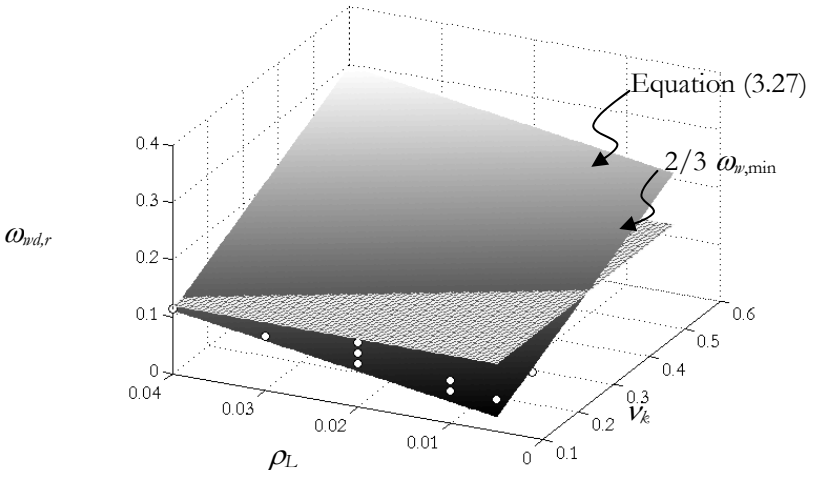

Figure 22 Plot of Equation (3.27) which gives the minimum amount of confining transverse reinforcement when ν_k > 0.20. The white dots represent the minimum amount of transverse reinforcement against buckling requested by prEN 1998-2 when $\nu_k \leq 0.20$. It is evident that when $\nu_k \leq 0.20$ the provisions against buckling are more stringent than the confining provisions

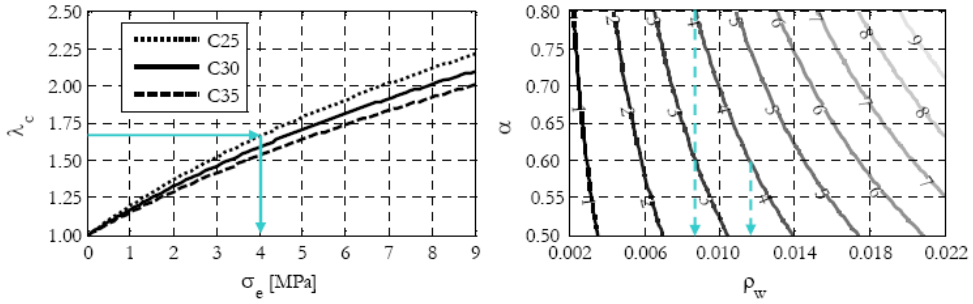

Figure 23 Evaluation of the range of transverse reinforcement ratio values ρ_w corresponding to a given value of the confinement parameter λ_c

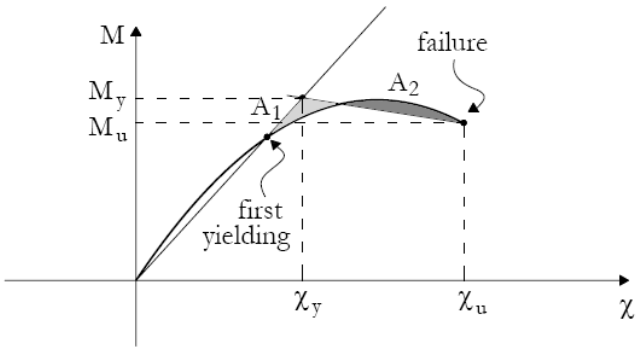

Figure 24 Construction of the bilinear approximation of the nonlinear skeleton curve of the pier section behaviour

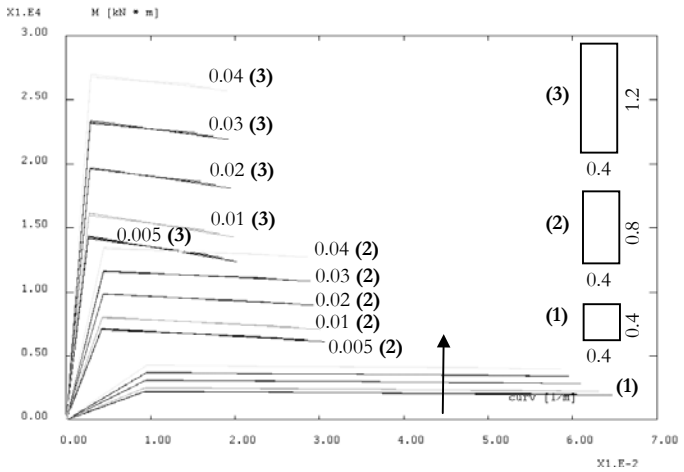

Figure 25 Bilinear skeleton curves corresponding to sections characterized by different aspect ratios (section depth and width are expressed in m) and different longitudinal reinforcement ratios. The remaining parameters are common to all the sections: concrete C25, ν_k = 0.60, λ_c = 1.4

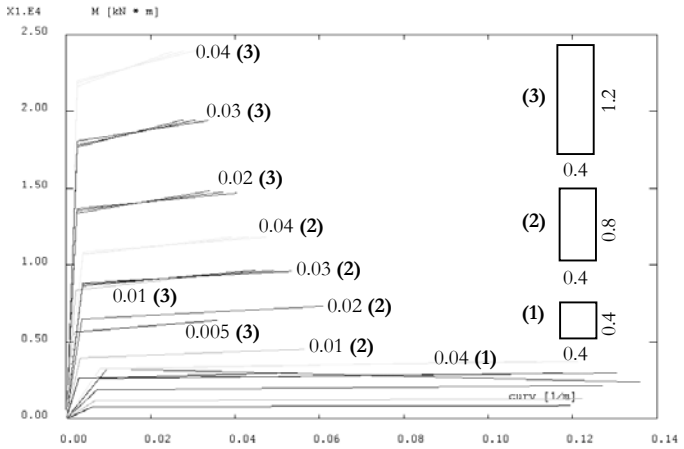

Figure 26 Bilinear skeleton curves corresponding to sections characterized by different aspect ratios (section depth and width are expressed in m) and different longitudinal reinforcement ratios. The remaining parameters are common to all the sections: concrete C25, ν_k = 0.10, λ_c = 1.4

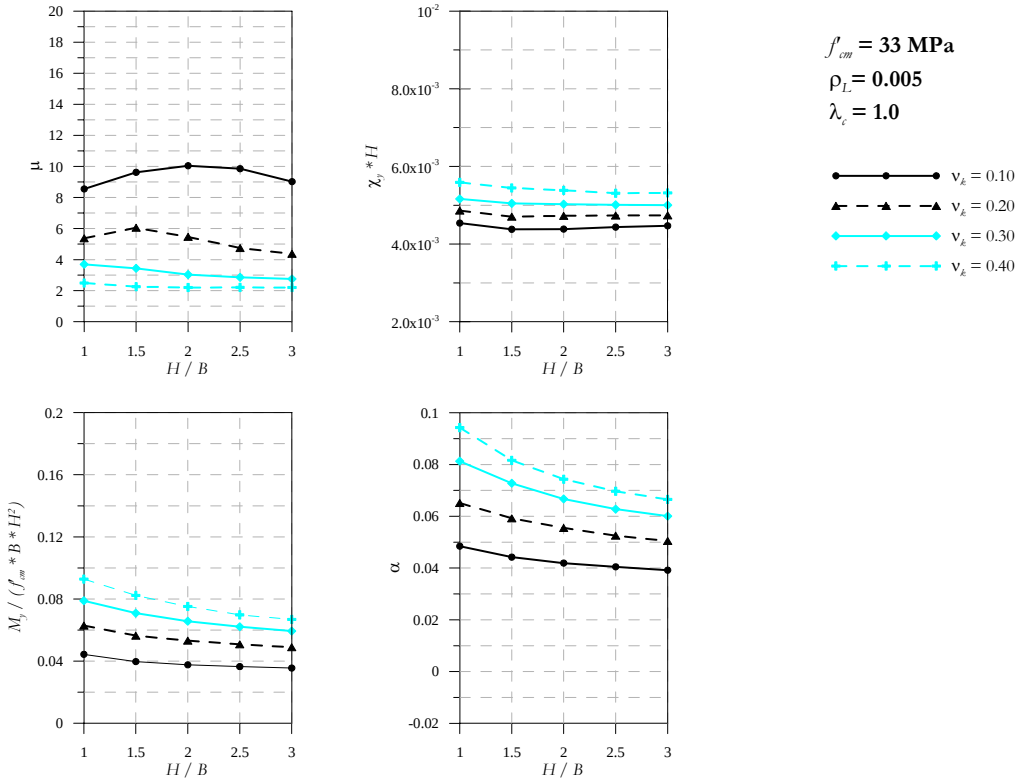

Figure 27 Results of the parametric analysis (f'_{cm} = 33 MPa, ρ_L = 0.005, λ_c = 1.0)

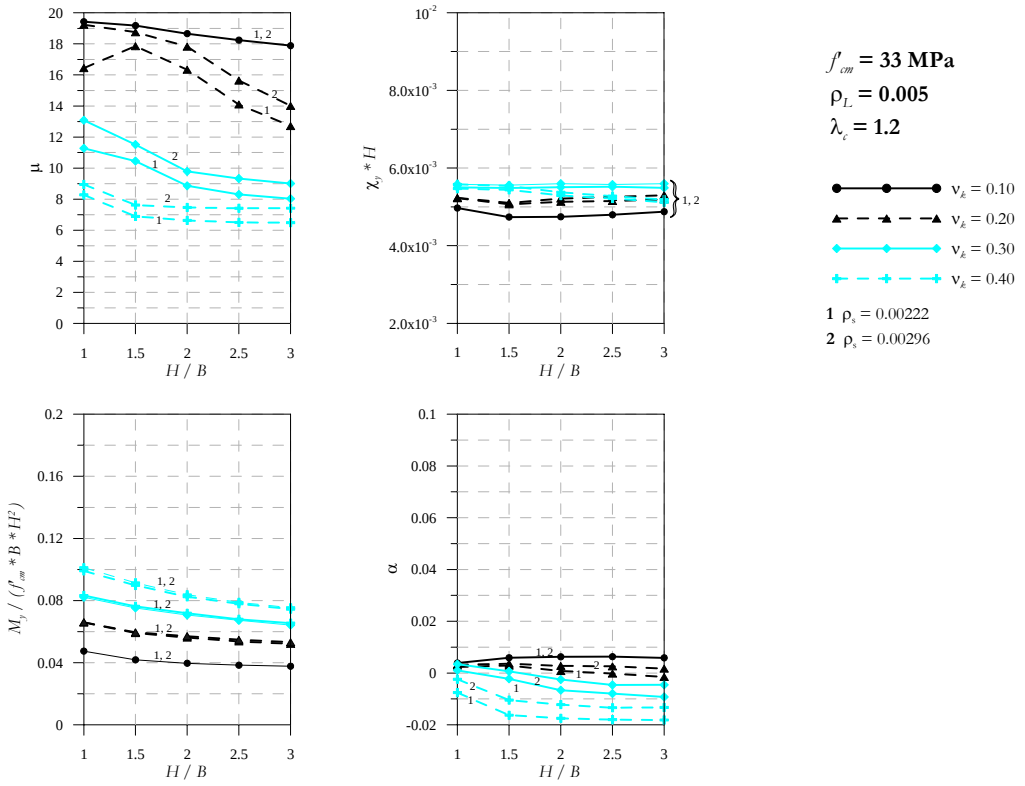

Figure 28 Results of the parametric analysis (f'_{cm} = 33 MPa, ρ_L = 0.005, λ_c = 1.2)

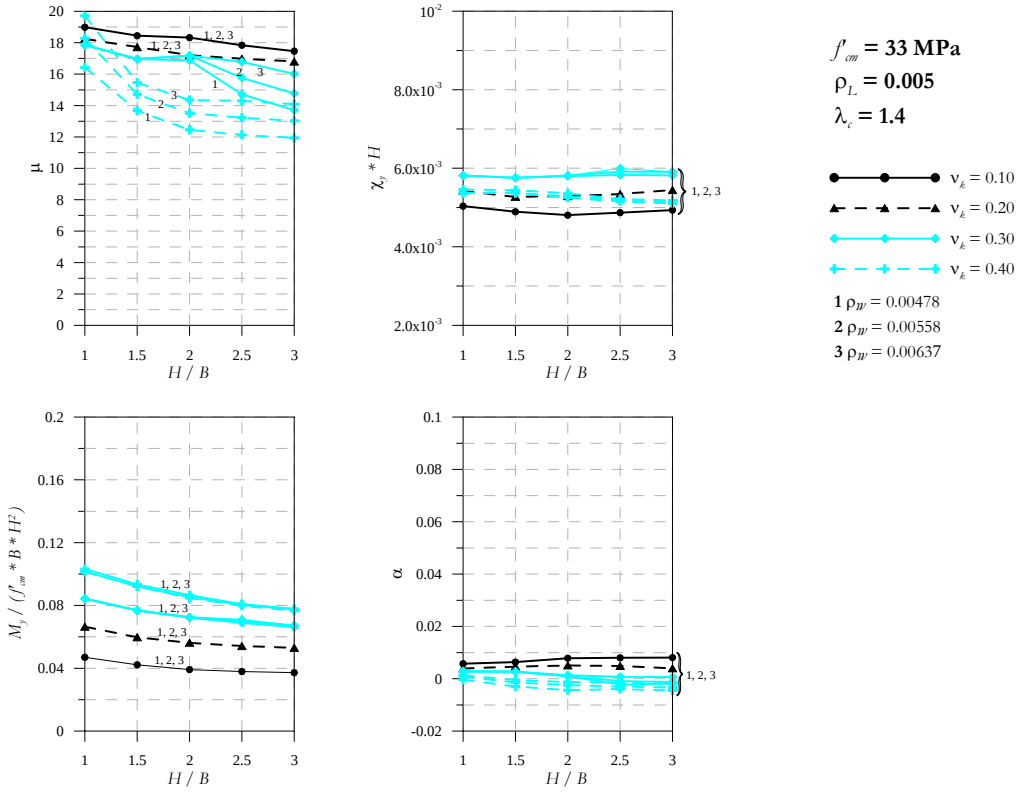

Figure 29 Results of the parametric analysis (f'_{cm} = 33 MPa, ρ_L = 0.005, λ_c = 1.4)

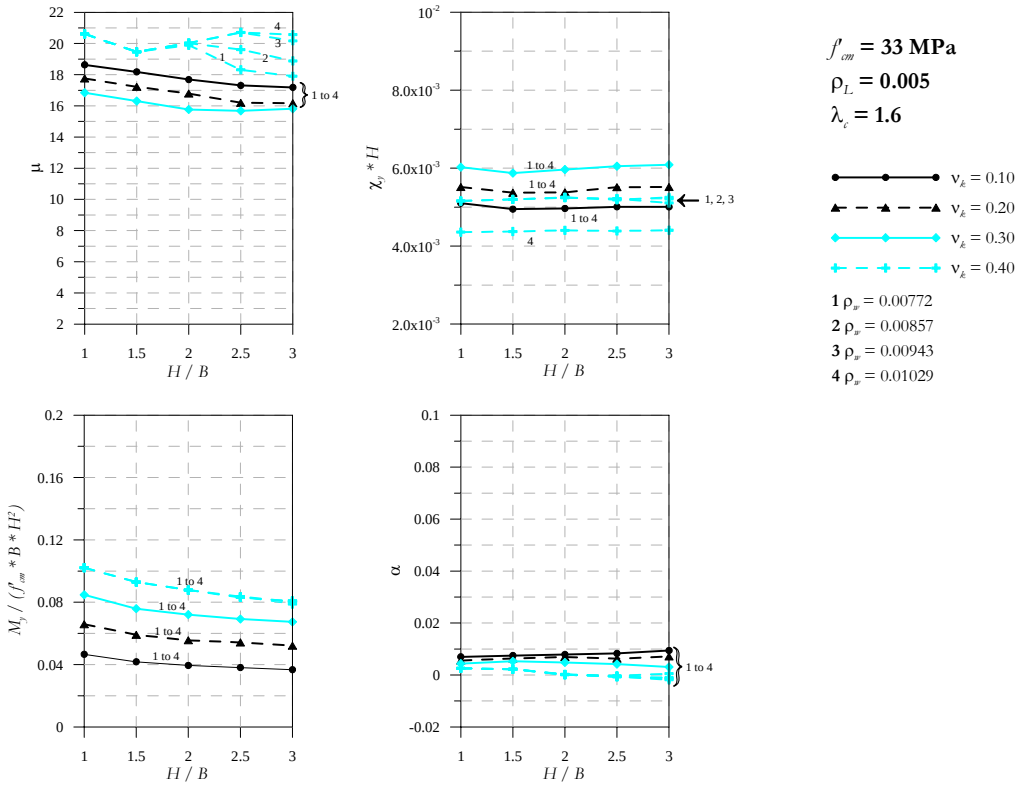

Figure 30 Results of the parametric analysis (f'_{cm} = 33 MPa, ρ_L = 0.005, λ_c = 1.6)

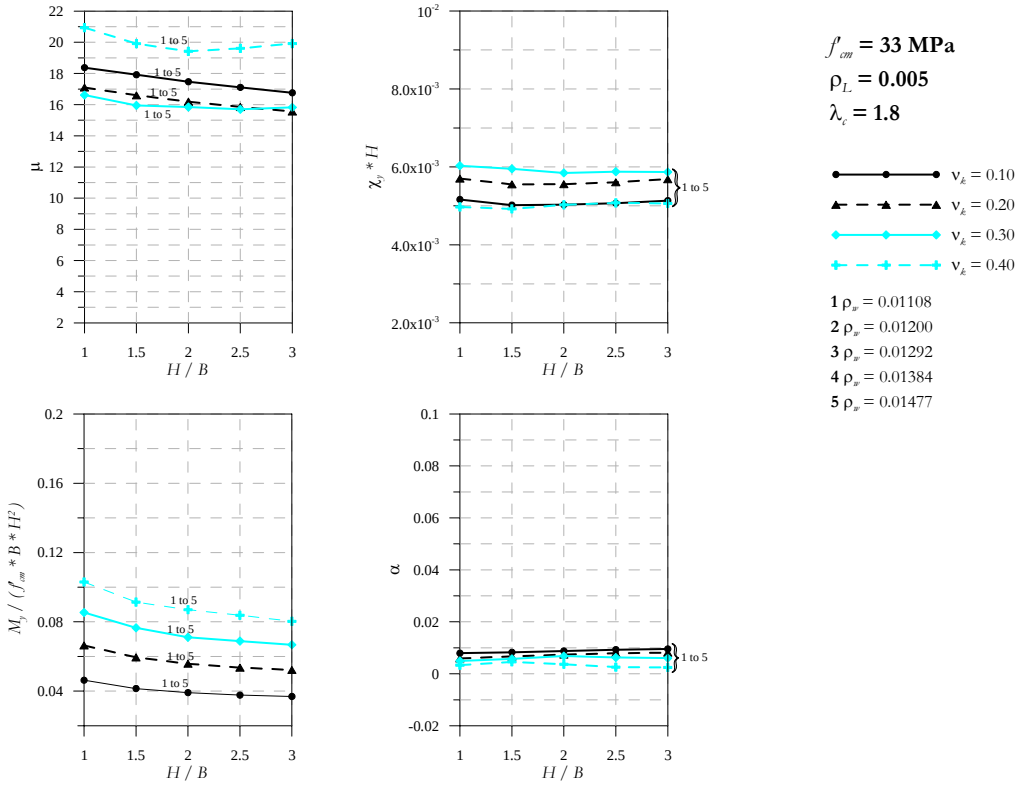

Figure 31 Results of the parametric analysis (f'_{cm} = 33 MPa, ρ_L = 0.005, λ_c = 1.8)

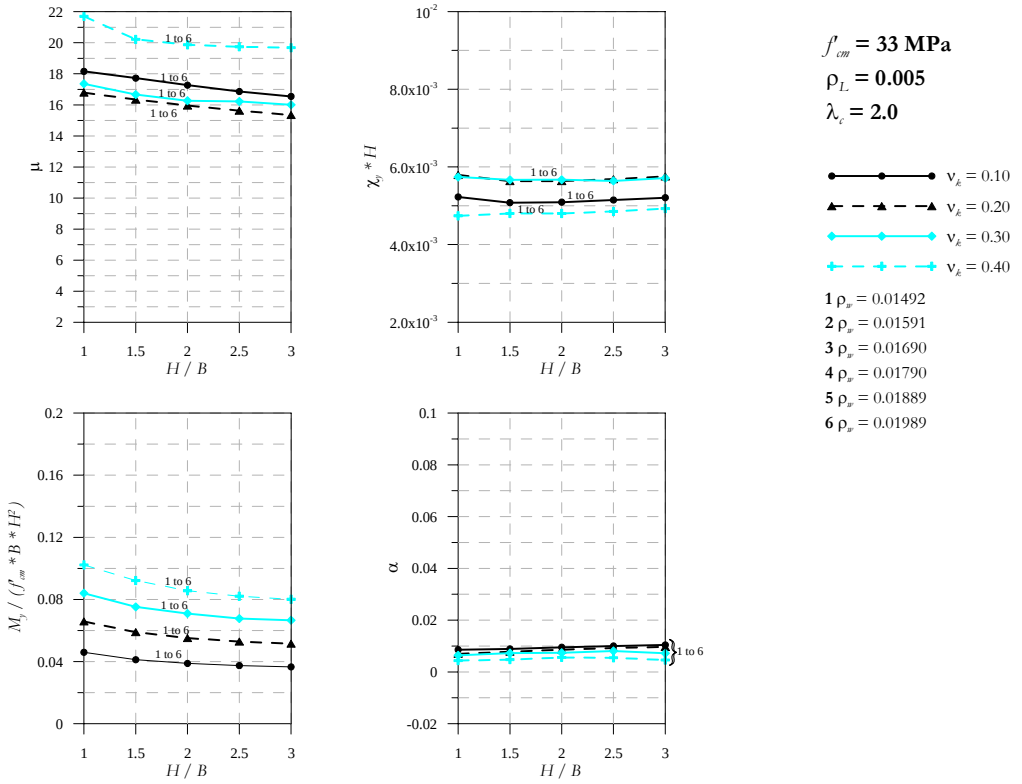

Figure 32 Results of the parametric analysis (f'_{cm} = 33 MPa, ρ_L = 0.005, λ_c = 2.0)

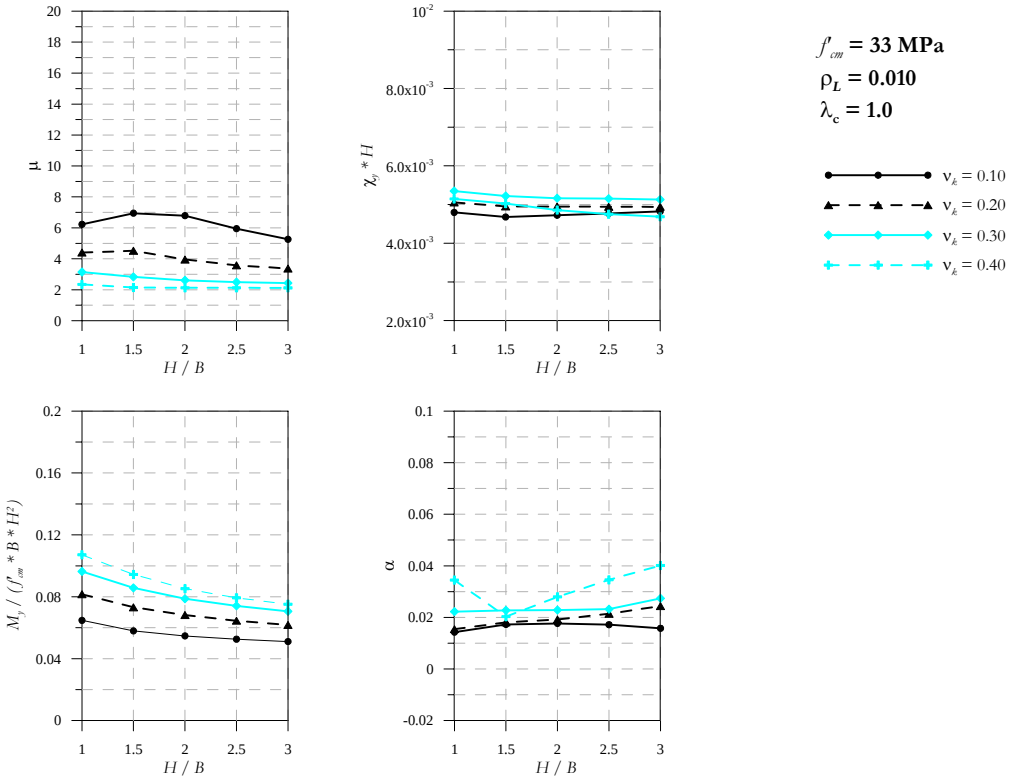

Figure 33 Results of the parametric analysis (f'_{cm} = 33 MPa, ρ_L = 0.010, λ_c = 1.0)

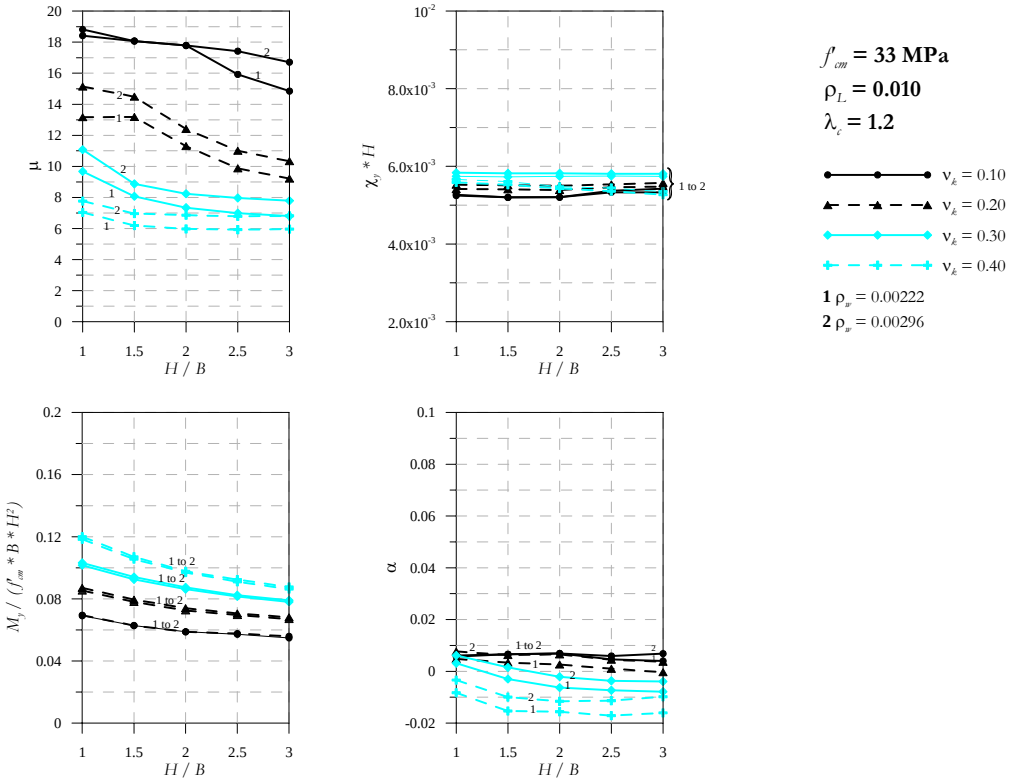

Figure 34 Results of the parametric analysis (f'_{cm} = 33 MPa, ρ_L = 0.010, λ_c = 1.2)

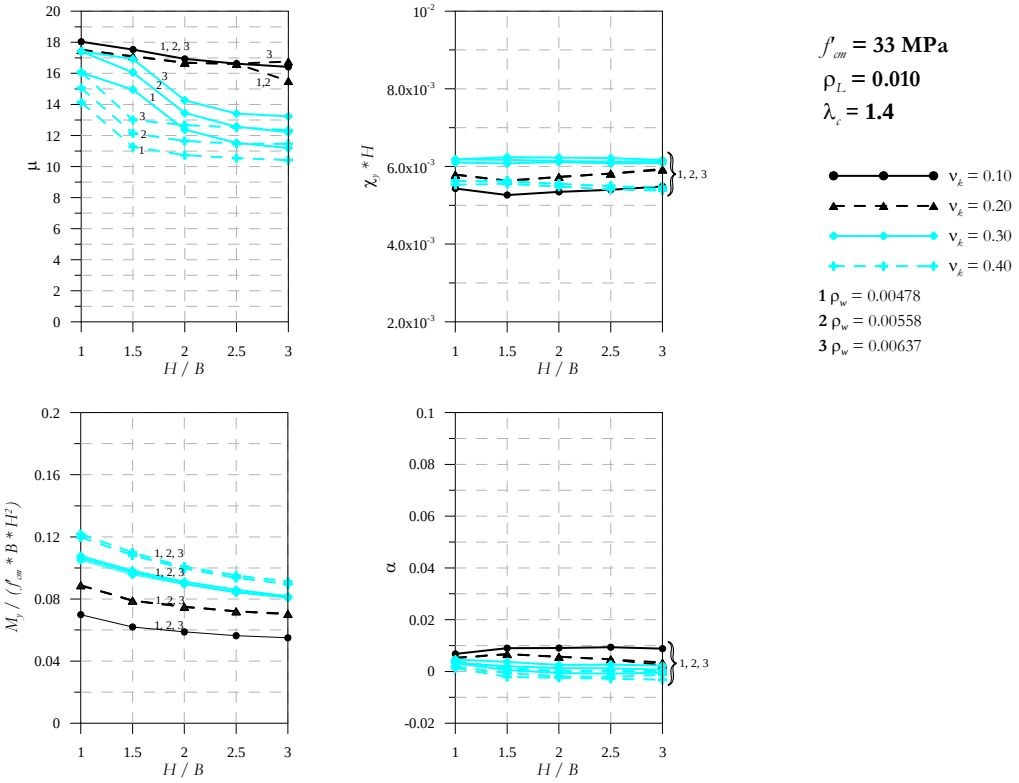

Figure 35 Results of the parametric analysis (f'_{cm} = 33 MPa, ρ_L = 0.010, λ_c = 1.4)

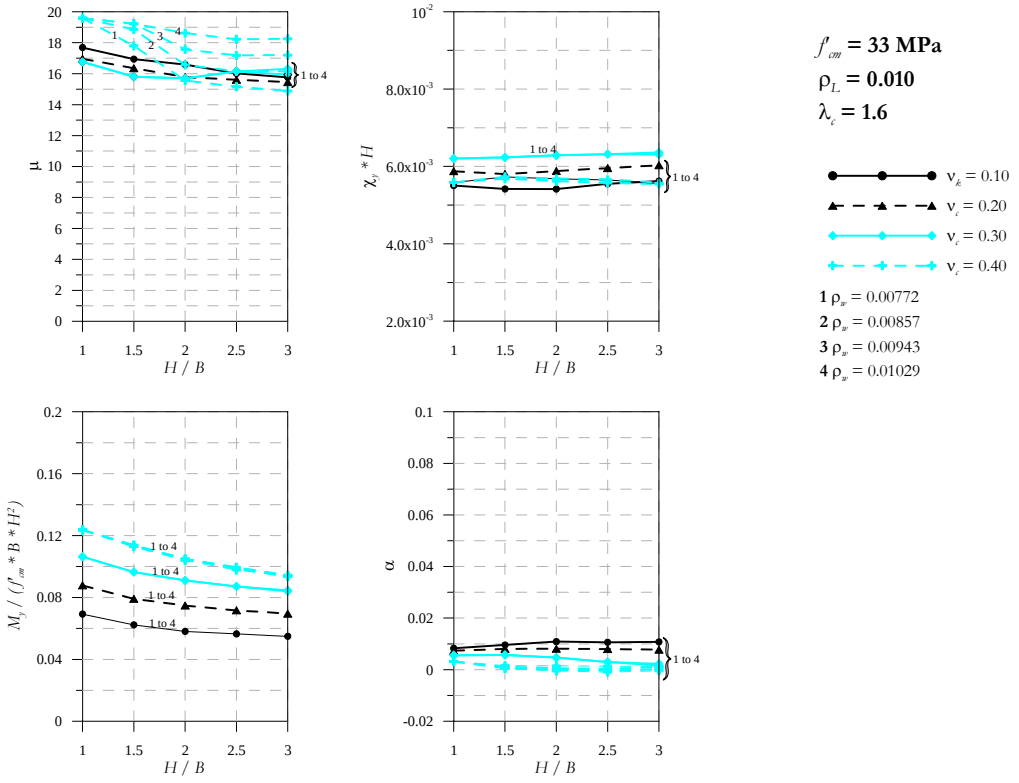

Figure 36 Results of the parametric analysis (f'_{cm} = 33 MPa, ρ_L = 0.010, λ_c = 1.6)

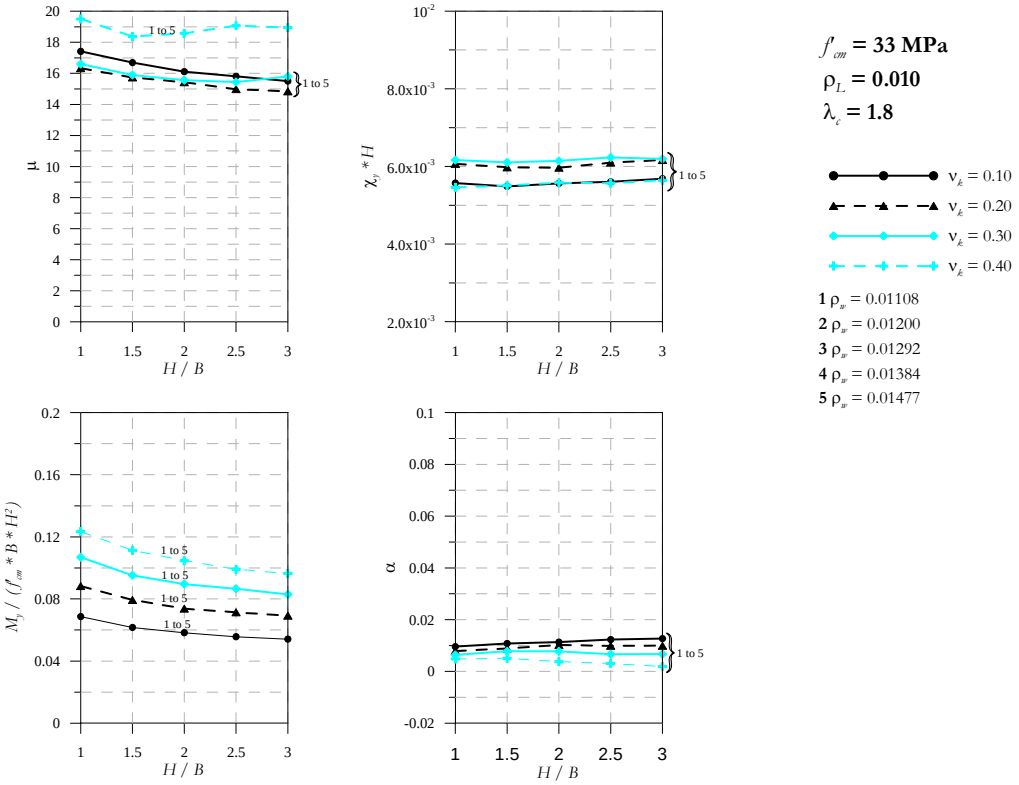

Figure 37 Results of the parametric analysis (f'_{cm} = 33 MPa, ρ_L = 0.010, λ_c = 1.8)

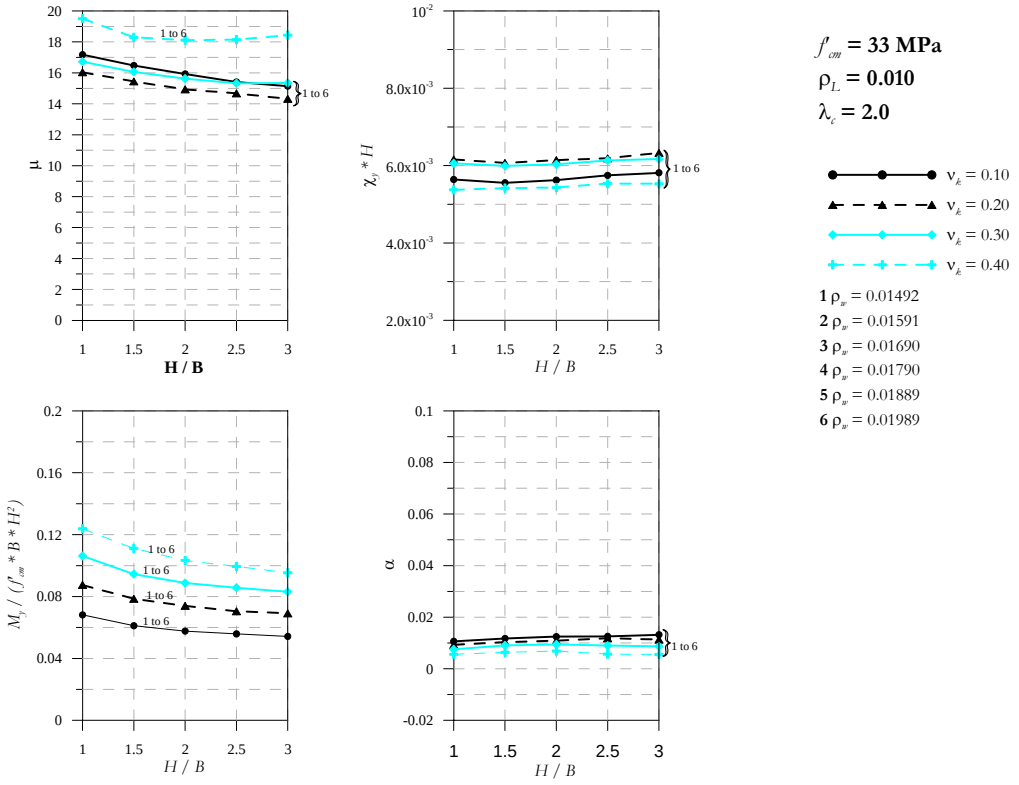

Figure 38 Results of the parametric analysis (f'_{cm} = 33 MPa, ρ_L = 0.010, λ_c = 2.0)

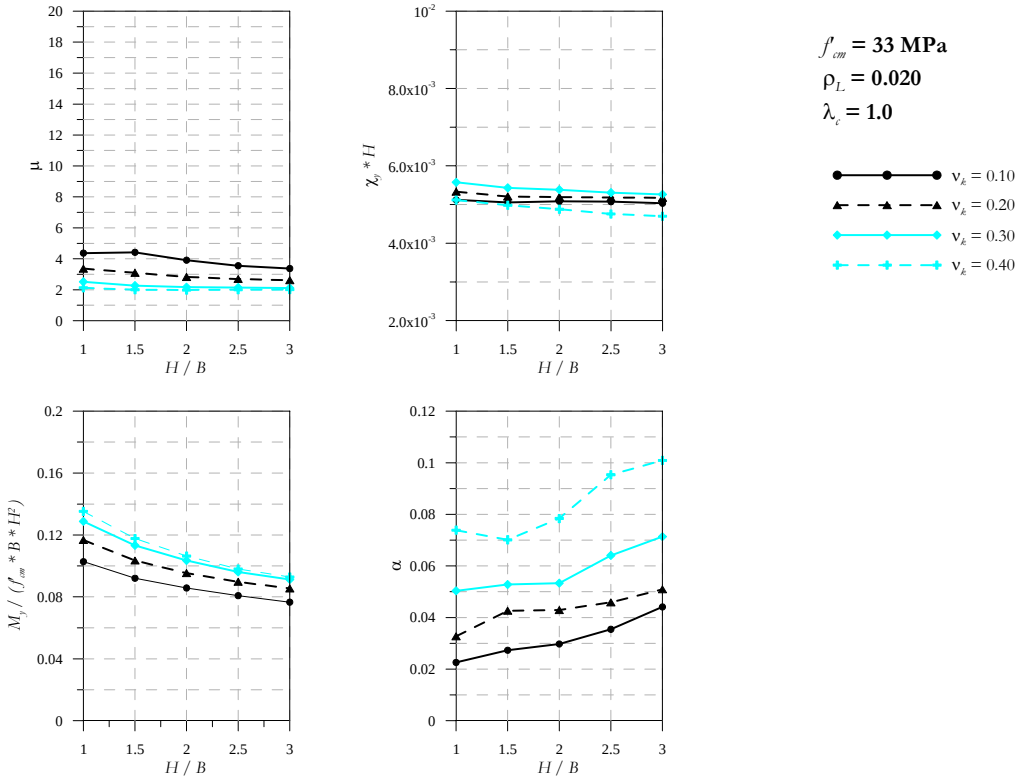

Results of the parametric analysis (f'_{cm} = 33 MPa, ρ_L = 0.020, λ_c = 1.0)

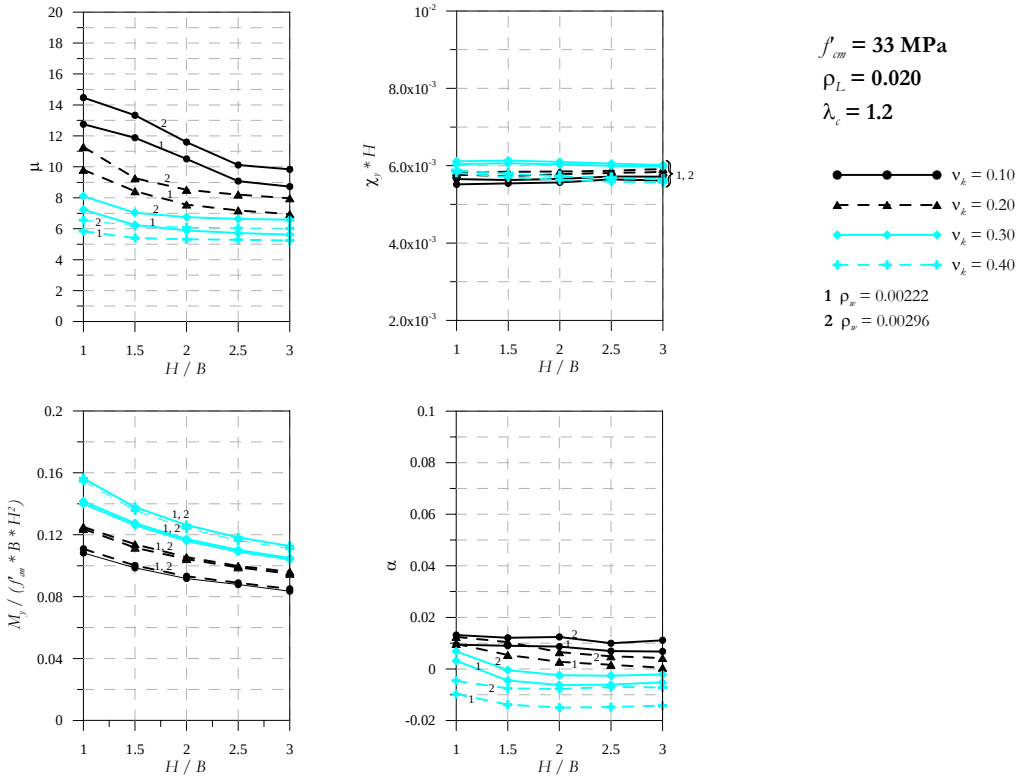

Figure 39 Results of the parametric analysis (f'_{cm} = 33 MPa, ρ_L = 0.020, λ_c = 1.2)

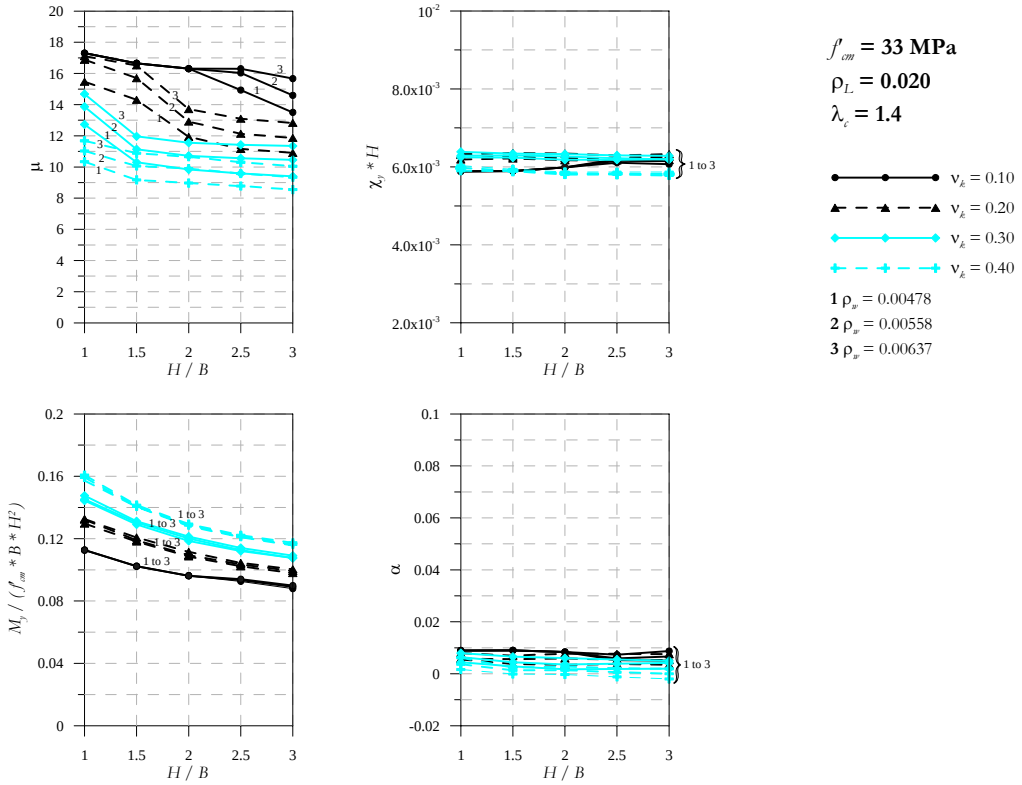

Figure 40 Results of the parametric analysis (f'_{cm} = 33 MPa, ρ_L = 0.020, λ_c = 1.4)

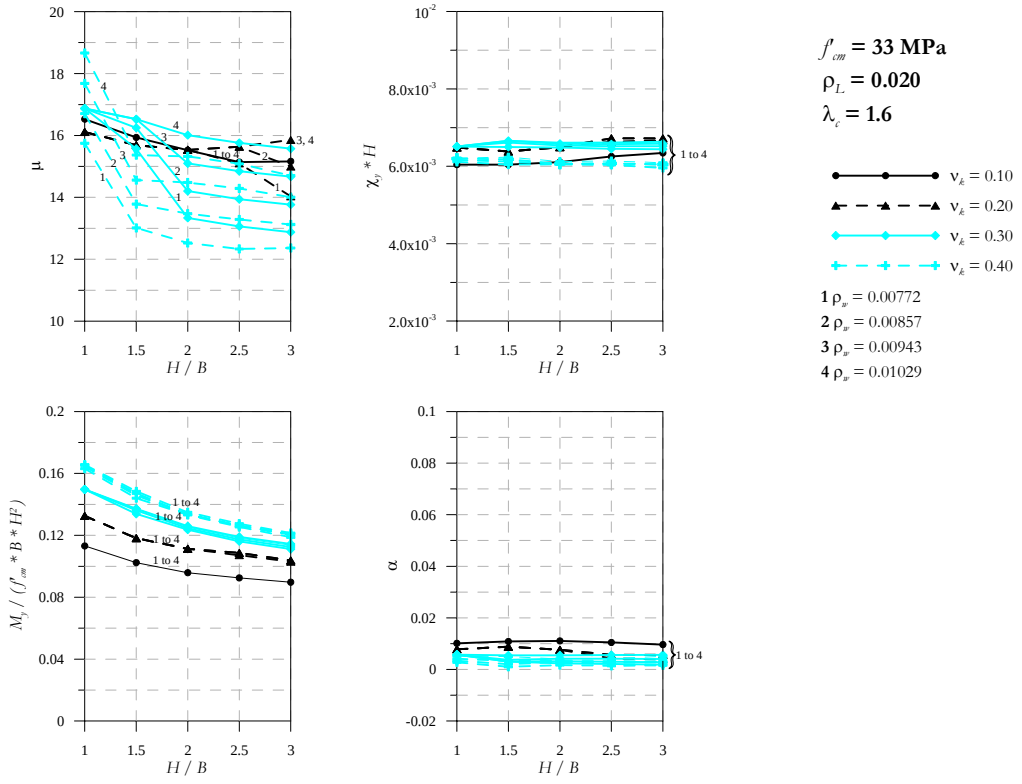

Figure 41 Results of the parametric analysis (f'_{cm} = 33 MPa, ρ_L = 0.020, λ_c = 1.6)

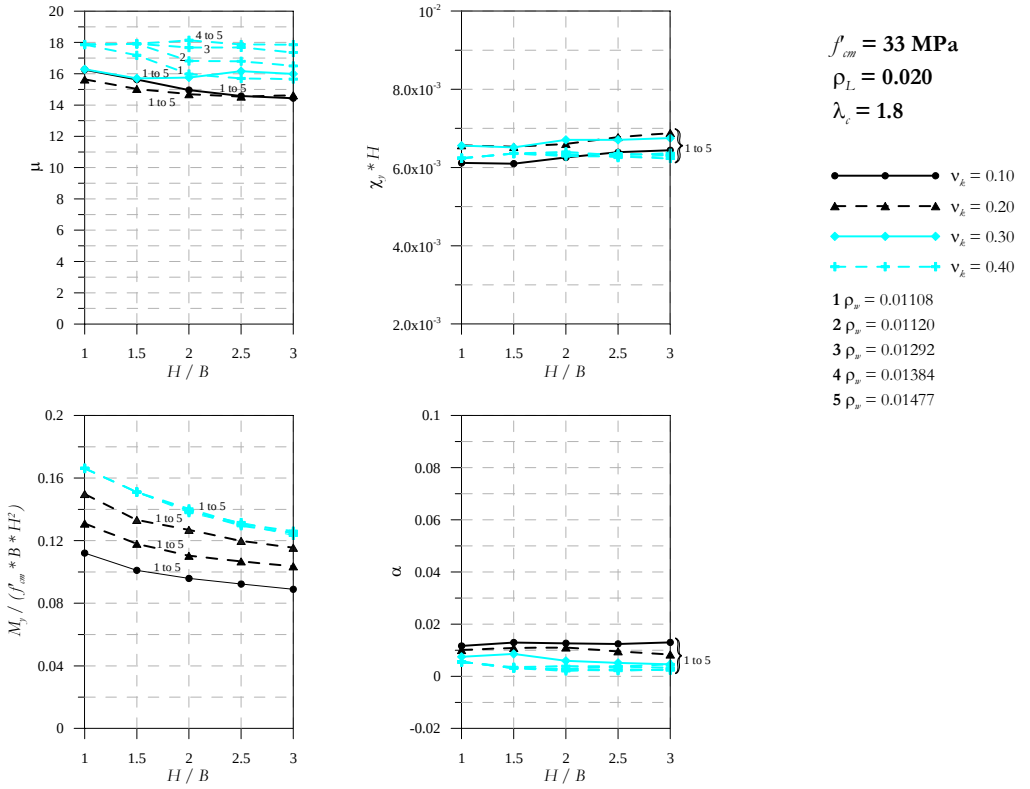

Figure 42 Results of the parametric analysis (f'_{cm} = 33 MPa, ρ_L = 0.020, λ_c = 1.8)

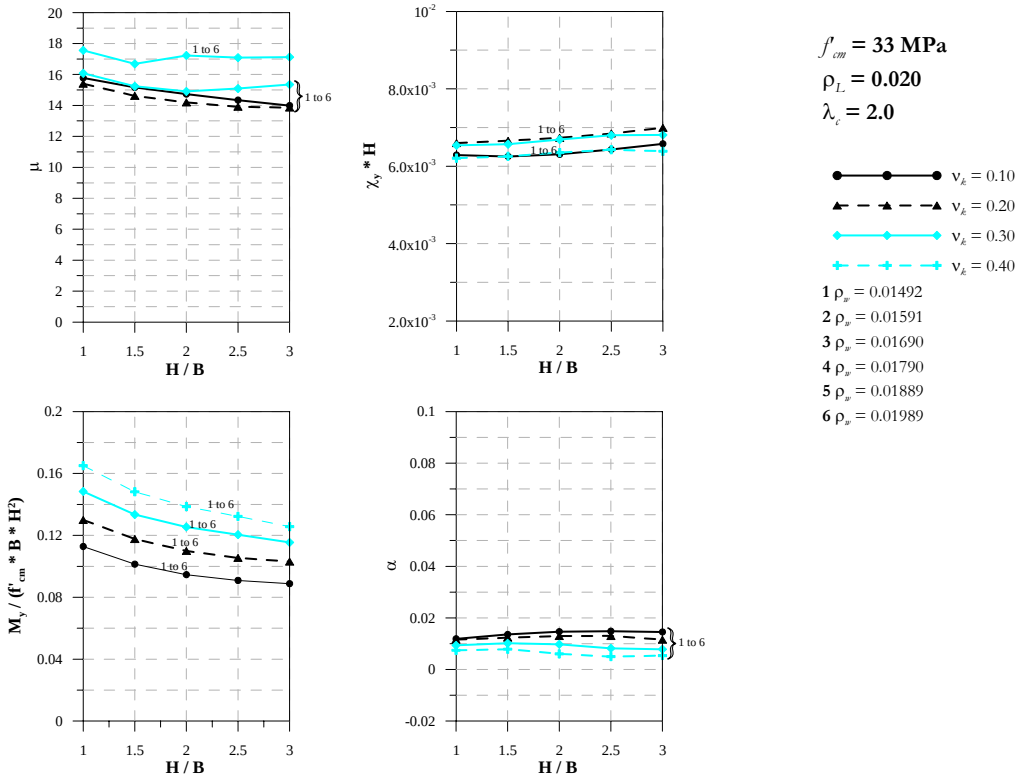

Figure 43 Results of the parametric analysis (f'_{cm} = 33 MPa, ρ_L = 0.020, λ_c = 2.0)

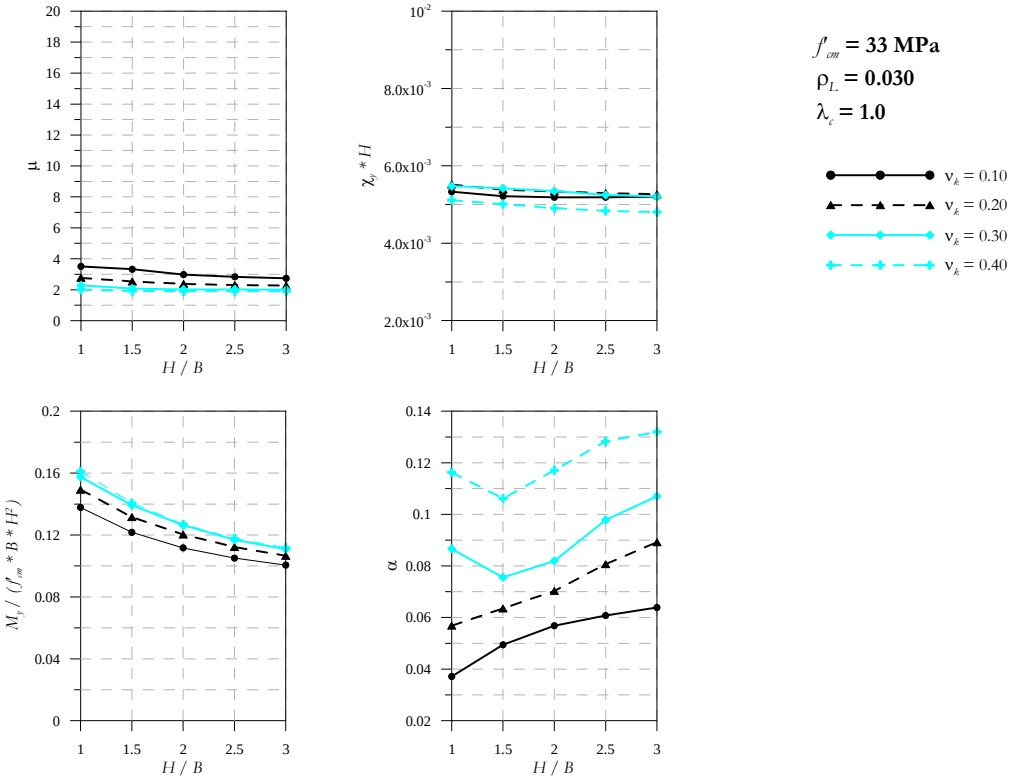

Figure 44 Results of the parametric analysis (f'_{cm} = 33 MPa, ρ_L = 0.030, λ_c = 1.0)

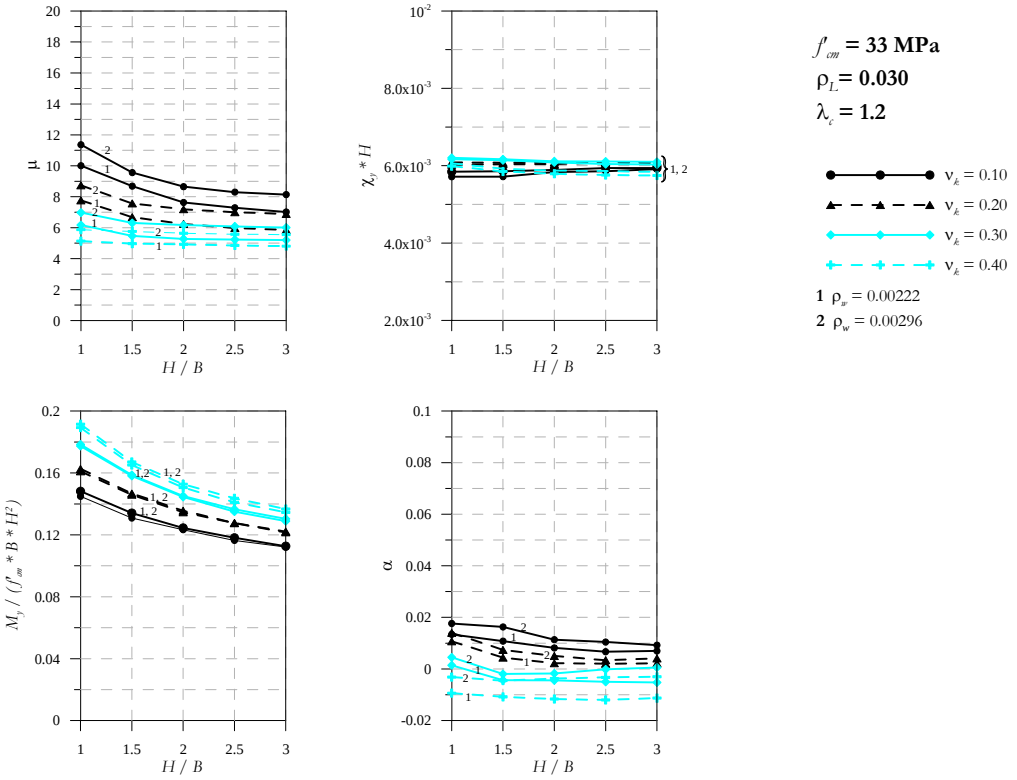

Figure 45 Results of the parametric analysis (f'_{cm} = 33 MPa, ρ_L = 0.030, λ_c = 1.2)

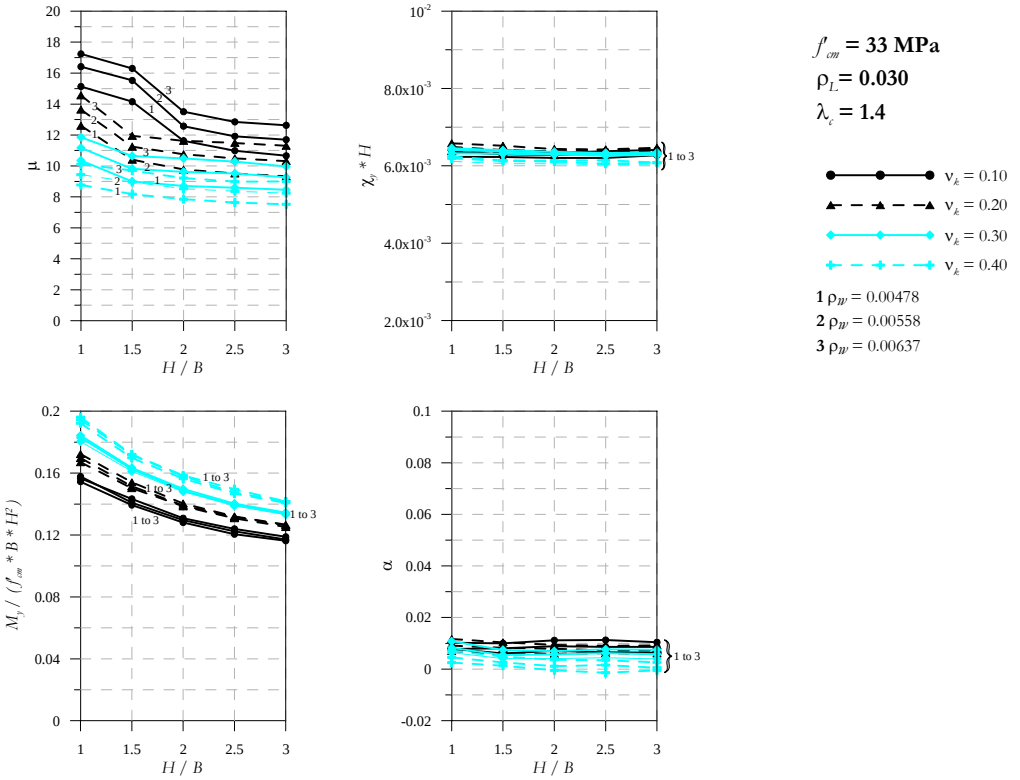

Figure 46 Results of the parametric analysis (f'_{cm} = 33 MPa, ρ_L = 0.030, λ_c = 1.4)

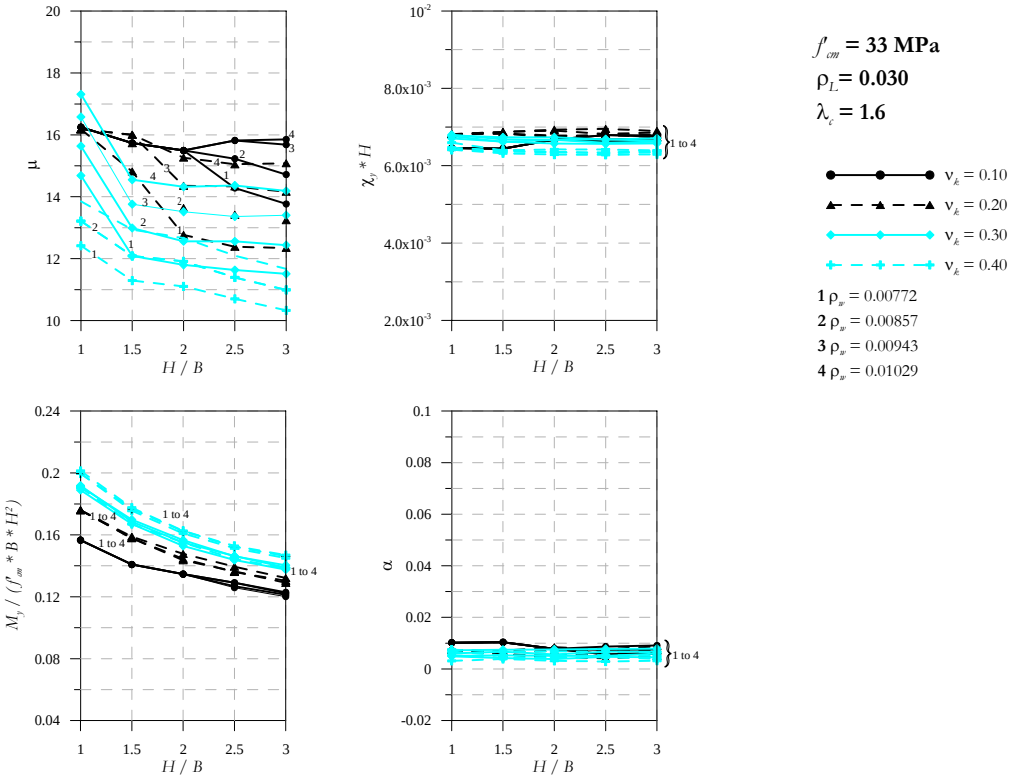

Figure 47 Results of the parametric analysis (f'_{cm} = 33 MPa, ρ_L = 0.030, λ_c = 1.6)

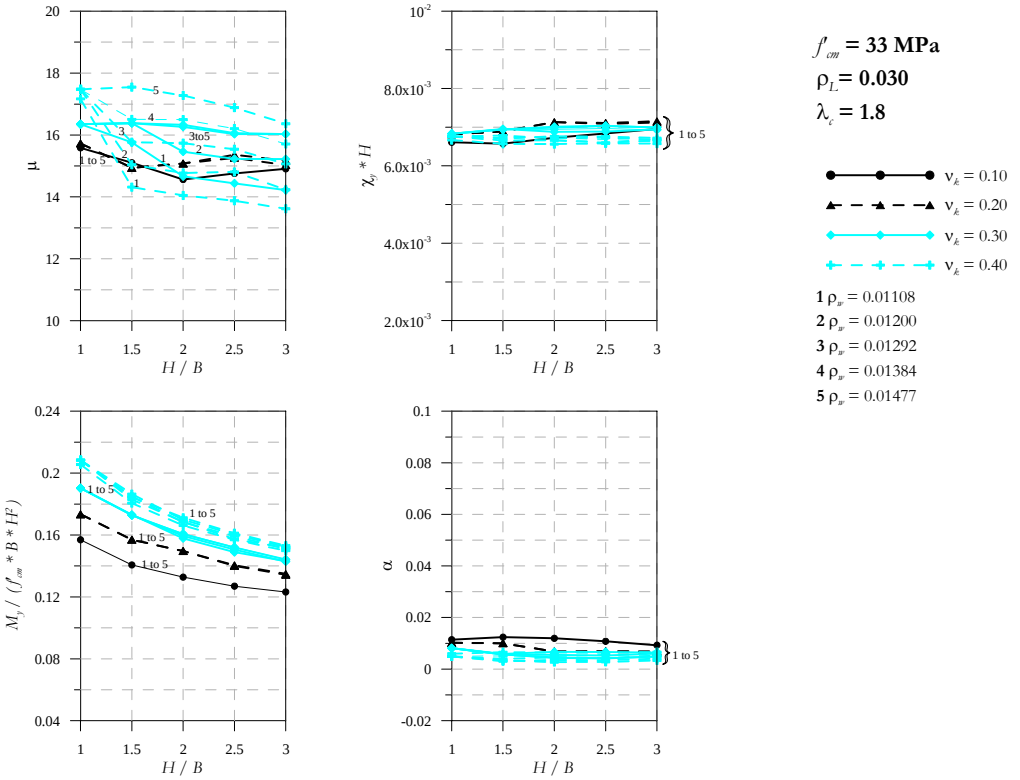

Figure 48 Results of the parametric analysis (f'_{cm} = 33 MPa, ρ_L = 0.030, λ_c = 1.8)

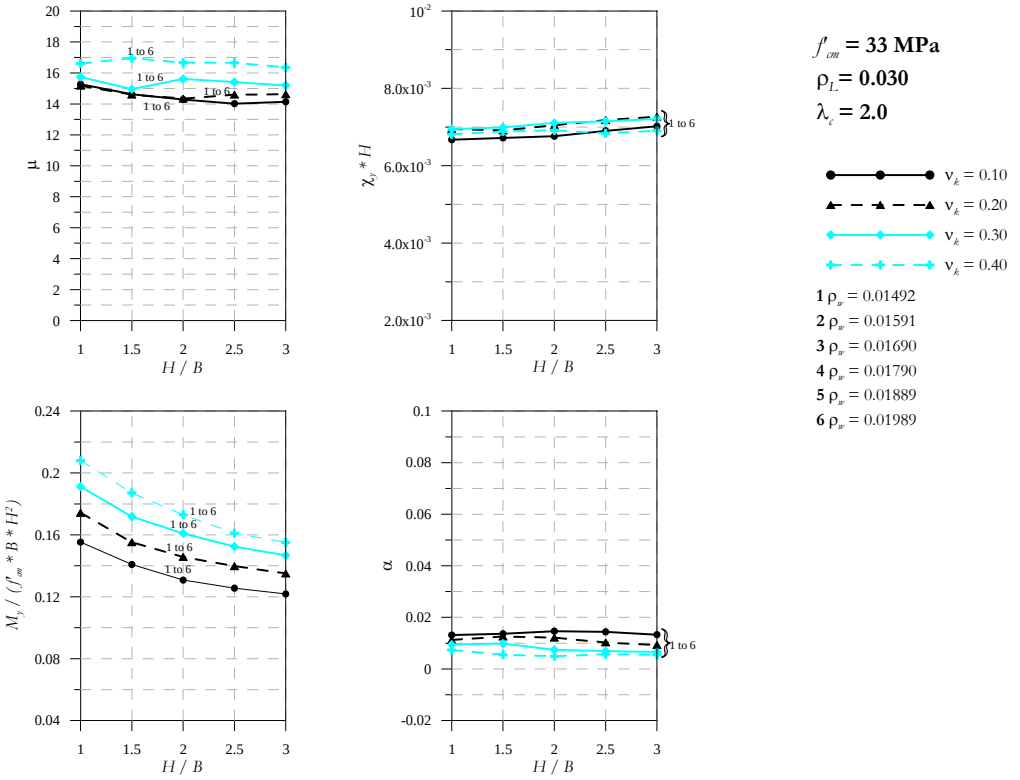

Figure 49 Results of the parametric analysis (f'_{cm} = 33 MPa, ρ_L = 0.030, λ_c = 2.0)

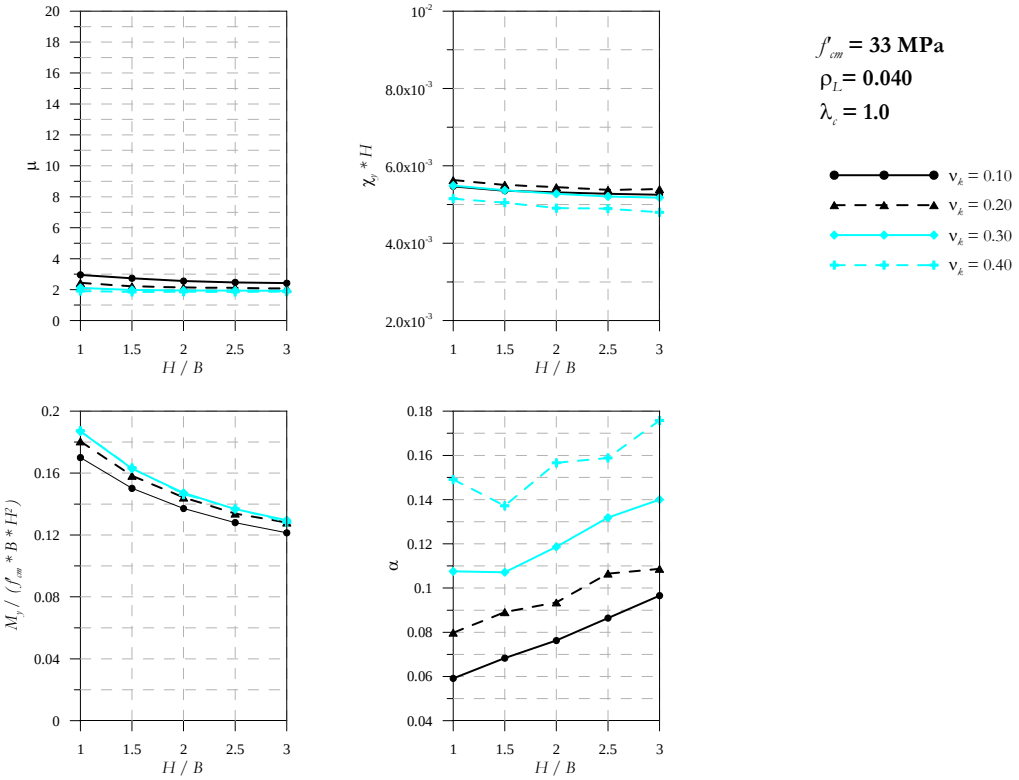

Figure 50 Results of the parametric analysis (f'_{cm} = 33 MPa, ρ_L = 0.040, λ_c = 1.0)

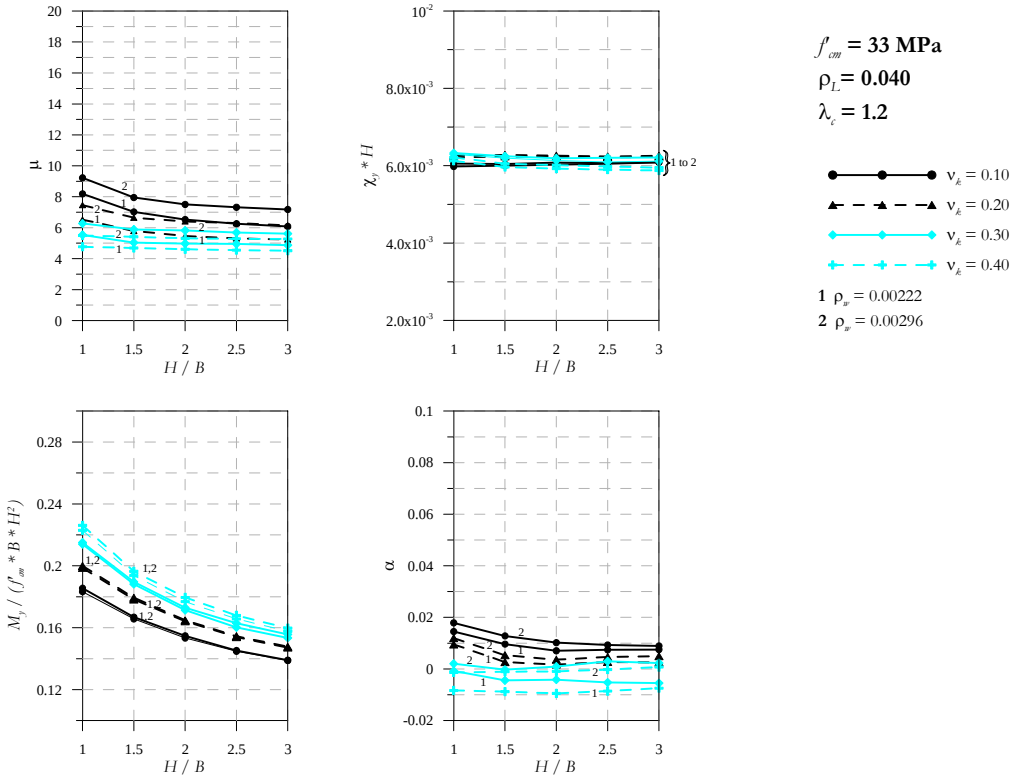

Figure 51 Results of the parametric analysis (f'_{cm} = 33 MPa, ρ_L = 0.040, λ_c = 1.2)

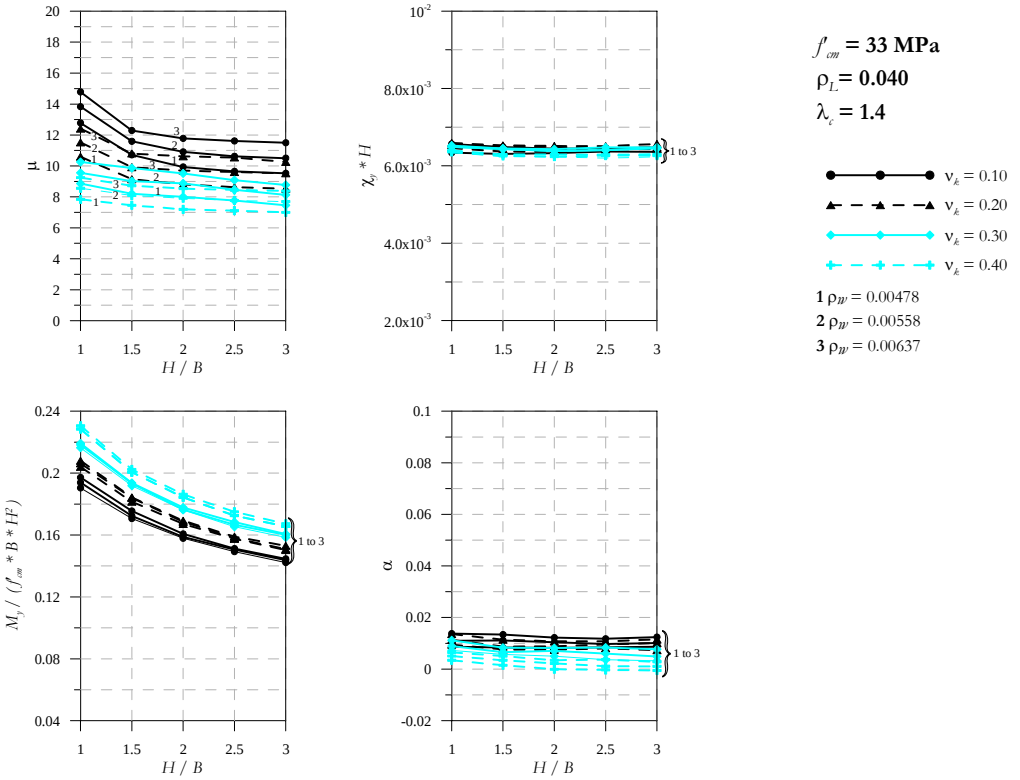

Figure 52 Results of the parametric analysis (f'_{cm} = 33 MPa, ρ_L = 0.040, λ_c = 1.4)

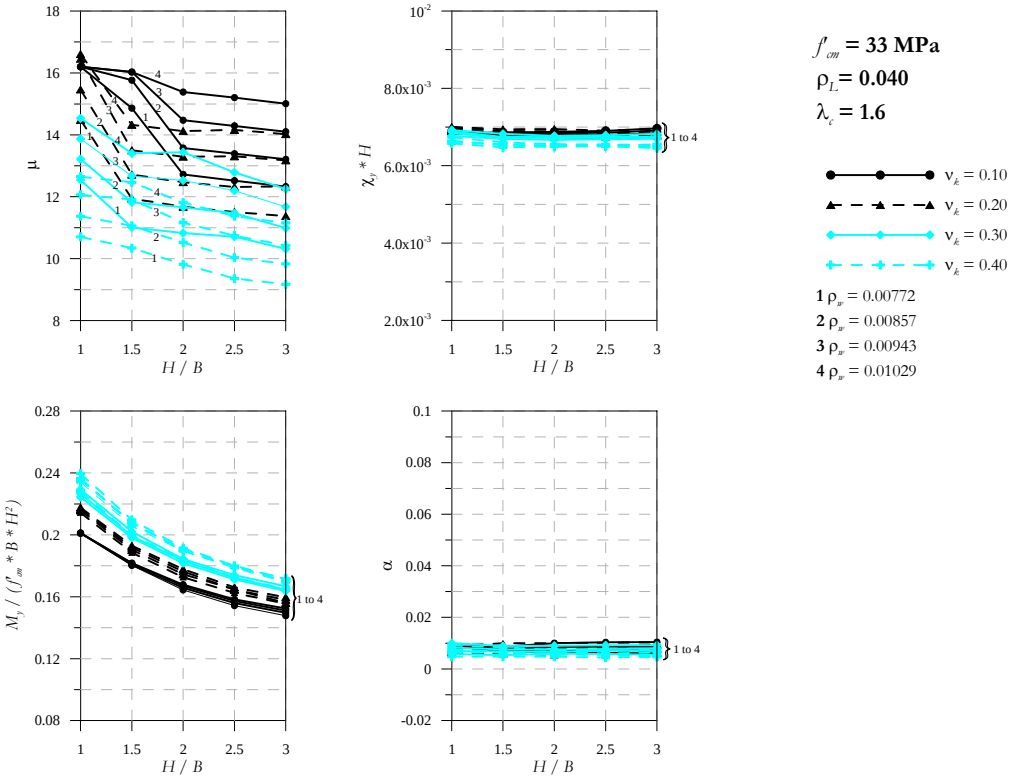

Figure 53 Results of the parametric analysis (f'_{cm} = 33 MPa, ρ_L = 0.040, λ_c = 1.6)

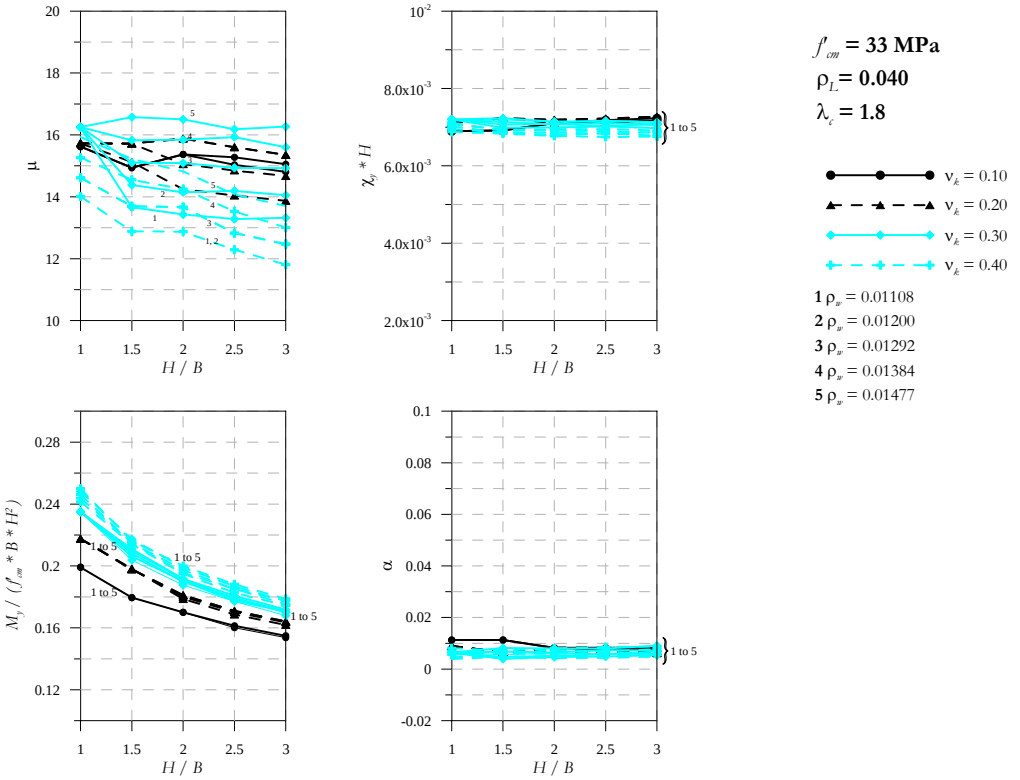

Figure 54 Results of the parametric analysis (f'_{cm} = 33 MPa, ρ_L = 0.040, λ_c = 1.8)

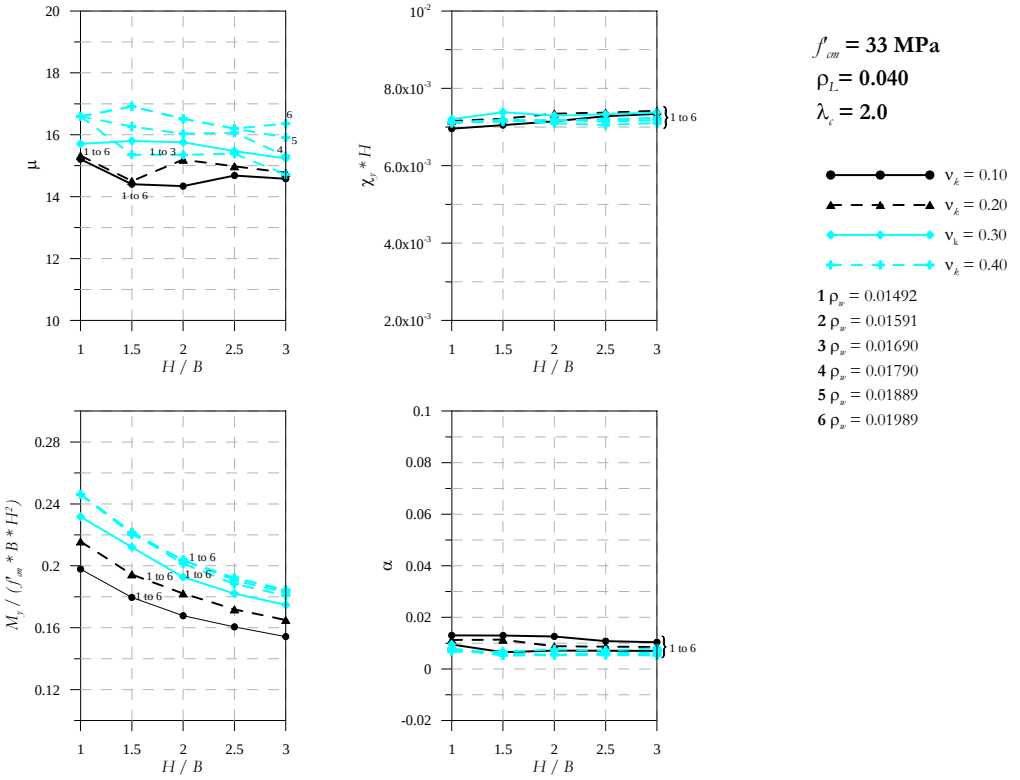

Figure 55 Results of the parametric analysis (f'_{cm} = 33 MPa, ρ_L = 0.040, λ_c = 2.0)

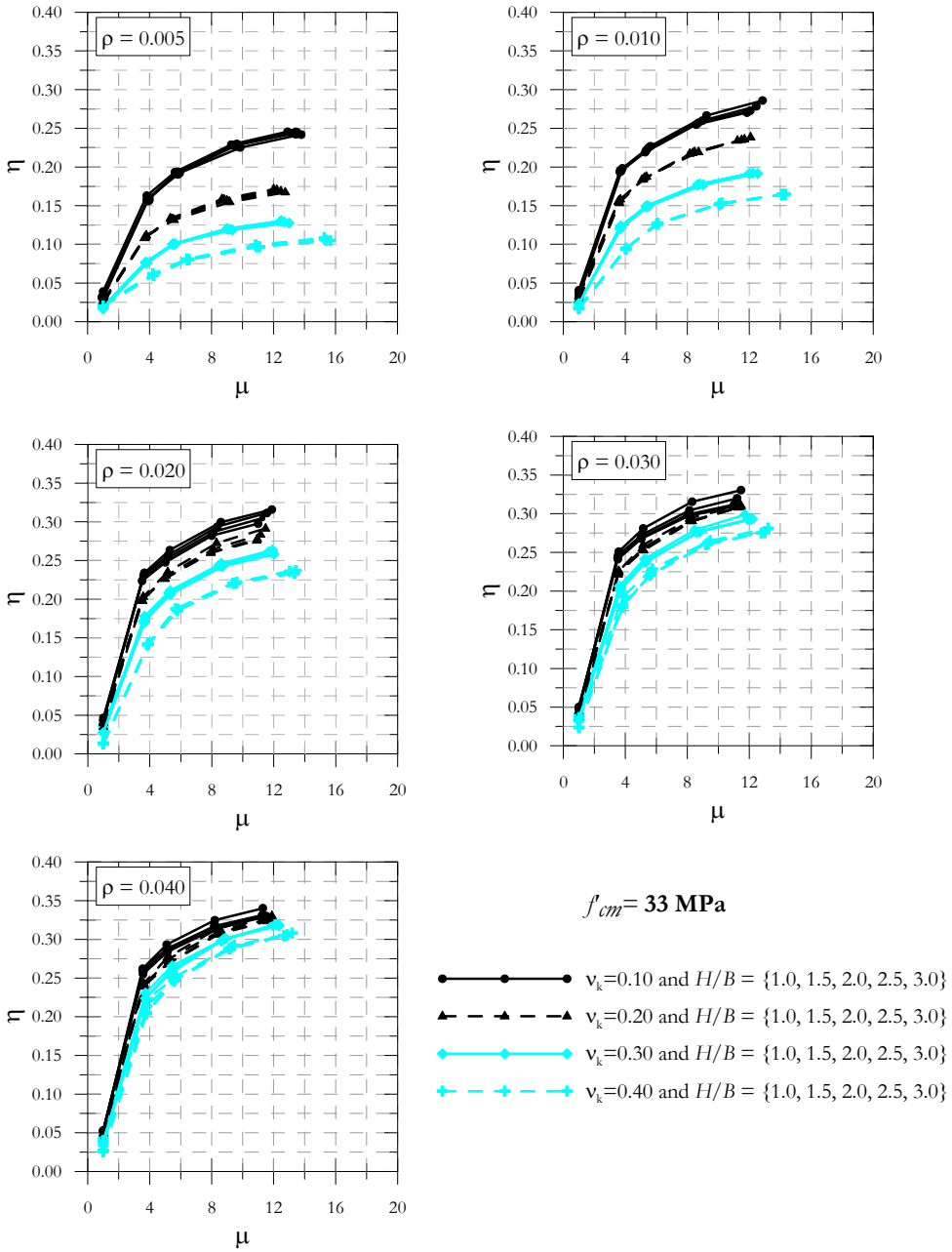

Figure 56 Parameter that represents the hysteretic energy dissipated by piers

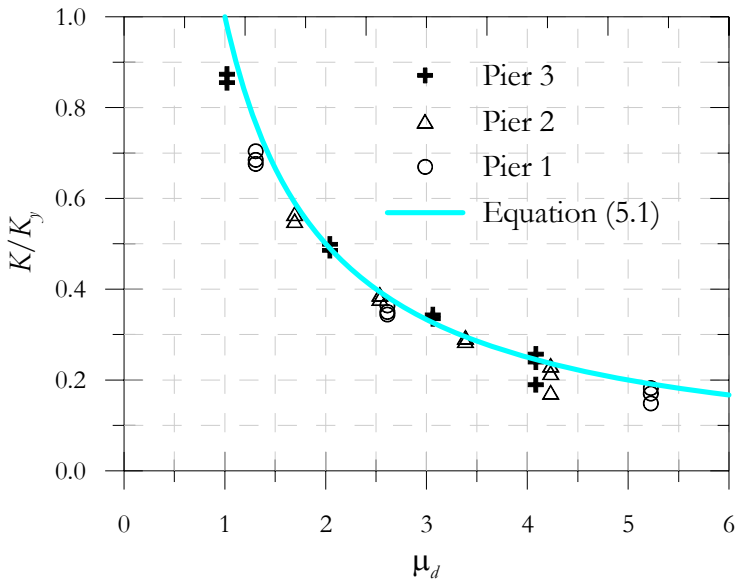

Figure 57 Comparison between Equation (5.1) and experimental results obtained from three piers characterized by different shear span ratio: 1.75 for Pier 1, 3.50 for Pier 2 and 5.25 for Pier 3.

PART B

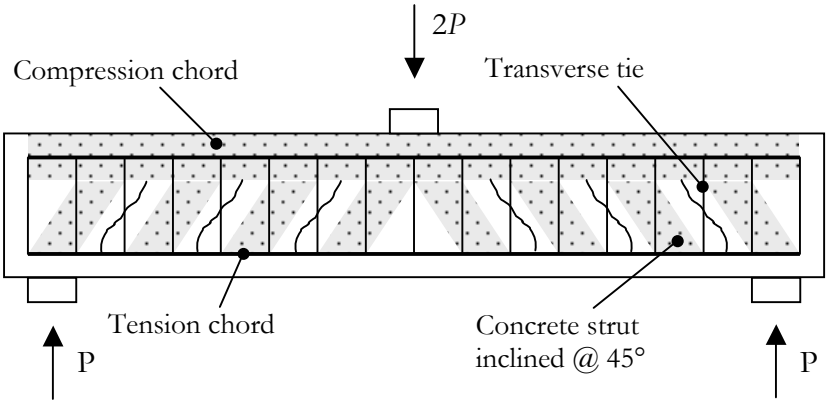

Figure 58 Ritter-Morsch model

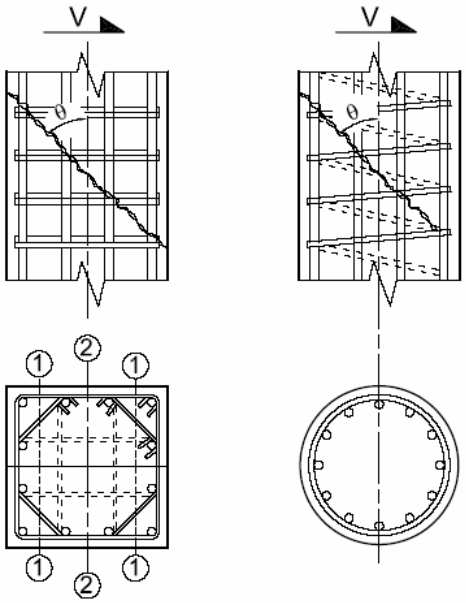

Figure 59 Effectiveness of transverse reinforcement for shear resistance of columns (adapted from Priestley *et al.* [1996])

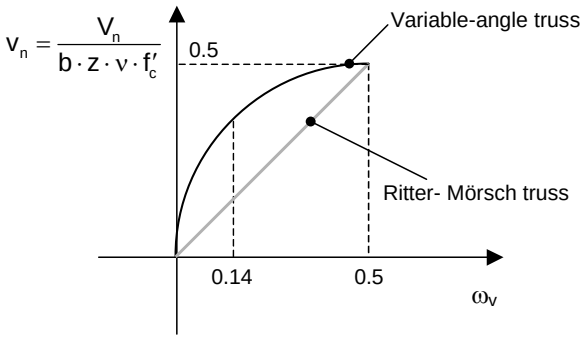

Figure 60 Dimensionless shear strength v as a function of the mechanical percentage of web reinforcement, ω_v

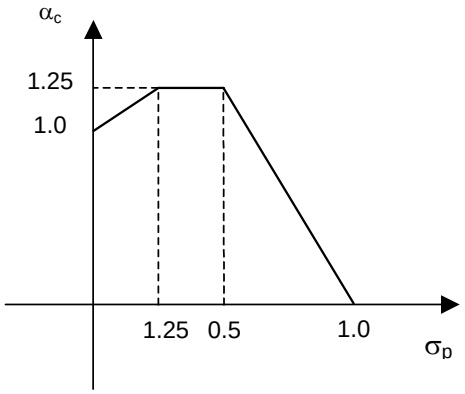

Figure 61 Values of factor α_c affecting Equation (8.5) for members subjected to axial compressive loads

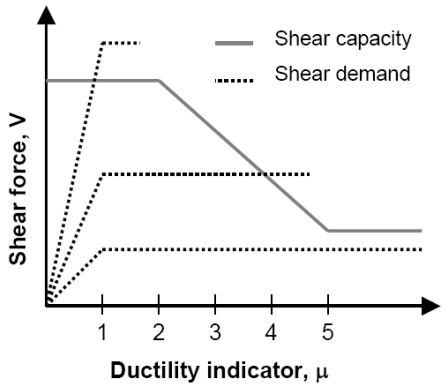

Figure 62 Applied Technology Council Model for shear strength degradation

Figure 63 Relationship between ductility and strength of concrete shear-resisting mechanisms (adapted from Priestley *et al.* [1994])

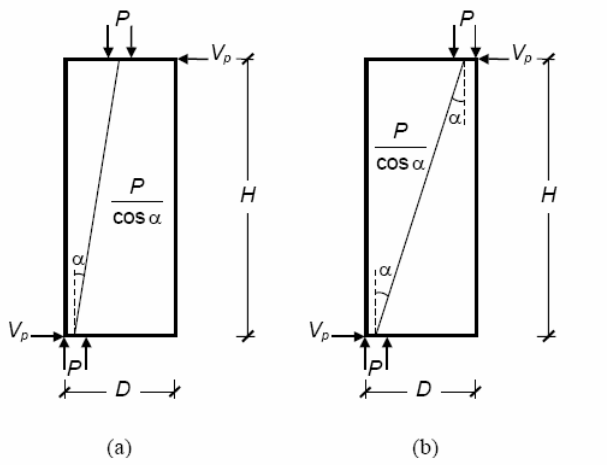

Figure 64 Contribution of axial force to column shear strength for (a) simple bending and (b) reversal bending (adapted from Priestley *et al.* [1994])

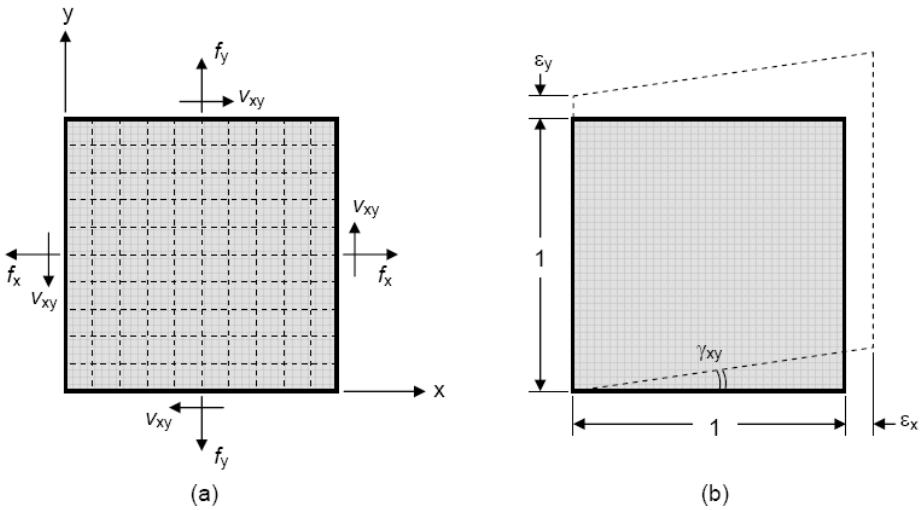

Figure 65 CFT of a reinforced concrete membrane element

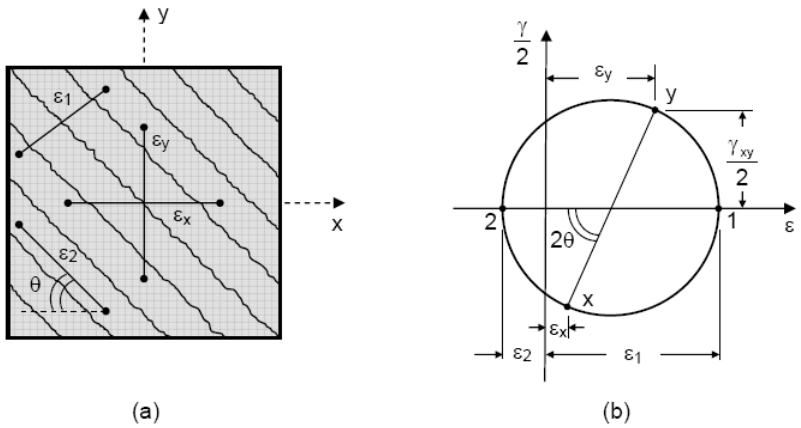

Figure 66 Mohr's circle for average strains

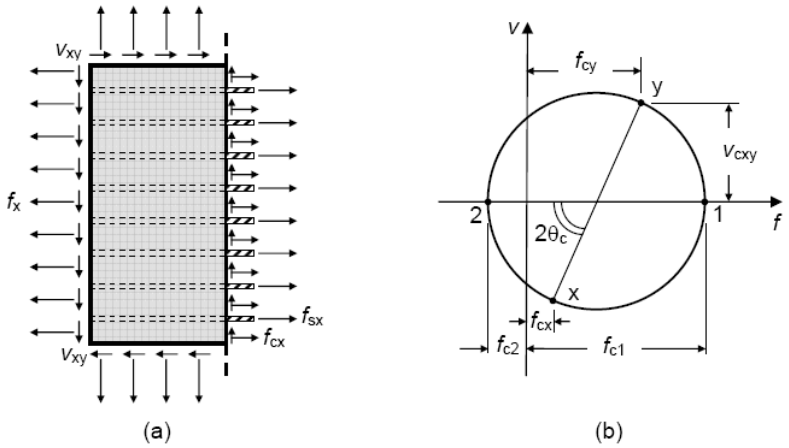

Figure 67 Mohr's circle for average stresses

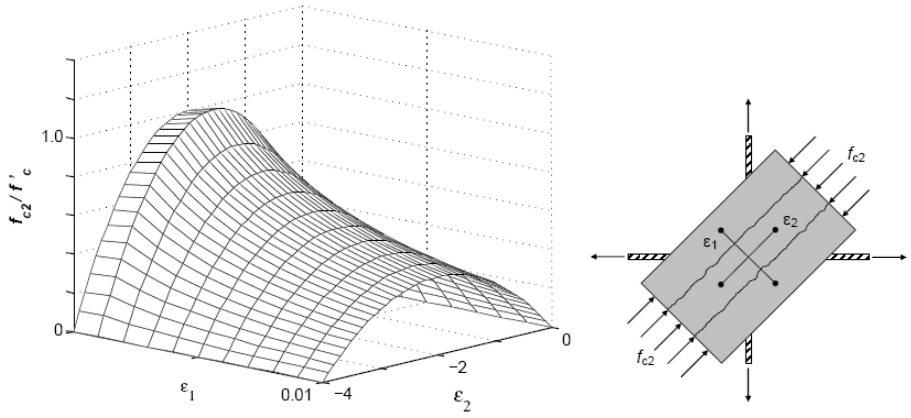

Figure 68 Average stress-strain relationship for cracked concrete in compression

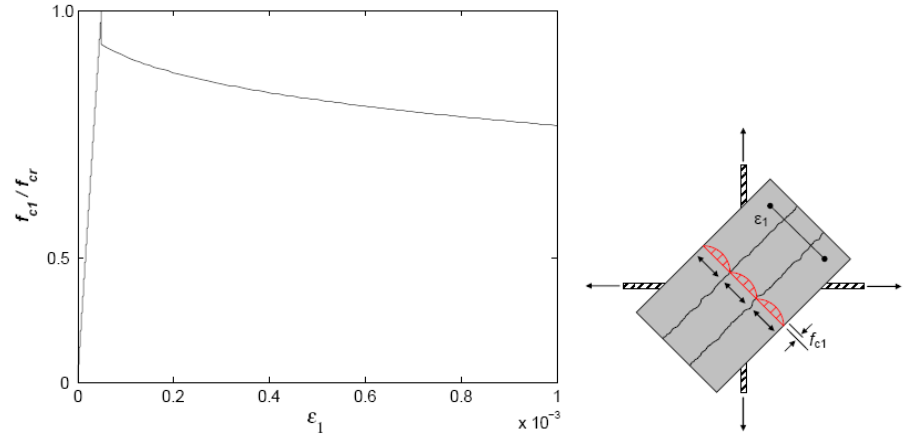

Figure 69 Average stress-strain relationship for cracked concrete in tension

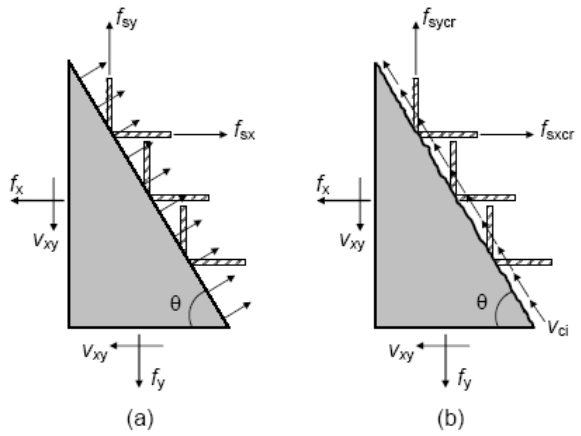

Figure 70 (a) Calculated average stresses. (b) Local stresses at a crack

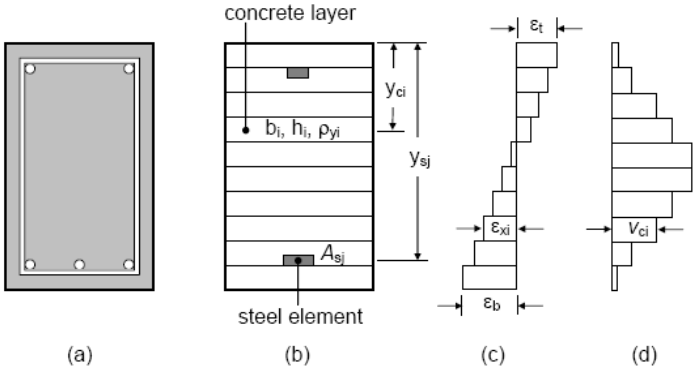

Figure 71 Layered model of the member section

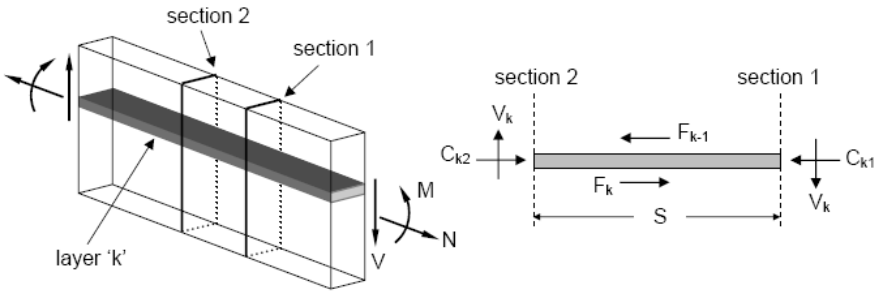

Figure 72 Free-body diagram for concrete layer k

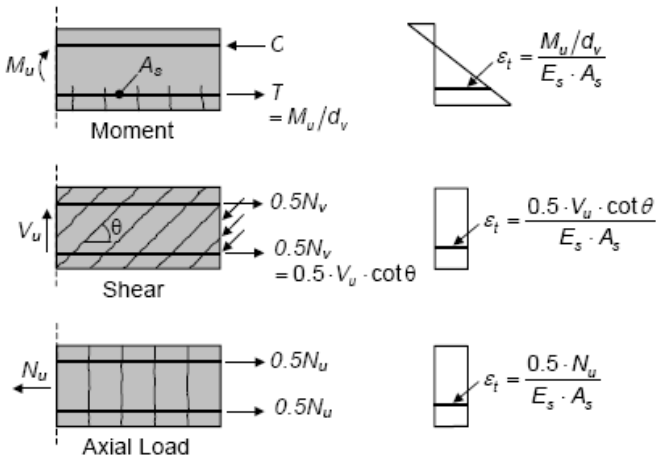

Figure 73 Determination of strain ε_x for a non-prestressed beam

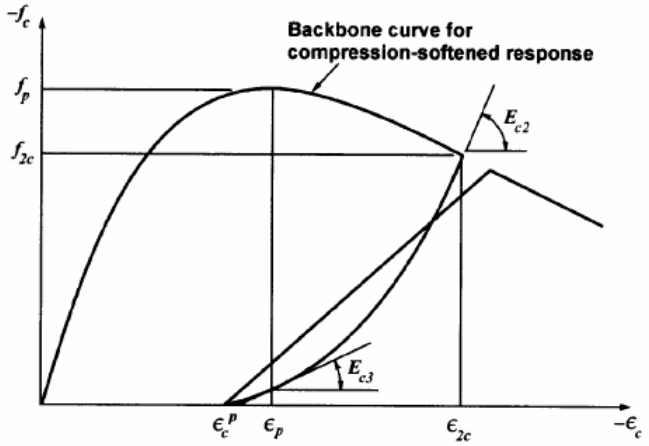

Figure 74 Hysteresis model for concrete in compression: unloading branch (from [Palermo and Vecchio, 2003])

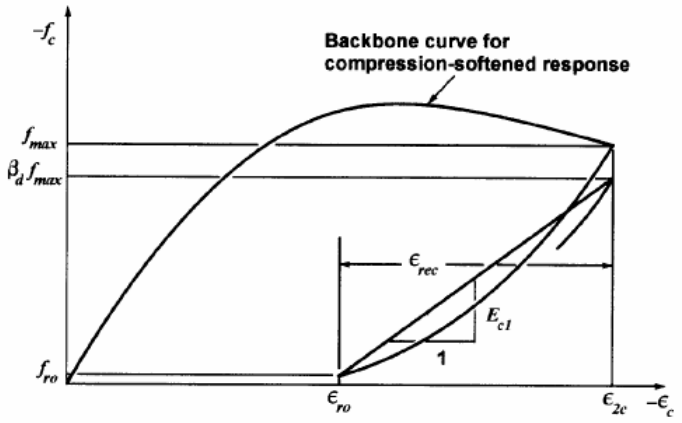

Figure 75 Hysteresis model for concrete in compression: reloading branch (from [Palermo and Vecchio, 2003])

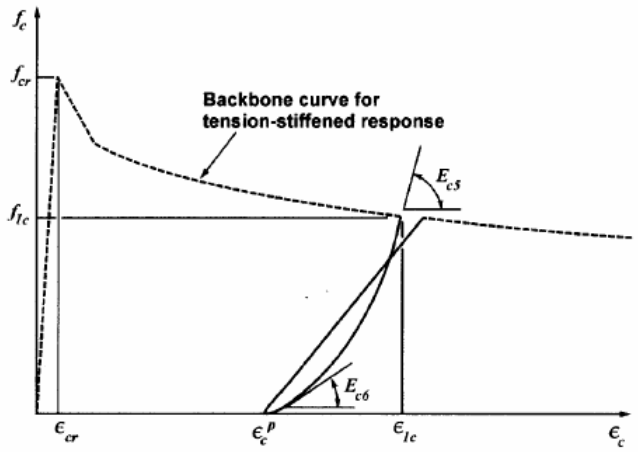

Figure 76 Hysteresis model for concrete in tension: unloading branch (from [Palermo and Vecchio, 2003])

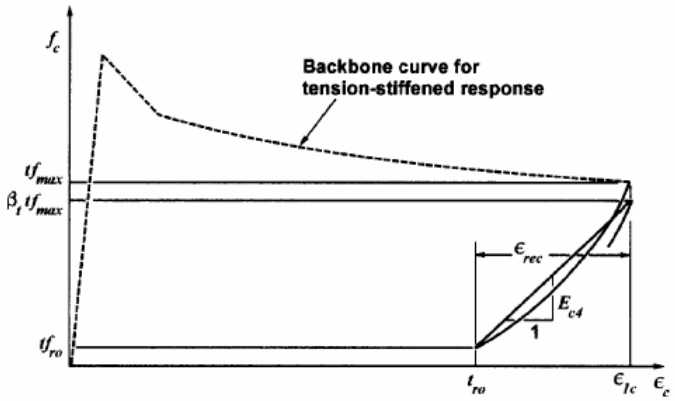

Figure 77 Hysteresis model for concrete in tension: reloading branch (from [Palermo and Vecchio, 2003])

European Commission

EUR 22885 EN – Joint Research Centre – Institute for the Protection and Security of the Citizen
Title: Simplified models/procedures for estimation of secant-to-yielding stiffness, equivalent damping, ultimate deformations and shear capacity of bridge piers on the basis of numerical analysis
Author(s): Carlo PAULOTTO, Gustavo AYALA, Fabio TAUCER, Artur PINTO
Luxembourg: Office for Official Publications of the European Communities
2007 – 113 pp. – 21 x 29.7 cm
EUR – Scientific and Technical Research series – ISSN 1018-5593

Abstract
The present report gives charts and expressions for computing the equivalent stiffness and damping of bridge piers of rectangular hollow cross section at maximum displacement within the framework of displacement based design and assessment of bridges, based on the results of parametric non-linear cyclic fibre section analysis calibrated from full-scale experimental results. A state of the art review is presented concerning the different approaches that may be adopted to model shear effects in reinforced concrete columns concerning the different approaches that may be adopted to model the shear effects in reinforced concrete columns.

The mission of the JRC is to provide customer-driven scientific and technical support for the conception, development, implementation and monitoring of EU policies. As a service of the European Commission, the JRC functions as a reference centre of science and technology for the Union. Close to the policy-making process, it serves the common interest of the Member States, while being independent of special interests, whether private or national.